Bioactive Aurones, Indanones, and Other Hemiindigoid Scaffolds: Medicinal Chemistry and Photopharmacology Perspectives

Leticia Lazinski, Guy Royal, Maxime Robin, Marc Maresca, Romain Haudecoeur

Bioactive Aurones, Indanones and Other Hemiindigoid Scaffolds: Medicinal Chemistry and Photopharmacology Perspectives

Leticia M. Lazinski,[1,2] Guy Royal,[2] Maxime Robin,[3] Marc Maresca[4] and Romain Haudecoeur*[,1]

1. Univ. Grenoble Alpes, CNRS 5063, DPM, 38000 Grenoble, France.
2. Univ. Grenoble Alpes, CNRS 5250, DCM, 38000 Grenoble, France.
3. Mediterranean Institute of Marine and Terrestrial Biodiversity and Ecology (IMBE), Aix Marseille Univ., 27 boulevard Jean Moulin, 13385 Marseille, France
4. Aix Marseille Univ., CNRS, Centrale Marseille, iSm2, 13397 Marseille, France.

ABSTRACT

Hemiindigoids comprise a range of natural and synthetic scaffolds that share the same aromatic hydrocarbon backbone as well as promising biological and optical properties. The encouraging therapeutic potential of these scaffolds has been unraveled by many studies over the past years and uncovered representants with inspiring pharmacophoric features such as the acetylcholinesterase inhibitor donezepil and the tubulin polymerization inhibitor indanocine. In this review, we summarize the last advances in the medicinal potential of hemiindigoids, with a special attention to molecular design, structure-activity relationship, ligand-target interactions, and mechanistic explanations covering their effects. As their strong fluorogenic potential and photoswitch behavior recently started to be highlighted and explored in biology, giving rise to the development of novel

fluorescent probes and photopharmacological agents, we also discuss these properties in a medicinal chemistry perspective.

INTRODUCTION

Hemiindigoids are aromatic scaffolds derived from the better-known indigoids, themselves termed in reference to natural indigo, a famous chromophore used as a dye since the antiquity and whose structure was described by Baeyer in 1883.[1] Unlike indigoids, which are made of two symmetrical bicyclic aromatic units linked by an exocyclic carbon-carbon double bond, hemiindigoids display an "indigoid part" connected to a "stilbene part" through the double bond (Figure 1). Hemiindigoids are thus asymmetrical compounds, but they retain the existence of two isomers, called *Z* and *E*, instead of the *cis* and *trans* forms for indigoids. They consist of four main scaffolds, depending on the nature of the intracyclic atom embedded in the five-membered ring. The oxo scaffold, called aurone (in red in Figure 1), is certainly the most studied, as it occurs from natural sources, mainly plants. Indeed, over a hundred of natural aurones are known,[2] especially with polyphenolic substitution patterns, such as sulfuretin, maritimetin or hispidol (Figure 2), and numerous synthetic derivatives were developed for medicinal chemistry purposes.[3] Carbon-based counterparts are often called 2-arylideneindanones, or more simply indanones (in green in Figure 1). The aza and thio versions are known as hemiindigos and hemithioindigos (sometimes azaaurones and thioaurones, in blue and yellow in Figure 1, respectively). While these subclasses have been known for a long time (hemithioindigos were reported for the first time by Friedländer in 1906,[4] aurones by Geissman and Heaton in 1943)[5], their medicinal properties and unique photophysical behaviors have been studied only recently. Especially, the past ten years have

witnessed a great interest for hemiindigoids, aurones and indanones in the foreground, in several pharmaceutical domains such as cancer, neurodegenerative disorders, infectious diseases or inflammation. Meanwhile, the hemiindigo and hemithioindigo scaffolds emerged as reliable photoswitchable platforms for various applications, often allowing a reversible *Z*-to-*E* conversion using visible light with high bistability and favorable photophysical parameters. Recently, they even made a timid incursion in biology, paving the way for future exciting opportunities in photopharmacology, a field expanding rapidly. Thus, we propose herein to take stock of the advances in the medicinal chemistry and photochemistry of hemiindigoids achieved within the past ten years, and to identify the most promising perspectives these fascinating scaffolds can offer.

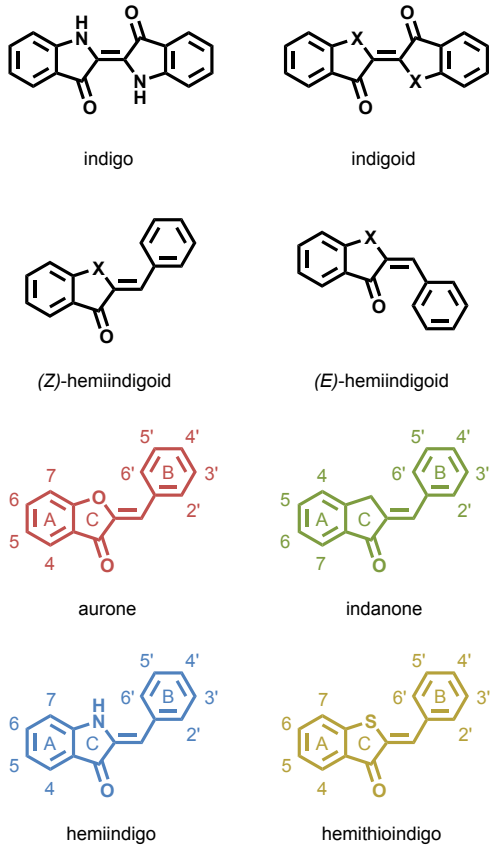

Figure 1. Structures of various indigoids and hemiindigoids.

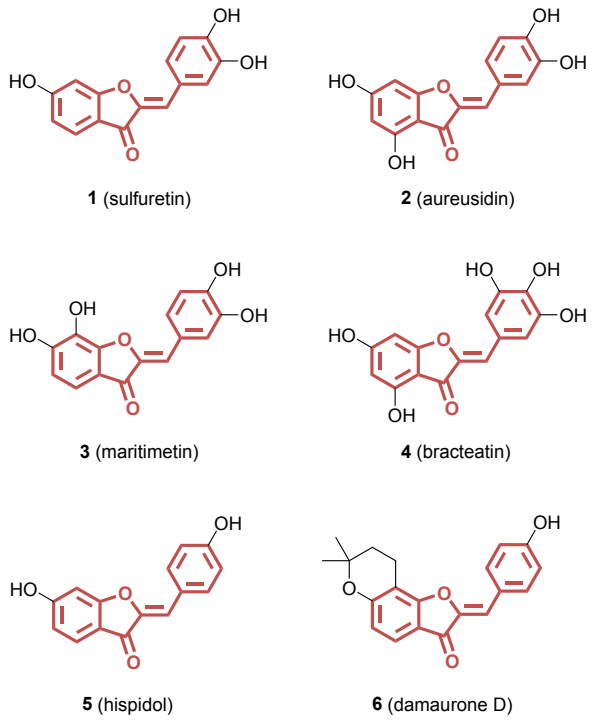

Figure 2. Structures of the best-known naturally occurring aurones.

MAIN SYNTHETIC METHODS OF HEMIINDIGOIDS

Numerous straightforward synthetic pathways were developed for preparing hemiindigoids over the years, and aurones received the closest attention, due to their natural origin. However, a large proportion of these methods followed pure synthetic chemistry objectives, and appears as not easy transferrable to pharmacomodulation endeavors. Thus, only synthetic routes allowing to reach hemiindigoids with various functionalization patterns are presented herein. Most of the available methods comprise the synthesis of the widely described aurone scaffold, but, with some adaptations, they can be extended to indanones, HI and HTI. In most cases, aldol condensation between the "indigo" part and a benzaldehyde constitutes the main path. The synthesis of the "indigo" part through intramolecular acylation most frequently precedes the condensation for

indanones and HTI when functionalization is desired, and the starting material is not commercially available. In the case of HI, functionalized indoxyl heterocycles are less described and conventional synthesis usually starts from 3-indolyl acetate or 1-acetyl-3-acetoxyindole, which are directly employed in the condensation step under basic conditions (Scheme 1).[6,7] Typically, for thioindoxyls, the synthesis starts from the conversion of a thiophenol into 2-(phenylthiol)-acetic acid, followed by the transformation into the corresponding acid chloride using $SOCl_2$ and, finally, ring closure through Friedel-Crafts in the presence of $AlCl_3$.[8] An alternative method employed very often for the synthesis of thioindoxyls is the lithium diisopropylamide (LDA)-mediated cyclization of 2-(methylthio)benzamides.[9] For indanones, the synthesis usually starts from arylpropionic acids and cyclization has been reported to occur in the presence of sulfuric acid, $Tb(OTf)_3$, P_2O_5 and methane sulfonic acid.[10–12] Then, as already stated, the last step of the synthesis is usually performed through aldol condensation in the presence of bases (*e.g.*, KOH, NaOH, NaH, piperidine) or acids (*e.g.*, AcOH, HCl, H_2SO_4), both of which are frequently used for indanones, aurones and HTI.[8,13–15] For aurones, neutral Al_2O_3 or "on-water" synthesis in refluxed H_2O are also employed as milder conditions for fragile substituents, but both methods include limitations.[16,17] Alternatively, for aurones and HTI, cyclization of 2'-hydroxychalcones[18,19] and 2'-nitrochalcones[20] respectively are frequently used methods that affords derivatives with good yields and functional group tolerance (Scheme 1). Overall, several other ingenious methods have been reported so far, such as the 5-*exo*-*dig* cyclization of substituted acetylene derivatives using Pd-, Ag- or Au-based catalysis,[21] or the Suzuki coupling of arylboronic acids with 2-bromomethylene derivatives,[22] but they globally appear as more difficult to implement in a medicinal chemistry context, due to the poor accessibility of variously substituted starting materials and/or the cost of reagents and catalysts.

Scheme 1. Main Synthetic Routes for the Preparation of Hemiindigoids.[a]

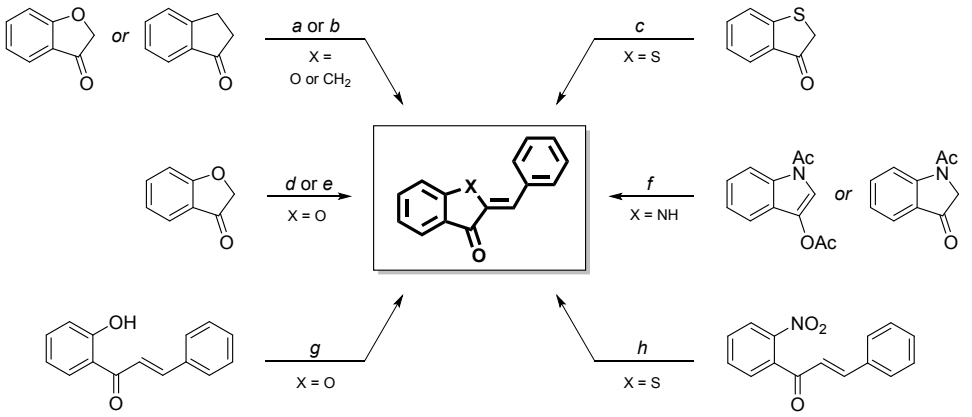

[a]Reagents and conditions: (a) arylaldehyde, KOH (10–50%), MeOH, H_2O; (b) arylaldehyde, AcOH, HCl, H_2O; (c) arylaldehyde, piperidine (cat.), EtOH; (d) arylaldehyde, Al_2O_3 (neutral), CH_2Cl_2; (e) arylaldehyde, H_2O; (f) arylaldehyde, NaOH, MeOH, H_2O; (g) $Hg(OAc)_2$, DMSO *or* pyridine; (h) S_8, DMSO, Et_3N.

BIOLOGICAL ACTIVITIES OF HEMIINDIGOIDS

Anticancer activities

Inhibition of tubulin polymerization. The targeting of microtubules is an attractive strategy for inducing cycle arrest of cancer cells, and several antitubulin drugs are already in clinical use.[23] In 2000, the National Cancer Institute (USA) discovered indanocine (**8**, Figure 3), an indanone derivative with strong antiproliferative activity (IC_{50} = 2.0–25 nM against seven multidrug-resistant lines). It acted as a cytostatic and cytotoxic agent, blocking tubulin polymerization at the

colchicine binding-site (IC_{50} = 1.7 μM) while selectively causing apoptosis of multidrug-resistant cancer cells.[24] As a consequence, in the last decade several studies reported new analogues, based on the indanone scaffold with colchicine- (**7**) and/or combretastatin-inspired substitution patterns —especially including the aromatic trimethoxy moiety, at positions 4, 5 and 6. One good illustration of this design strategy is compound **9**, which was found as a tubulin polymerization inhibitor with IC_{50} = 7.56 μM, able to cause a disruption of the microtubule network in a HeLa cells assay. Therefore, **9** acted as an efficient antiproliferative agent in an evaluation involving five human cancer cell lines (HeLa, A549, Bel-7402, PC-3, MDA-MB-231), yielding IC_{50} values of 0.17–0.6 μM.[25] Fused-indole derivative **10** exerted stronger effects in both tubulin polymerization (IC_{50} = 1.99 μM) and antiproliferative assays (IC_{50} = 0.03–0.04 μM against HeLa, A549, Bel-7402, PC-3 and K562 cell lines).[26] A series of aurone-based derivatives was globally found as equally potent, as illustrated by the comparable tubulin polymerization inhibition displayed by **11**, a close analogue of **9** (IC_{50} = 8.6 μM vs. 7.56 μM).[27] The introduction of a trimethoxylated aryl group at position 3 of the indanone scaffold afforded additional series of antimitotic agents. Among them, compound **12**, despite its modest antiproliferative action (IC_{50} = 4.0–10.0 μM against THP-1, HCT-116, MCF-7, T-47D and A549 cells), revealed a slightly improved action on tubulin (IC_{50} = 1.5 μM).[28] A molecular dynamics study and conformational modes analysis proposed a crucial role for the trimethoxylated ring A of **12** in the binding process. Indeed, the ring would be embedded between S8/S9 β-sheets, H8 α-helix and T7 loop of colchicine binding-site of the αβ-tubulin dimer, triggering robust hydrophobic interactions and hydrogen bonds, and causing perturbations in lateral contacts with microtubule.[29] Compound **13** is another example with submicromolar anti-polymerization activity (IC_{50} = 0.63 μM), but it showed disparate results in the antiproliferative test, exhibiting either a good (IC_{50} = 0.01–0.10 μM for MCF-7 and HCT cells) or a weak profile (IC_{50} = 4.9–11.0 μM for THP-1 and A549 cells), depending on the cell lines.[30] Regarding *in vivo*

potency, **13** induced a reduction of Ehrlich ascite carcinoma by 45.5% at 20 mg/kg (day 12) in Swiss-albino mice.[31] Analogue **14** was further investigated for its pharmacological properties but was found to exert only moderate anticancer activity.[32] All these molecules act through a similar mechanism, leading to cell cycle arrest at the G2/M phase and cell apoptosis.

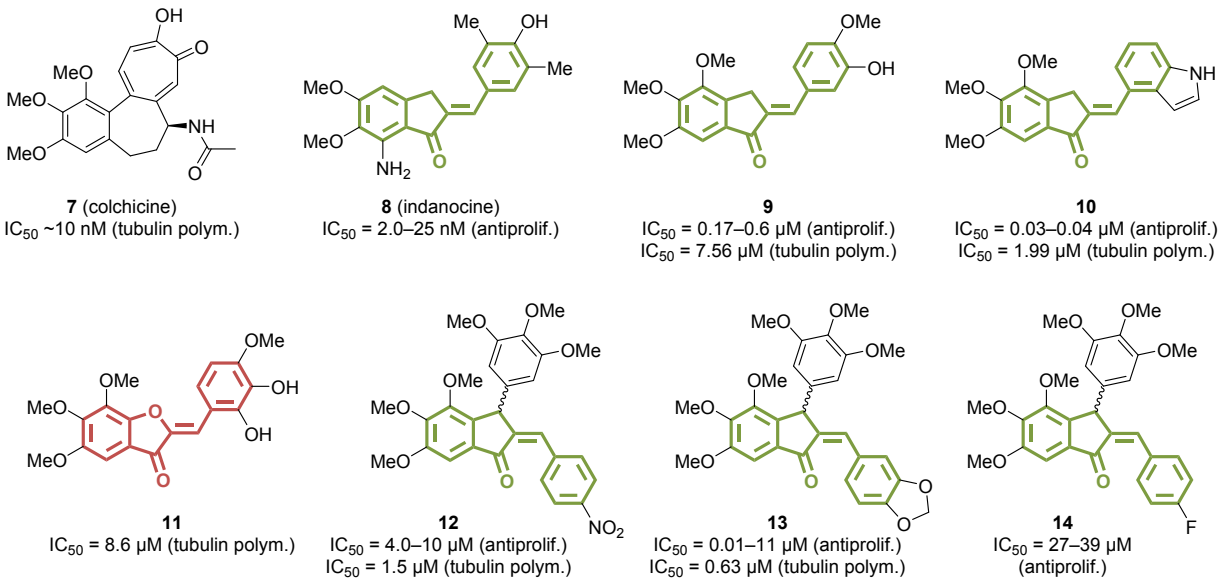

Figure 3. Structures and activities of tubulin polymerization inhibitors.

Targeting of collateral sensitivity in multidrug-resistance cancer cells. In the frame of multidrug resistance in cancer, it was found that specific compounds were able to target specifically tumors with resistant phenotypes, a counter-intuitive phenomenon that was termed collateral sensitivity. Several medicinal chemistry approaches were tried for exploiting such properties, through various mechanisms often involving efflux pumps. Ferrocene-based flavonoids, including aurone derivatives, were especially found to induce glutathione efflux in MRP1-transfected BHK-21 cells. Compound **15** (Figure 4) caused a significant net glutathione efflux in these cells after correction from the effect detected on wild-type BHK-21 cells (52% at 5 μM). This observation could be the source of the difference seen in terms of cytotoxic action for **15** against NCI-H69 cancer cells and

the resistant MRP1-overexpressing counterpart H69AR (EC_{50} >100 µM and 12 µM respectively, a >8.2 selectivity ratio).[33] Thus, the presence of MRP1 in the cells, initially providing defense against anticancer agents, enabled the rise of a collateral sensitivity phenomenon. Very recently, a series of hemiindigo derivatives was reported. Evaluated against both the MES-SA sensitive and multidrug-resistant cancer cell lines, most of the compounds selectively targeted resistant cells. Compound **16** was the most promising analogue, with antiproliferative IC_{50} values of 18 µM and 3.7 µM against MES-SA and MES-SA/Dx5 (a doxorubicine-induced resistant line) respectively, providing a selectivity ratio of 4.8. By contrast, aurone derivatives were far less active, although they shared similar selectivity ratios. Higher IC_{50} values of 60 µM and 15.0 µM were recorded for compound **17**, one of the best aurones in the series.[34] Surely, more work is needed for improving the modest observed ratios and to further assess the true potential of the hemiindigoid family at targeting collateral sensitivity.

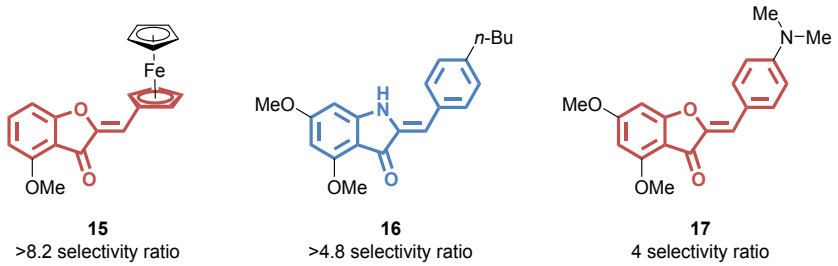

Figure 4. Structures and activities of collateral sensitivity inducers.

Inhibition of poly(ADP-ribose)polymerases (PARPs). The PARP-1 protein plays an important role in DNA damage repair, and thus constitutes a promising anticancer target for inhibitor development. Especially, targeted therapeutic strategies rely on the concept of synthetic lethality,[35] for example in the treatment of cancers with specific mutations, such as breast cancers (with mutated genes *BRCA*1 or *BRCA*2). Several agents and preclinical and clinical studies have been

reported to date, and among them aurone derivatives were found as potent inhibitors of PARP-1. Starting from an initial lead based on a dihydrobenzofuran scaffold (IC_{50} = 9.5 μM against PARP-1), modulation endeavor of Patel *et al.* led to the production of a first aurone series. While the sole presence of a naked B-ring did not improve the activity, better results were obtained upon phenol group insertion at position 4' (*e.g.*, IC_{50} = 0.75 μM for **18**, Figure 5). Crystallographic data of a **18**–PARP-1 complex (PDB code 4OQA, Figure 6A) showed that the resorcinol group was directed toward a hydrophilic pocket including side chains from Asp766, Asp770, Ser864, Asn868 and Arg878, without filling it however. Extended substituents were thus anchored to position 4' of the aurone scaffold. The piperazine moiety from compound **19** afforded improved IC_{50} (0.114 μM), among other piperazine- or morpholine-containing derivatives with submicromolar potencies. Indeed, the crystal structure of a morpholino counterpart of **19** bound to PARP-1 revealed the extent of additional interactions made with the hydrophilic pocket (PDB code 4OQB, Figure 6B).[36] Switching the flexible piperazine arm for a more rigid 5,6,7,8-tetrahydro-[1,2,4]triazolo[4,3-a]pyrazine heterocycle —among other tested scaffolds— gave compounds with two-digit nanomolar anti-PARP-1 activity. Compounds **20** and **21**, the most promising ones, were found active both against PARP-1 (IC_{50} = 30 nM and 27 nM, respectively) and PARP-2 (IC_{50} = 2 nM and 1.9 nM, respectively), but a wide range of derivatives with alternative heterocyclic substituents — in place of CF_3 or cyclopropyl— shared very similar values (IC_{50} = 30–67 nM against PARP-1 and 2.1–4.6 nM against PARP-2). The co-crystallization of **21** with a CATΔHD construct of PARP-1 —the catalytic domain with deletion of the autoinhibitory folded helical domain— revealed key interactions between the cyclopropyl part and hot spot residues from the adenosine binding pocket, such as Asn868 and Arg878. Upon further replacing the substituent at position 4', this time with benzimidazole derivatives, the IC_{50} values decreased, hitting single-digit nanomolar range with compound **22** (IC_{50} = 4 nM against PARP-1 and 0.7 nM against PARP-2). Structural data obtained

from another analogue, **23** (IC_{50} = 18 nM and 4 nM against PARP-1 and PARP-2, respectively), in complex with the CATΔHD construct, showed that the benzimidazole moiety pointed toward Arg878. Interestingly, the selectivity profile of compounds **20**–**23** against several PARP isoforms (PARP-1 and 2, TNKS1 and 2) strongly vary: if **20** and **21** are highly selective of PARP-1 and 2 (IC_{50} = 30 nM and 2 nM for PARP-1 and PARP-2, respectively, *vs.* >1000 nM for TNKS1 and 2) and could serve as chemical probes without interfering with other isoforms, **22** is by contrast a pan-isoform low nanomolar inhibitor (IC_{50} = 0.7–8.8 nM for PARP-1, PARP-2, TNKS1 and TNKS2), and **23** is only partially selective. Finally, compounds **20** and **21** showed PARP-specific cytotoxicity in *BRCA*1-mutant cells.[37] Interaction patterns of **21** and **23** were rationalized through crystal structure examination (PDB codes 6NRI and 6NRF, Figures 6C and 6D respectively).

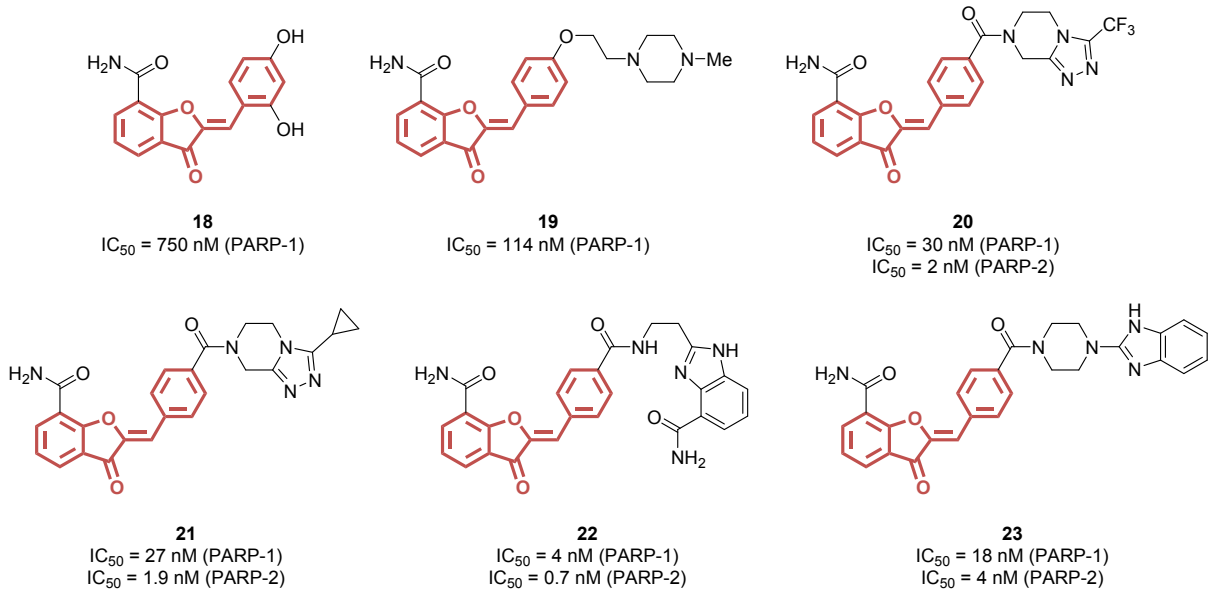

Figure 5. Structures and activities of PARP inhibitors.

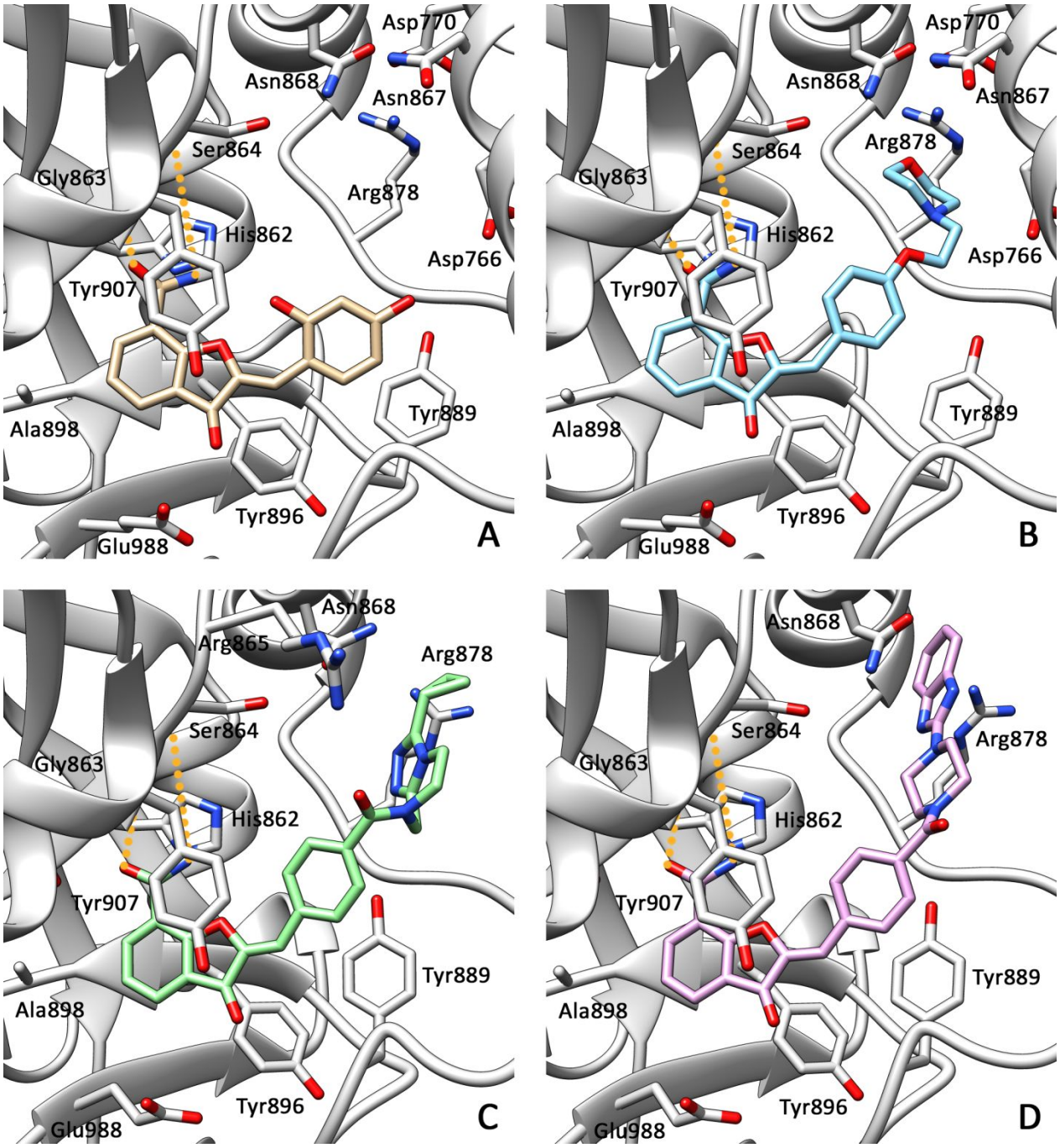

Figure 6. Compared crystal structures of **18** (A, gold, PDB code 4OQA), a morpholino analogue of **19** (B, cyan, PDB code 4OQB), **21** (C, green, PDB code 6NRI) and **23** (D, pink, PDB code 6NRF) in complex with PARP-1.

Inhibition of tyrosinase. Human tyrosinase catalyzes the first two steps of melanogenesis, and is a key target for reducing melanin formation *in vivo*. Besides the implications in dermocosmetics, the inhibition of human tyrosinase could mitigate the melanin-induced resistances of melanoma against a wide range of classical anticancer therapies, such as chemotherapy, immunotherapy or radiotherapy.[38] However, only few human tyrosinase inhibitors are known, as most studies focus on assays against tyrosinase from the mushroom *Agaricus bisporus*, which eventually appears as a deceptive model.[39] After a first report in 2006 focusing on cellular melanogenesis inhibition,[40] polyhydroxylated aurones were also described as chemical tools able to adopt versatile behaviors against both *Agaricus bisporus* mushroom and bacterial tyrosinases. Indeed, while monophenol and catechol substitutions at the B-ring led to the production of either substrates (4'-hydroxy and 3',4'-dihydroxy, such as **24**, Figure 7) or activators (2'-hydroxy and 3'-hydroxy, such as **25**) of tyrosinases, the resorcinol counterpart allowed to reach efficient inhibition of the isolated enzymes.[41,42] Compound **26** was especially associated with IC_{50} values of 4–9 μM against mushroom and bacterial enzymes, and was found to inhibit another tyrosinase, from *Polyporus arcularius* (IC_{50} = 34 μM).[43] A resorcinol-based indanone counterpart, **27**, was also identified with very similar potency (IC_{50} = 12.3 μM, K_i = 10.3 μM) against mushroom tyrosinase,[44] and was even highlighted as a more potent inhibitor in another study (IC_{50} = 0.034 μM and 1.39 μM using L-tyrosine and L-DOPA as a substrate, respectively).[14] Compound **28**, a close derivative of **27** with an additional fused phenyl ring, also showed some interesting activity (IC_{50} = 0.15 μM).[45] Alternatively, 4'-dimethylamino and 4'-diethoxymethyl groups introduced on the indanone scaffold yielded promising results (IC_{50} = 6–8 μM), as illustrated by compound **29**.[46] In addition, embedding a hydroxypyridine-*N*-oxide (HOPNO) moiety on the aurone scaffold afforded a series of three compounds with high activity against human tyrosinase, bearing either a 4-hydroxy, a 6-hydroxy, or a 4,6-dihydroxy substitution pattern. Compound **30** reached a K_i of 350 nM and

exhibited a similar potential to thiamidol, a reference molecule in the field of human tyrosinase targeting. QM/MM dynamics were performed in order to rationalize the binding of this compound to the dicopper center. As expected, the HOPNO moiety would interact with the metals while the rest of the aurone structure would provide contacts with various residues of the second coordination sphere, such as Ile368 and the flexible 302–310 loop, especially His304, Lys306 and Arg308. However, cell-based assays provided underwhelming results, and **30** seemed to suffer from its low solubility and membrane-crossing issues (IC_{50} = 85.3 µM in a whole-cell context using human melanoma cells).[47]

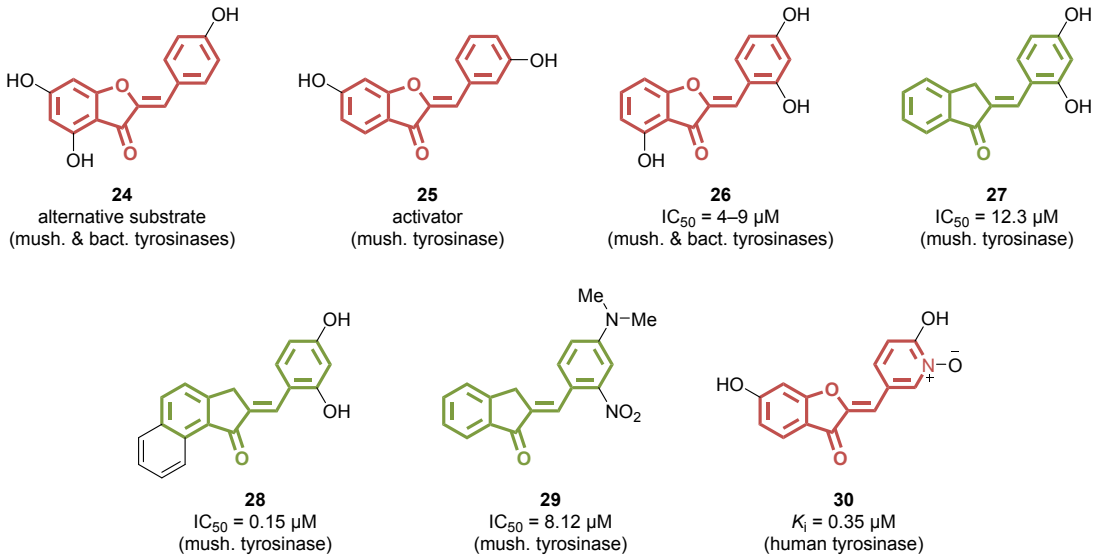

Figure 7. Structures and activities of tyrosinase inhibitors.

Inhibition of proto-oncogene serine/threonine-protein (PIM) kinases. PIM kinases are seen as important therapeutic targets in the frame of anticancer therapy since several years. Overexpressed in hematologic cancers and solid tumors, the three isoforms PIM1, PIM2 and PIM3 are both involved in numerous cancer-related disorders, such as cell proliferation or apoptosis. Thus, the development of PIM inhibitors recently attracted attention.[48] Initially, a virtual screening involving more than 5,000,000 compounds yielded 532 candidates evaluated against PIM1 kinase, eventually

affording five active molecules at 5 μM. Among them, the indolaurone derivative **31** (Figure 8) was found as a promising submicromolar 'hit' inhibitor (IC_{50} = 410 nM against PIM1),[49] interacting with PIM1 ATP-binding cleft (PDB code 3UMX, Figure 9A),[50] but suffered from poor kinase selectivity and metabolic stability. Thus, modulation efforts were undertaken in order to improve the profile of **31**. The 7-amino and 6-hydroxy groups, and the indole B-ring were all modulated independently for identifying the most beneficial features. It clearly appeared that a piperazinyl moiety was favorable at position 7, while a methoxy group gave the best results at position 6. Thus, variations of the B-heterocyclic ring of an otherwise optimized scaffold afforded two compounds with low nanomolar activity, **32** and **33** (IC_{50} = 3 nM and 2 nM, respectively). Compound **32** was especially co-crystallized with PIM1 kinase (PDB code 3UMW, Figure 9B), and seemed to bind also at the ATP-binding site. While the piperazine ring formed two crucial hydrogen bonds with Asp128 and Glu171, the extra methyl group introduced at position 6 was found to be set in a hydrophobic pocket, endorsing its higher potency, as compared with the hydroxy group of the parent compound **31**. Many other hydrogen bonds were observed, especially between the aurone carbonyl and Asp186 and Lys67, and between the heterocyclic B-ring and Glu121. In addition, **32** showed a far better kinase-selective profile, as revealed by tests performed against a large panel of kinases. Contrariwise, **33**, which shared a similar PIM1 inhibition potency, was associated with a global lower selectivity, while exhibiting an identical interaction pattern, just as its 6-azaindole derivative (PDB codes 5VUC and 5VUA, Figures 9C and 9D respectively). Cell-based assays confirmed the ability of **32** to inhibit the phosphorylation of BAD, a PIM1 substrate, and to cause apoptosis with a cell cycle arrest at the G1 phase, consistent with PIM1 inhibition effects already documented.[51] Then these compounds were modulated for reaching a better activity against PIM3. Indeed, **32** was found to be less active against PIM3 than PIM1 (IC_{50} = 25 nM vs. 3 nM). By combining the heterocyclic moieties at the B-rings of **25** and **26**, and by introducing an

additional methyl group on the methylene bridge between the aurone scaffold and the piperazine group, the authors designed compound **34**, which displayed a better anti-PIM3 activity (IC_{50} = 2.5 nM) while retaining a good PIM1 inhibitor profile (IC_{50} = 1.9 nM) and *in vivo* efficacy against pancreatic cancers in mice.[52] A further exploration of the impact of a substituent at position 6 of X3 B-ring heterocycle afforded a series of compounds with very high activity against PIM1. Among the studied molecules, 6'-fluoro and 6'-chloro derivatives were found to be particularly promising, both in the 6-methoxy and 6-hydroxy series. Compound **35** especially combined an excellent anti-PIM1 activity (IC_{50} = 1.4 nM) with a decent effect against PIM2 (IC_{50} = 140 nM) and good ADMET properties. The presence of the extra chlorine group allowed to hamper off-target interactions, including with other kinases, while improving the affinity for PIM2, thereby opening a way for reaching selective pan-PIM inhibitors.[53] A very recent study focused on PIM1 inhibitors discovery based on the aurone scaffold with hydroxy substitution at the A-ring. While submicromolar results were obtained for 3'-methoxy analogues, the best values were shown by B-heterocyclic compounds, reminiscently of the work of Nakano *et al*. The use of the B-ring of **35** was successful (IC_{50} = 8.8 nM for the 4-hydroxy-6-methoxy derivative), but compound **36**, based on another heterocyclic scaffold, also displayed potent inhibition of PIM1 (IC_{50} = 18 nM), indicating that some room still exists for a further development of aurone or hemiindigoid analogues.[54]

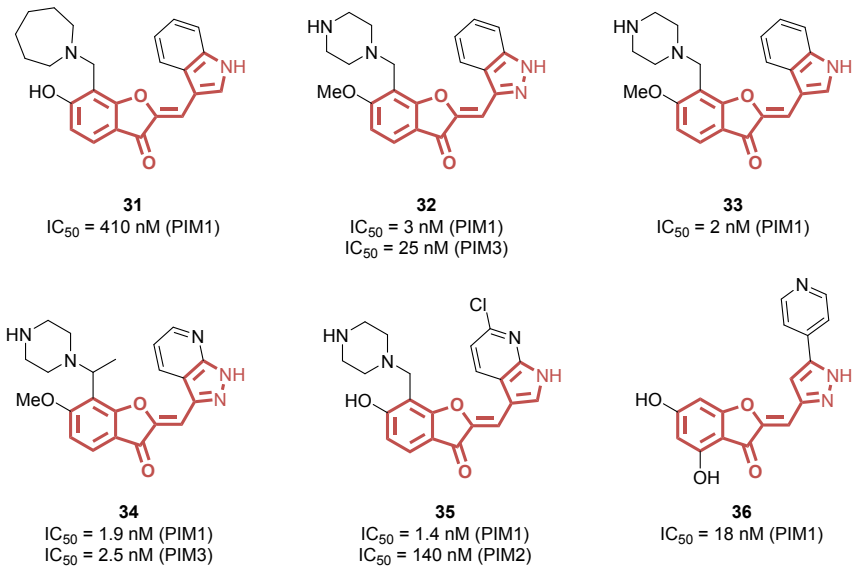

Figure 8. Structures and activities of PIM inhibitors.

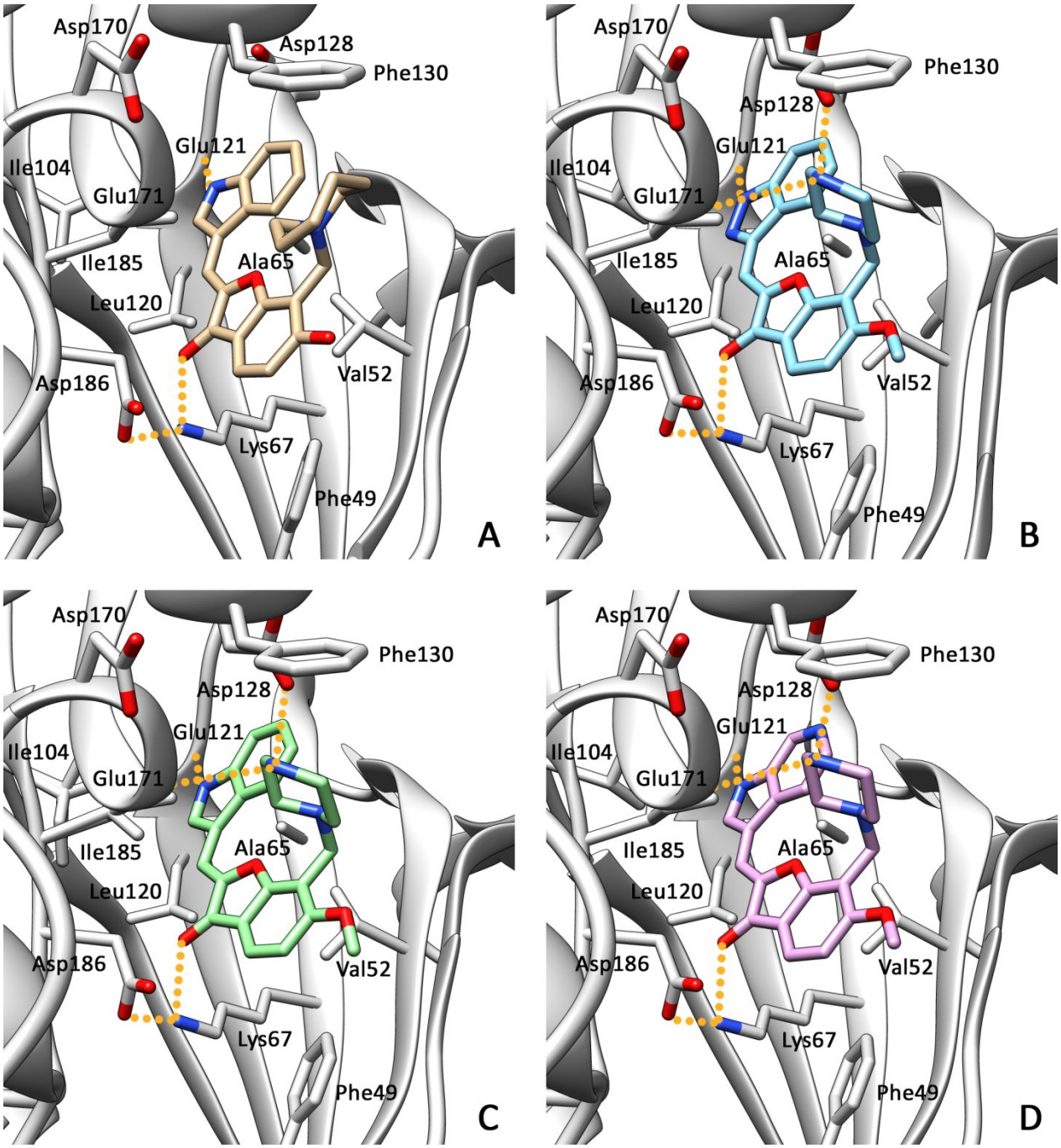

Figure 9. Compared crystal structures of **31** (A, gold, PDB code 3UMX), **32** (B, cyan, PDB code 3UMW), **33** (C, green, PDB code 5VUC) and its 6-azaindole derivative (D, pink, PDB code 5VUA) in complex with PIM1.

Targeting of other kinases, cancer-related proteins and pathways. Hemiindigoid derivatives were also associated with sporadic hit discovery, targeting kinases or other proteins and signaling pathways linked to cancer. In the Wnt pathway, the protein-protein interaction between the Frizzled 7 receptor and the PDZ subdomain of Dishevelled protein (Dvl) could contribute significantly to tumorigenesis.[55] Thus, compound **37** (Figure 10) was identified among eighteen other potential inhibitors from a 7-million structure virtual screening. Evaluated through SPR analysis, **37** was the most promising candidate for inhibiting the interaction (K_d = 11.2 μM).[56] Another target, retinoic acid receptor (RAR) was successfully modulated in the treatment of acute promyelocytic leukaemia.[57] Therefore, efforts were undertaken for developing active ligands for anti-cancer therapy. An adamantyl aurone derivative, **38**, was discovered among other flavonoids as a RARα antagonist, with an IC_{50} value of 4.42 μM. However, the selectivity of compound **38** for RARα was not assessed, although it constitutes a crucial indicator of its potential as anticancer agent.[58] For kinases, protein phosphorylation is a crucial process for cellular activities, that is known to be deregulated in cancer and linked to protein mutations, and thus these enzymes are often considered as relevant targets for cancer therapy, and several of them included hemiindigoids in their respective inhibitor portfolio. Compound **39** was discovered as a potent allosteric inhibitor of Akt, a kinase involved in the regulation of p53 activation in several cancers, with an IC_{50} value of 207 nM.[59] This aurone derivative demonstrated anti-proliferative and anti-metastatic effects *in vivo* against lung cancer models, and was thus further chemically modulated for affording **40**, a close analogue with enhanced properties. Compound **40** especially showed an improved inhibition of isolated Akt (IC_{50} = 66 nM) and was associated with an extension of the pre-G_0/G_1 cell-cycle phase in HL-60 leukemia cells and a pro-apoptosis effect.[60] Compound **41** was identified as a submicromolar inhibitor (IC_{50} = 0.735 μM) of Aurora B kinase (AURKB), an enzyme overexpressed in cancer cells and involved in mitosis and tumorigenesis. Exhibiting a good

selectivity for AURKB among a panel of kinases, **41** managed to target the enzyme in a cellular context, as attested by the observed accumulation of cancer cells in the G_2/M phase, and induced a global significant reduction of a human liver tumor weight *in vivo*.[61] In addition, aurone compounds **42** and **43** emerged from virtual screenings conducted respectively against CK2 and c-KIT, two protein kinases involved in cancer. In each case these "hits" are active at the low micromolar level, with an IC_{50} value of 6.0 μM for **42** against CK2 (a crystal structure of the **42**–CK2 complex is depicted in Figure 11, corresponding to PDB code 3WIL),[62] and IC_{50} values of 15.6 μM and 1.4 μM for **43** against WT and D816V mutant c-KIT kinases, respectively.[63] A further exploration of anti-CK2 properties of aurones afforded numerous compounds with nanomolar activities, with a clear beneficial effect of substituents at position 3'. Compound **44** was one of the most active aurones of the series (IC_{50} = 3.3 nM).[64] Altogether, these studies constitute promising starting points for further modulation endeavors. Besides kinases, histone deacetylases (HDACs) are also widely associated with cancer development. A series of aurones, tested against HDAC 1, 2 and 6, afforded compound **42** as the most promising compound with moderate micromolar potency (IC_{50} = 5.1–27 μM), making this molecule a potential anticancer multitarget agent.[65] These results were contested by another study which hypothesized a false-positive result caused by fluorescence interferences during the test.[66] However, aureusidin (Figure 2), already identified by Zwick *et al.*, was confirmed to induced HDAC inhibition in a more recent phytochemical work. Aureusidin was especially found as an efficient inhibitor of HDAC4 (K_i = 0.80 μM), but delivered far less activity against other subtypes (K_i = 1.66–4.55 μM against HDAC 2, 7, 8).[67] A set of interactions was predicted through molecular docking with the zinc via the catechol group, and with His158, Gly330 and Pro298. A small series of aurones was also evaluated against a class III HDAC, sirtuin 1 (SIRT-1), and yielded compound **38** as the best inhibitor (IC_{50} = 1 μM).[68] Another enzyme, tyrosyl-DNA phosphodiesterase (TDP1), known for its capacity to repair DNA lesions induced by anticancer

drugs, was targeted by extended aurone derivatives. Compound **46** combined a good activity (IC_{50} = 63 nM against TDP1) with a high selectivity index and a sensitizer profile for topotecan cytotoxic action in A-549 and HEK-293 cell lines.[69] Finally, the targeting of G-quadruplex DNA has recently emerged as a new approach for anticancer agent development. A small series of indanones with indole-based B-rings was proposed. Compound **47** appeared as particularly interesting, as it provided a high level of stabilization for oncogene-related G-quadruplex topologies ($\Delta T_{1/2}$ = 12.4–24.3 °C for c-myc, c-kit1 and c-kit2) while not targeting telomeric quadruplex ($\Delta T_{1/2}$ = –0.4 °C) and classical duplex DNA ($\Delta T_{1/2}$ = 2.8 °C).[70] Such a specificity appears as mandatory for the development of anticancer G-quadruplex ligands that would not trigger genomic instability.

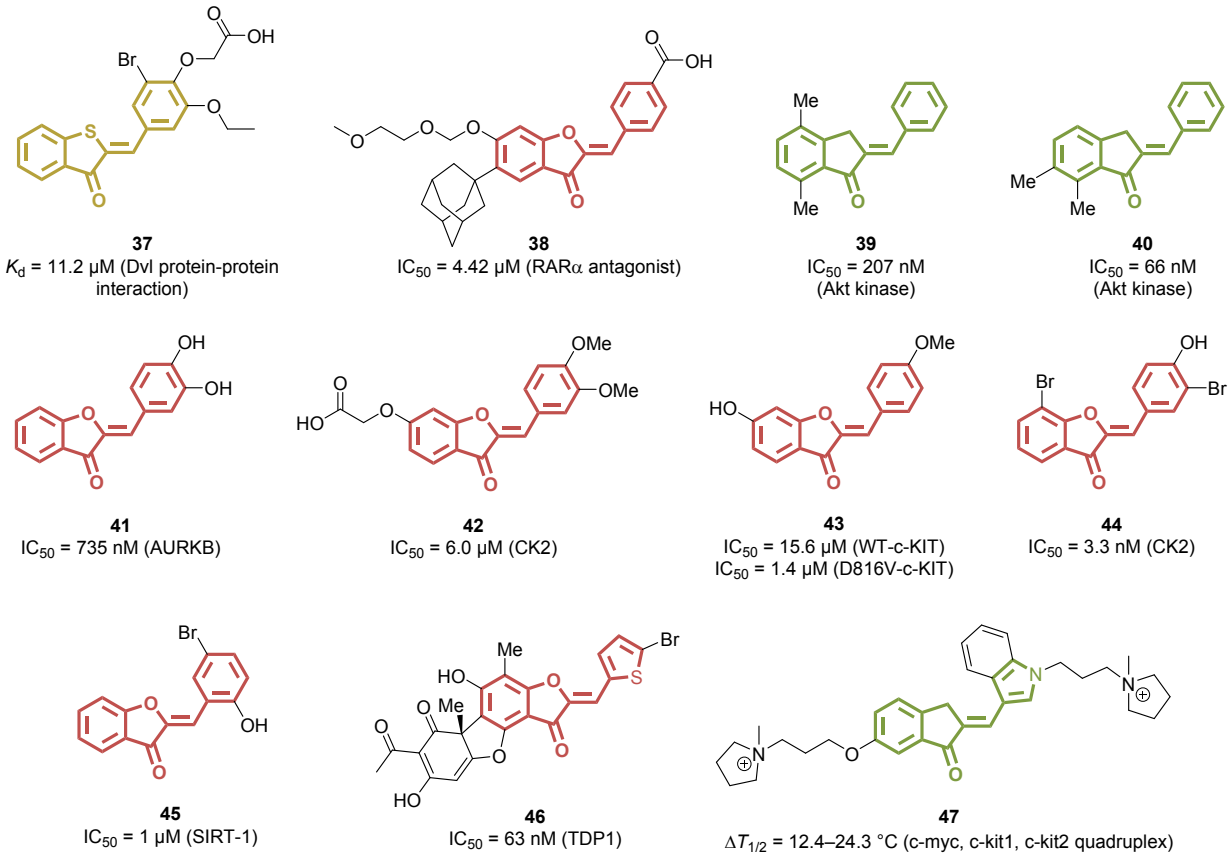

Figure 10. Structures and activities of inhibitors of other cancer-related targets.

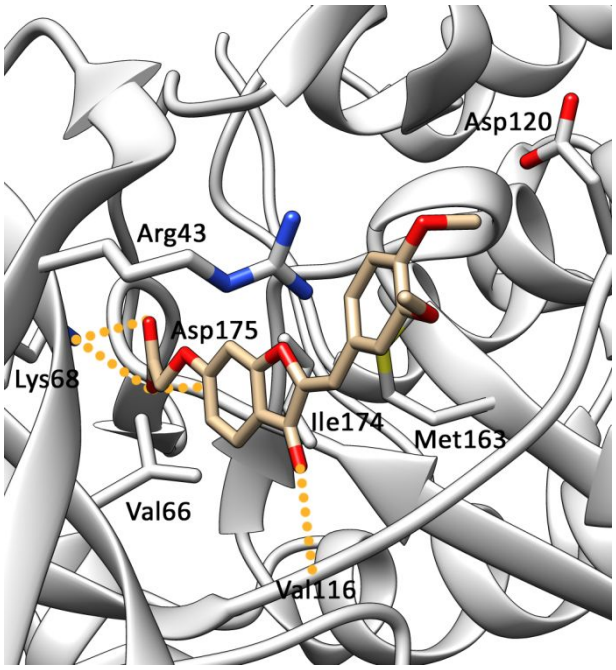

Figure 11. Crystal structure of **42** in complex with CK2 (PDB code 3WIL).

Screenings for cytotoxic and antiproliferative activities. Besides the specific targeting of a key process or a biomolecule involved in oncogenicity or cancer progression, numerous pharmacochemical or phytochemical studies relied only on basic antiproliferative or cytotoxicity assays, often involving the widely used MTT dye, with mixed results. Several articles reported hemiindigoids (especially aurones and indanones) with very limited anticancer potential, yielding low activity both in antiproliferative and cytotoxicity experiments (IC_{50} >10 μM in all cases). However, some compounds were found as micromolar or submicromolar cytotoxic or antiproliferative agents. For example, a pharmacomodulation effort around 3'-substituted indanones afforded compound **48** (Figure 12) as the most active analogue in a cytotoxicity assay, but with prohibitive action against normal cells as well, leading to a very low selectivity index shared by all the derivatives of the series.[71–74] A similar lack of selectivity was recorded regarding ferrocene derivatives.[75] The indanone scaffold, associated with an heterocyclic B-ring, also

provided a series of extended cytotoxic compounds in the micromolar range, such as compound **49**, which showed IC_{50} values between 0.23 and 2.89 μM against the growth of a panel of sixty cancer cell lines.[76] Disparate results were also reported through recent phytochemistry works that led to the isolation of new aurone structures from plants. Besides moderate activities recorded from classical polyhydroxyaurones, compound **50** and its 4'-prenylated analogue showed low micromolar values in some cases (IC_{50} = 3.4 μM against NB4 cells and 3.5 μM against SH-SY5Y cells, respectively).[77,78] The isoprenylated aurone **51**, extracted from *Rosa damascena*, showed IC_{50} values in the same range in a cytotoxicity assay (IC_{50} = 3.4 μM and 4.8 μM against SHS-SY5Y and NB4 cell lines, respectively).[79] Unsurprisingly, linking an aurone derivative to the well-known antimitotic compound podophyllotoxin boosted the cytotoxicity of the resulting hybrid agents, especially for **52** (IC_{50} = 0.10–0.97 μM against MCF-7, A549, DU-145 and MDA MB-231 cells). The aurone scaffold was found to contribute to the activity however, as demonstrated by the results obtained with podophyllotoxin analogue etoposide (IC_{50} = 1.9–3.1 μM in the same conditions).[80] Antiproliferative assays also led to promising results in some cases. Furanoaurone **53** was evaluated against sixty cancer cell lines and afforded a median IC_{50} of 4.1 μM.[81] A series of 10-hydroxyindanones with various B-rings gave inhibition values in the same order of magnitude, with compound **54** reaching the low micromolar range (IC_{50} = 2.5 μM against U-251 cells). The low pro-apoptotic action of this compound suggests a different mechanism that was not unraveled.[82] Finally, the 7-acetoxyaurone **55** was the only compound with submicromolar potency against PC-3 prostate cancer cells (IC_{50} = 0.74 μM).[83]

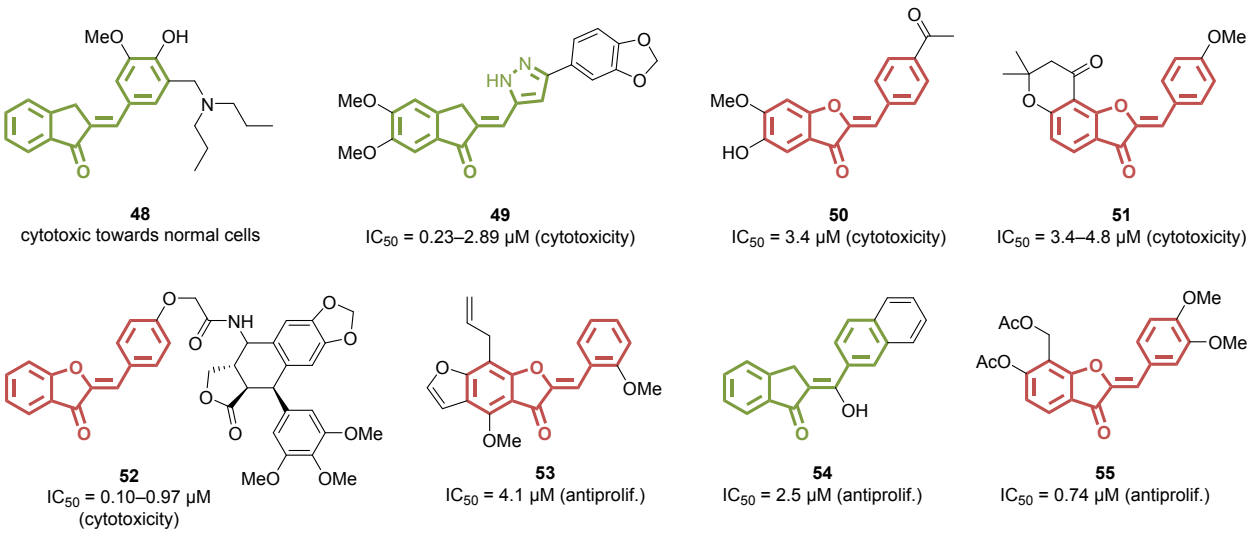

Figure 12. Structures and activities of cytotoxic and antiproliferative compounds.

Neurochemical activities.

Inhibition of monoamine oxidases (MAO-A and MAO-B). Monoamine oxidases (MAO) are responsible for the oxidation of various neurotransmitters, such as dopamine or 5-hydroxytryptamine. In the AD context, MAO are involved in the neurodegeneration process via oxidative stress and Aβ indirect production, and MAO inhibitors have shown beneficial effect on cognitive function for AD patients. Selective anti-MAO agents are thus needed, and hemiindigoids have displayed promising profiles. 4'-Dialkylamino indanones were first identified through a multitarget study involving the development of agents with both MAO inhibition, anti-aggregation, antioxidant and metal chelation properties. In this context, only low micromolar inhibitors were discovered. Compound **56** (Figure 13) shared a very similar profile with analogues bearing variously substituted 4'-amino substituents (IC_{50} = 35.2–41 μM against MAO-A and 7.5-10.9 μM against MAO-B for **56** and its *N*-dimethyl, *N*-diethyl and *N*-methylethyl derivatives), indicating a

good tolerance to alkyl groups length in that position. Replacing the 5-hydroxy group of **56** by a methoxy led to a complete loss of anti-MAO-A activity, but did not significantly change the anti-MAO-B potential (IC_{50} = 19 μM).[84] The study of a small series of aurones against MAO-A and MAO-B afforded results similarly advocating for a beneficial effect of a *N*-dialkyl group at position 4'. Indeed, while interesting values were obtained for a 4'-chloro analogue, the best results were provided by **57** and, to a lesser extent, by its 6-hydroxy derivative (IC_{50} = 99 nM *vs.* 240 nM against MAO-B, and 270 nM *vs.* 980 nM against MAO-A, respectively).[85] A diversification of the 4-dialkylamino group yielded more active analogues, reminiscently of the previous work involving indanones. *N*-Methylethyl compound **58** reached an IC_{50} of 28 nM against MAO-A (IC_{50} = 810 μM against MAO-B), a value significantly different from other tested dialkylamino substituents, including pyrrolidine, piperidine, morpholine and piperazine moieties. Interestingly, a 6-methoxy derivative bearing a 4'-piperidino group provided the better inhibition of MAO-B, an observation relevant with the previously described tolerance for an additional methyl group at this position in the indanone series.[86] However, the presence of a 4'-dialkylamino group did not appear as mandatory for anti-MAO activity. Even simple aurones, such as naturally occurring sulfuretin and hispidol (Figure 2), managed to potently inhibit the action of MAO-A (IC_{50} = 4.16 μM vs. 0.26 μM). The latter was also identified as a low micromolar inhibitor of MAO-B (IC_{50} = 2.5 μM).[87] Other B-substituted aurones mostly failed to significantly improve MAO-A and MAO-B inhibition potency, but some individual compounds were interesting for their ability to target both enzymes. Anthracenyl derivative **59** (K_i = 0.11 μM and 0.20 μM against MAO-A and MAO-B, respectively)[88] and furanyl indanone **60** (IC_{50} = 0.18 μM and 0.04 μM against MAO-A and MAO-B, respectively)[89] were overall the best anti-MAO agents among them. Modulation efforts around the indanone scaffold provided another series of compounds variously substituted at the B-ring. If the indanone counterpart of hispidol was less active against MAO-A (IC_{50} = 1.67 μM), several

analogues reached inhibition values below 200 nM. In addition, compound **61**, among others, showed an impressive effect on MAO-B inhibition (IC_{50} = 5 nM) together with a good MAO-B *vs.* MAO-A selectivity (>600-fold ratio between the measured IC_{50} values).[90] A further functionalization of substituents at the A- and B-rings of the indanone scaffold led to three extended molecules, without a clear benefit both in terms of anti-MAO-B inhibition and selectivity ratio however. Compound **62** was found as the most promising ligand of the series (IC_{50} = 262 nM against MAO-B, selectivity ratio >36).[91] A ratio of 180 was reached by hemithioindigo **63** (IC_{50} = 0.35 μM against MAO-B, 63 μM against MAO-A), the best value among a series of 10-hydroxy derivatives.[92] A recent study focusing on the B-ring modulation of 5,6-dimethoxyindanones did not afford more active molecules against MAO-B, even if compound **64** displayed an exquisite selectivity for the enzyme over MAO-A (IC_{50} = 0.02 μM vs. 58 μM, respectively, a selectivity ratio >2500), eventually highlighting once more the beneficial effect of 4'-amino derivatives.[93] However, the higher selectivity was obtained with indolaurone **65**, with a ratio >38,000. The molecule was one of the best known hemiindigoid inhibitor of MAO-B (IC_{50} = 2.6 nM) while being completely inactive against MAO-A (IC_{50} >100 μM).[94]

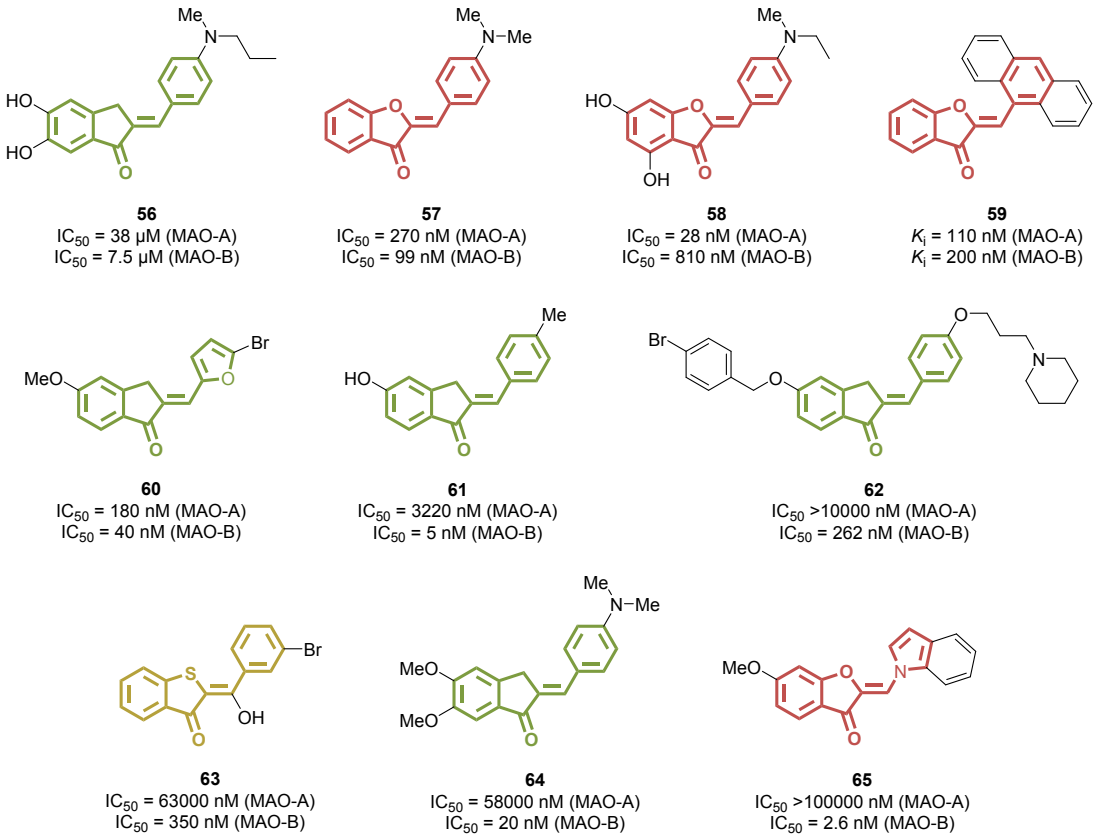

Figure 13. Structures and activities of MAO inhibitors.

Inhibition of cholinesterases (AChE and BuChE). Cholinesterases catalyze the hydrolysis of cholinergic neurotransmitters, assuring a crucial role for cholinergic neurons deactivation and various neurological functions, such as memory or cognition. However, in the AD context, a depletion of cholinergic neurotransmitters occurs, and inhibitors of cholinesterases are able to mitigate the symptoms of the disease. A selective inhibition of acetylcholinesterase (AChE) or butyrylcholinesterase (BuChE) is often required, depending on the stage of AD progression. Thus, two drugs were put on the market, including the well-known donepezil (**66**, Figure 14), whose structure is closely related to hemiindigoids. Starting from donepezil, a first study focused in 2012 on the modulation of the A-ring with the introduction of various alkylpiperidine substituents and the swapping of the initial piperidinyl fragment of donepezil with aromatic groups, eventually

affording indanones. Compound **67** (Figure 14) was found as the most potent AChE inhibitor, more efficient than the parent compound donepezil in *in vitro* assays (IC_{50} = 1.8 nM), with a good selectivity (IC_{50} = 9.5 μM against BuChE, a >5,000 ratio). Substituting the nitrogen atom afforded a series of benzylpyridinium derivatives, reminiscently of the donepezil structure. Compound **68** especially shared a similar profile than **67** (IC_{50} = 1.9 nM and AChE-vs.-BuChE selectivity ratio >5,000), with a very high activity recorded against human AChE (IC_{50} = 0.8 nM).[95] Transpositions into an aurone scaffold led to less active compounds with decreased selectivity, as witnessed by a direct comparison between compounds **69** (IC_{50} = 52 nM and 1,620 nM against AChE and BuChE, respectively) and **68**.[96] Introducing an extra carbonyl linker between the pyridinium moiety and the phenyl ring only produced far less active molecules, in the micromolar range.[97] Replacing the pyridinyl ring of the indanone scaffold by a phenyl counterpart overall maintained the inhibition potency (IC_{50} = 9.1 nM against AChE), but modifying the alkyl linker length or the nature of the amino group at position 6 of the indanone scaffold led to an activity drop.[98] These observations were confirmed by another study, which thus focused on the modification of the B-ring of indanones. Various amino substituents were introduced at position 4', leading to activities in the low nanomolar range, but with no clear improvement in terms of anti-AChE effect or AChE-*vs*.-BuChE selectivity. The most promising compounds bore NEt_2, NMePr and NPr_2 groups, showing IC_{50} values in the 15–20 nM range against eeAChE, together with 75–125 selectivity ratios. Assays involving human AChE resulted in an activity drop to IC_{50} = 400–1,000 nM however.[99] Moving the alkylpiperidine moiety at position 6 of an aurone series allowed to partially retain the AChE inhibition potency. Only few compounds were found as submicromolar inhibitors. Among them, compound **70** and its alkylpyrrolidine analogue provided the best measured effects (IC_{50} = 0.40 μM and 0.75 μM respectively). Again, introducing a $(CH_2)_3$ linker was overall slightly detrimental.[100] Actually, the position of the alkylamino group seemed to exert only a limited impact

on the activity. A further study proposed to compare several aurone series, bearing the alkylamino group either at position 6 or 4'. While the latter substitution afforded the best compounds, such as **71** (IC_{50} = 0.16 μM and 7.9 μM against AChE and BuChE, respectively), the inhibition values did not differ greatly from the 6-substituted analogues, which provided results in the same range than **70**.[101] Similarly, swapping to an indanone scaffold did not cause a significant change in the inhibition potency. As an illustration, compound **72**, which resembles to a reverse indanone-based **70**, gave nearly identical AChE inhibition values (IC_{50} = 0.3 μM).[102] However, shortening the linker between the B-ring and the piperidine moiety resulted in the production of aurone **73**, with a far better AChE inhibition efficacy (IC_{50} = 8.8 nM against eeAChE, 37 nM against the human enzyme), a remarkable exception among several other amino analogues which provided little or no improvement of the previously described activities.[103] Another series of 4'-substituted indanones was first reported in 2016, bearing this time amino groups directly bound to the B-ring. The results were overall underwhelming, with IC_{50} values around ten times higher than **71** and **72**.[104] However, a further study proposed to persevere with a series of indanones with directly bound extended piperazinyl substituents at position 4'. The other amino group of these piperazines was systematically functionalized with aromatic substituents, yielding significantly longer compounds with a far more promising activity. Analogue **74**, bearing a terminal pyrimidine group, reached an IC_{50} value of 25 nM against AChE (IC_{50} = 2.43 μM against BuChE, a ~100 ratio).[105] Positively charged piperazinium derivatives were recently reported, leading to a globally weaker inhibition effect against AChE, but with a very variable action against BuChE. If compound **75** displayed a similar level of activity against AChE and BuChE (IC_{50} = 0.32 μM and 0.43 μM, respectively), the allylpiperazinium analogue showed a far greater gap between IC_{50} values (IC_{50} = 0.43 μM against AChE vs. 25 μM against BuChE, a ~60 ratio). Hence, these results demonstrated that this series of compounds enables a fine-tuned management of the AChE-*vs*.-BuChE selectivity, depending on

the desired applications.[106] Finally, sporadic studies reported hemiindigoid analogues as AChE/BuChE inhibitors. If the aurone series of Mughal et al. was almost inactive,[107] the 2'-(2-aminoquinoline)indanone **76** was associated with an inhibition value in the nanomolar range (IC_{50} = 15 nM against AChE), with a predicted high ability to cross the blood-brain barrier.[108] More recently, indanones bearing phenylcarbamate groups at position 3' were evaluated, yielded inhibitors with reversed selectivity, such as compound **77** (IC_{50} = 21 µM *vs.* 0.31 µM against AChE and BuChE, respectively, a selectivity ratio of ~70).[109]

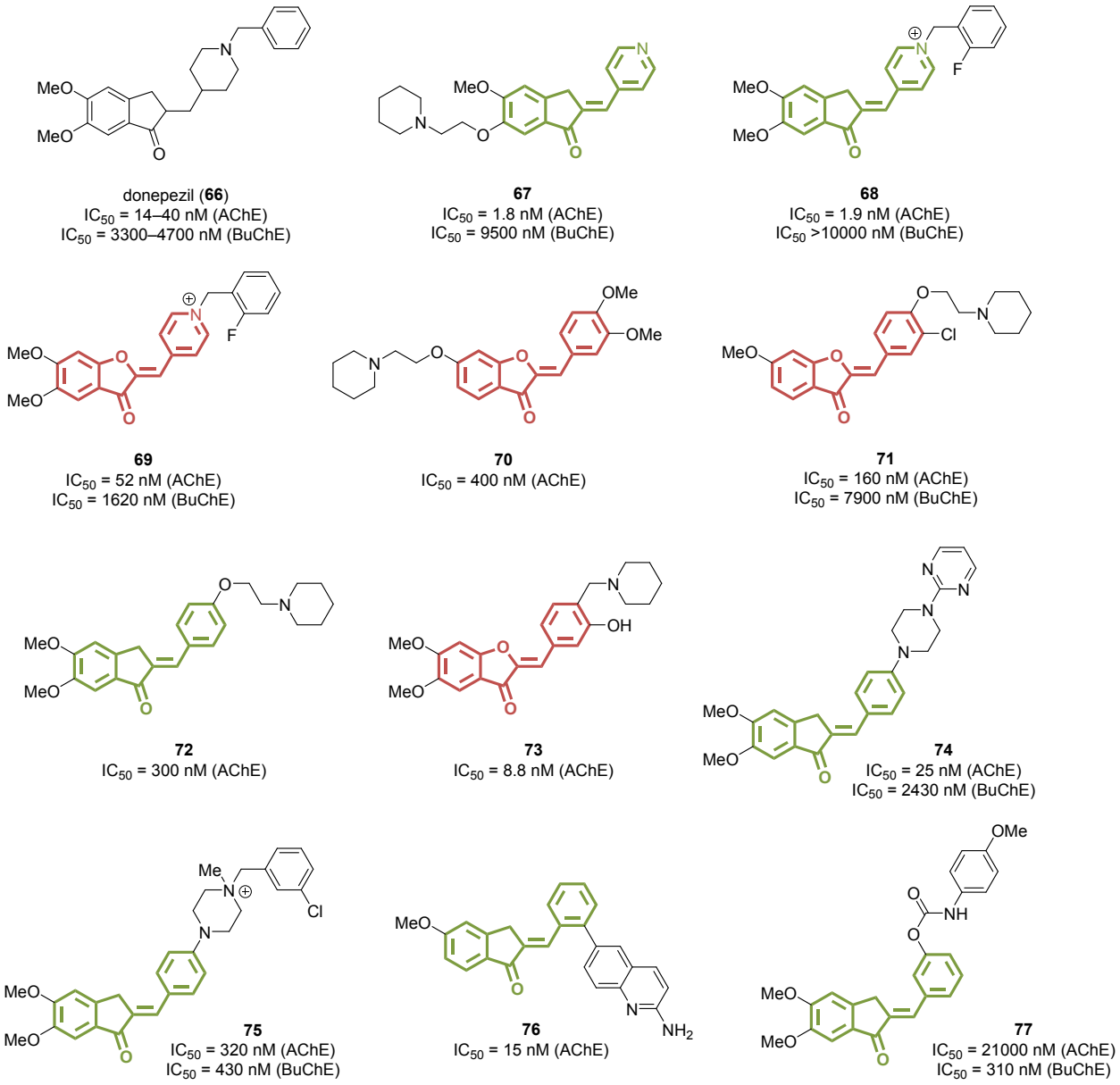

Figure 14. Structures and activities of AChE and BuChE inhibitors.

Activities related to Aβ, tau and α-synuclein peptides. Neurological amyloid diseases are characterized by the aggregation of particular proteins into the brain, especially Aβ and tau peptides in Alzheimer's disease (AD) and α-synuclein in Parkinson's disease (PD). Indeed, these events lead to the formation of amyloid plaques and neurofibrillary tangles (NFTs) that provoke neuronal dysfunction and degeneration. Thus, anti-aggregation agents could reduce the progression of the

disease, and numerous studies are dedicated to the identification of new molecules of interest. A significant part of hemiindigoid-based compounds evaluated for their ability to prevent Aβ peptides aggregation originated from so-called multitarget studies. However, in most cases, they actually reported formerly identified anti-MAO and/or anti-ChE agents secondly tested for their aggregation inhibition properties. Thereby, many hemiindigoids from the literature only provided moderate to weak activity, with IC_{50} values higher than 10 μM or merely inhibition percentages at 20 or 25 μM, without further characterization. Several previously mentioned neurochemical agents fall into this category, including **56**, **58**, **64** (Figure 13), **73**, **74** or **77** (Figure 14).[84,86,93,99,103,105,109] However, a more active analogue was discovered by Wang *et al*. Indeed, the 4'-nitro analogue of **64**, compound **78** (Figure 15), displayed a higher potency for self-induced $Aβ_{1–42}$ aggregation inhibition (IC_{50} = 1.8 μM), while retaining the anti-MAO-B profile already observed in the series (IC_{50} = 0.03 μM). Interestingly, **78** was also able to moderately induce the disaggregation of Aβ fibrils (IC_{50} = 7.9 μM).[93] A survey involving many polyhydroxylated flavonoids identified the aurone maritimetin (Figure 2) as the most potent compound against Aβ aggregation in a Thioflavin T assay (IC_{50} = 2.7 μM). However, maritimetin showed actually a weak action against fibrils formation in electron microscopy experiments.[110] As the Aβ peptides result from a sequential cleavage of APP by β-site APP cleaving enzyme 1 (BACE1), this enzyme is also a Aβ-related target of interest for AD treatments. A first indanone series provided extended BACE1 inhibitor **79** as the lead compound, with only micromolar activity however (IC_{50} = 2.5 μM).[111] The further study by Gabr *et al.*, which afforded compound **76** (Figure 14) as an efficient inhibitor of AChE, revealed the nanomolar potency of the molecule against BACE1 as well (IC_{50} = 13.1 nM).[108] The impact of hemiindigoids on tau peptide aggregation was far less studied, but a series of aurones showed promising results. Several polyhydroxylated derivatives still inhibited more than 50% of the

aggregation of AcPHF6, a model of tau, at a concentration of 1 μM. Aureusidin (Figure 2) was especially found as one of the most promising molecules (62% inhibition of AcPHF6 aggregation at 1 μM), able to prevent fiber formation and elongation through atomic force microscopy analyses.[112] A further, recent study confirmed the general potential of hemiindigoids by identifying indanone-based inhibitors of AcPHF6. The indanone bracteatin (Figure 2) counterpart especially led to a ~90% inhibition of fiber formation at 10 μM.[113] In addition, compounds **80** and **81** were found as potent GSK3β inhibitors (IC_{50} = 310 nM and 450 nM, respectively), a kinase involved in tau hyperphosphorylation in AD pathological context.[114,115] Besides, the detection of β-amyloid plaques and neurofibrillary tangles, which compose the senile plaques that characterize AD from aggregated Aβ and tau peptides, is a crucial element for a diagnosis of the disease as early as possible. The hemiindigoid scaffolds allowed the development of such probes, revealing a very high affinity for their targets. Hence, radioiodinated hemiindigo compound **82** was found to bind both tau and Aβ aggregates with exquisite affinities (K_i = 17 nM and 31 nM, respectively). *In vivo* experiments confirmed the potency of this molecule to successfully stain NFTs in specific brain sections related to AD.[116] The scaffold hopping into indanones retained partially the activity: the indanone counterpart of **82** showed a K_i of 240 nM for brain homogenates from an AD patient. However, the introduction of the ^{135}I substituent at position 5 yielded compound **83**, which displayed a better affinity (K_i = 100 nM).[117] The further insertion of a methoxy group at position 6 improved the affinity values to low nanomolar levels, as observed for compound **84** (K_i = 12 nM against $Aβ_{1–42}$ and 29 nM against AD patients brain homogenates). The radiolabeled molecule was found to stain β-amyloid plaques, and showed enhanced uptake in brain compared to previously described indanones.[118] Indanones also succeeded to label α-synuclein fibrils from PD brain tissues. Compound **85** especially showed a very good affinity (K_D = 39 nM) while being fairly

selective *versus* Aβ fibrils (K_D = 390 nM, a ten-fold ratio).[119] No data were reported regarding the activity of hemiindigoids against other amyloid-type proteins, such as prions, human islet amyloid polypeptide or systemic amyloid A. Hence, the evaluation of their aggregation inhibition properties against these targets could provide new treatments for various diseases.

Neuroprotection and other neurochemical effects. Several naturally occurring aurones were identified as neuroprotective agents through various degeneration and neurotoxicity models. Aureusidin (Figure 2) was found among other flavonoids as an inhibitor of CDK5/p25 (IC_{50} = 3.5 μM), a deregulated variation of physiological p35 or p39-regulated CDK5, involved in abnormal phosphorylation events related to neuronal cell death in the frame of AD.[120] This activity could be responsible for the attenuation of glutamate-induced neurotoxicity measured in HT22 neuronal cells, moderate at micromolar concentrations (EC_{50} = 11.9 μM) but reaching 97% at 40 μM.[121] The analogue sulfuretin (Figure 2) also showed a significant effect on the same model, leading to a 93% improvement of cell viability at 10 μM, a potency shared with other flavonoids, such as flavanones and chalcones. In addition, sulfuretin allowed a 1.8-fold attenuation of glutamate-induced ROS generation at 5 μM.[122] A further study provided an EC_{50} value of 3.5 μM against glutamate-induced HT22 cell death.[123] In addition, sulfuretin exerted neuroprotection effects by inhibiting 6-hydroxydopamine-induced neuronal cell death,[124] and by attenuating Aβ-induced neurotoxicity.[125] Through an activation of Akt/GSK3β and ERK signaling pathways, the compound also prevented MPP^+-induced neuronal cell death, highlighting a potential beneficial role in protection against PD.[126] Potent antioxidant properties could be partly responsible of this multiple neuroprotective action. Damaurone D (Figure 2) shared a favorable effect in MPP^+-induced neurotoxicity. In addition, it showed an attenuation of α-synuclein expression, accumulation and fibrillation, a promising profile for the development of an anti-PD agent.[127] Naturally occurring aurones **86**

(Figure 15) and *(Z)*-7,4'-dimethoxy-6-hydroxy-aurone-4-O-*β*-glucopyranoside also provided interesting results respectively on 6-hydroxydopamine-induced (IC_{50} = 2.9 µM)[128] and H_2O_2-induced neurotoxicity[129] models. The latter compound was further identified as an anxiolytic agent through an elevated plus maze test on rats. Finally, hispidol (Figure 2) was associated with antidepressant properties, as it allowed a dose-dependent decrease in immobility times in forced swimming and tail suspension tests performed on mice.[130]

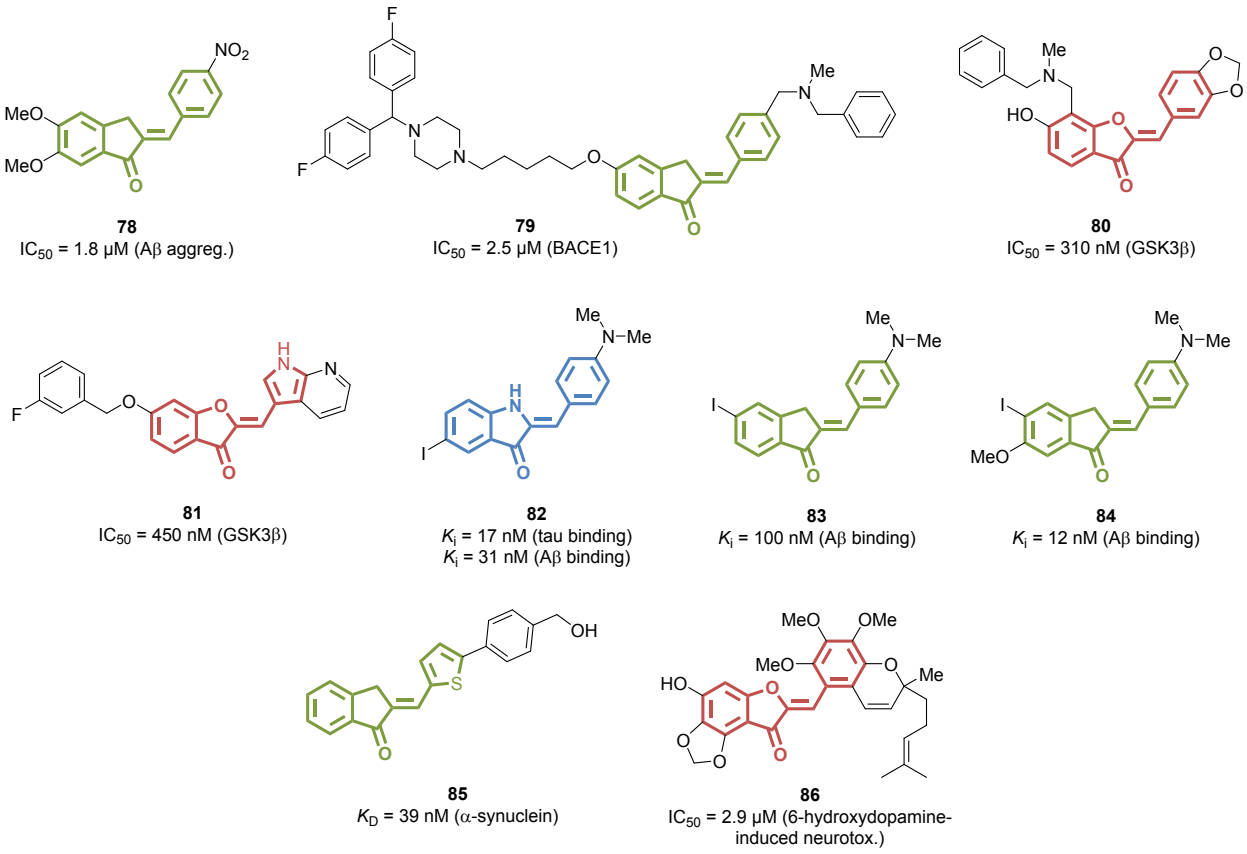

Figure 15. Structures and activities of compounds with various neurochemical activities.

Anti-infective activities.

Anti-bacterial activities. The growing concern of bacterial resistance has put back the quest for new anti-bacterial agents to the forefront of the pharmaceutical scene. As standard antibiotics chemical classes are progressively dismissed, the development of new scaffolds appears as a crucial need for treating bacterial infections in the next decades. Among these new chemical agents, several hemiindigoid-based series emerged. First, aurone derivatives with bicyclic B-rings were developed for their antibacterial activities. Quinoline-based analogues were especially investigated, and afforded compounds with weak effects. The *N*-allyl compound **87** (Figure 16) was identified as one of the most promising agents in a first study, exhibiting a MIC value of 33 μM against *Pseudomonas aeruginosa*, while being almost inactive against a panel of other Gram positive (*Staphylococcus aureus*, *Bacillus subtilis*, *Clostridium tetani*) and Gram negative (*Escherichia coli*, *Vibrio cholerae*) strains. The activities provided by the rest of the series were only marginal.[131] A second report focused on 2-chloroquinolin-3-yl derivatives. Again, most of the results obtained were underwhelming, even if some analogues showed a modest selective activity against *B. subtilis* over *S. aureus*.[132] Switching to bicyclic chromone B-rings afforded far more active agents. Especially, the dimethyl analogue **88** reached the low micromolar range against *P. aeruginosa* and *S. aureus*. The measured MIC value of 1.6 μM was notably lower than the MIC of ciprofloxacin and gentamicin.[133] Aurones with other various structures were also identified. The evaluation of a series of furoaurones against several Gram positive and Gram negative bacteria revealed a good potency of several derivatives. Compound **89** especially showed MIC values between 4.4 and 8.8 μM against *B. subtilis*, *S. aureus*, *E. coli* and *P. vulgaris* and could be an inhibitor of cyclooxygenase-II, according to docking studies.[134] Several studies only reported inhibition zones in mm, identifying compounds with structural diversity, such as **90**, which

displayed a similar result than ampicillin, but with no MIC values measured.[135] However, in all of these studies, no data regarding a potential general cytotoxicity was included, and the reported putative antibacterial compounds could actually be cytotoxic agents, as exemplified by the study of Tiwari *et al.* which showed both antibacterial activity and cytotoxic activity ferrocenyl aurone analogues.[75] Thus, a recent study examined the antibacterial activity of a series of substituted aurones, with a particular attention to their potential cytotoxic action. Among forty compounds, **91** was found as the most promising analogue with a specific activity against Gram positive strains, especially nisin-resistant *B. subtilis* (MIC of 3.9 μM), through a hypothesized alteration of the membrane. Surprisingly, **91** was also able to inhibit *Helicobacter pylori* and *Vibrio alginolyticus* selectively among other Gram negative bacteria (MIC of 15.6 and 3.9 μM, vs. >500 μM for thirteen other strains). The molecule did not exhibit any cytotoxic effect at these concentrations (IC_{50} = 190–340 μM against BEAS-2B and IMR-90 cells).[136] Aurones were also identified as antitubercular compounds in a high-throughput screening. Among a large diversity of chemical structures, three aurones emerged, including compound **92** which showed the best effect against *Mycobacterium tuberculosis* (IC_{90} = 4.8 μM) together with a low cytotoxicity (selectivity index of 17).[137] Further exploring the aurone and hemiindigo chemical spaces, Campaniço *et al.* discovered a series of compounds with very high activity against tuberculosis. Indeed, some *N*-acetyl hemiindigo analogues reached MIC_{90} and MIC_{99} values below 1 μM. Among them, compound **93** combined a good activity (MIC_{90} of 0.65 μM, MIC_{99} of 0.74 μM) with a low toxicity at these concentrations (CC_{50} = 19 μM against HEK293T cells). Several analogues were even able to inhibit multidrug-resistant and extensively drug-resistant clinical *M. tuberculosis* isolates.[138] The de novo design of a HtrA (High-temperature requirement A) inhibitor, a protease from *H. pylori* presumed to be a potential therapeutic target, finally afforded one hemithioindigo derivative, compound **94**, with a K_D value of 12 μM.[139]

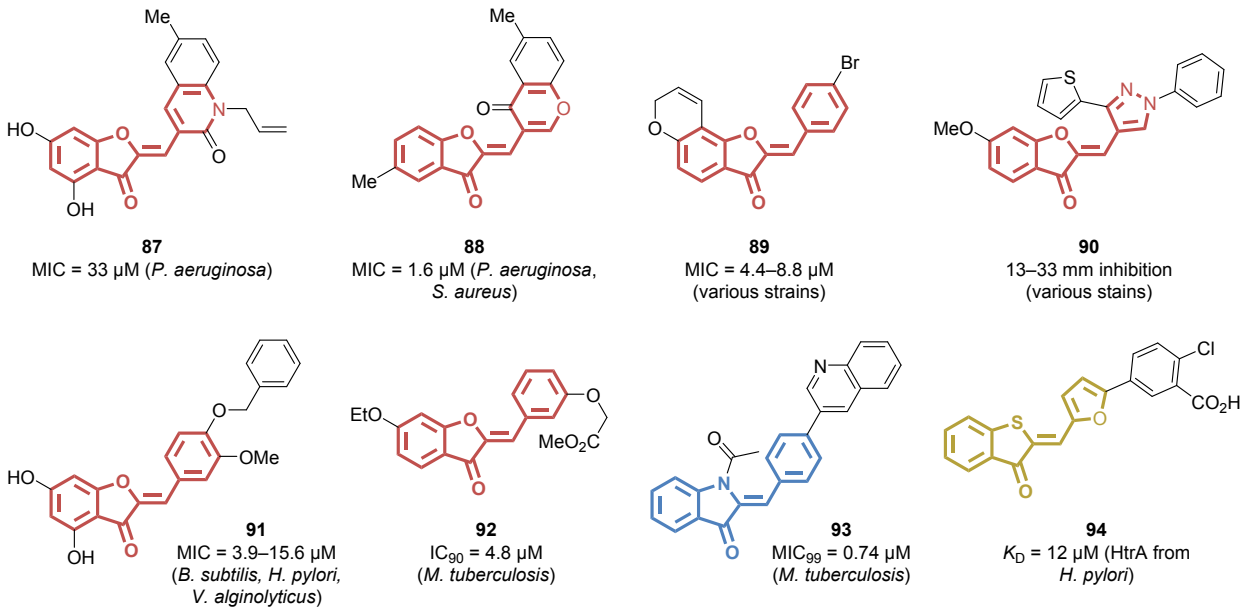

Figure 16. Structures and activities of anti-bacterial compounds.

Antifungal activities. In a similar way, pathogenic fungi are becoming increasingly resistant to widely used antifungals. The corresponding infections thus pose a serious threat to the global health, especially considering *Candida*, *Aspergillus*, *Pneumocystis* and *Cryptococcus* species, that cause more than 90% of fungi-related deaths. In the literature, a significant portion of antifungal results were produced through general antimicrobial screenings, performed preliminary against bacterial strains. Indeed, several hemiindigoid series already mentioned in the previous section yielded low to absent activities against a variety of fungus, especially *Candida albicans*, *Aspergillus niger* or *Fusarium oxysporum*.[131,132,136] However, some derivatives showed actual activity. Compound **88** (Figure 16) afforded MIC values of 14–17 μM against *A. niger* and *A. flavus*, and comparable results were obtained with the antifungal reference nystatin.[133] Compound **89** showed a weaker profile, with MIC values of 18–35 μM against *A. niger* and *C. albicans*,[134] and **90** inhibited *A. niger*, *F. oxysporum* and *Penicillum italicum* with promising inhibition zone values similar than griseofulvin.[135] However, several hemiindigoid molecules were discovered

through dedicated antifungal studies. A series of substituted aurones was evaluated against *Candida* species. Among several phenyl-based and heterocyclic B-rings, compounds **95** and **96** (Figure 17) were identified as the most potent inhibitors, with IC_{50} values between 10 µM and 18 µM against three species: *C. albicans*, *C. glabrata* and *C. tropicalis*. Compound **95** was able to prevent *C. albicans* biofilm formation at these concentrations.[140] Furanoindanones were also evaluated with various heterocyclic B-rings, but the MIC values obtained were globally underwhelming. One of the best compounds, **97**, inhibited *Rhizophus oryzae*, *Mucor mucido*, *A. niger* and *C. albicans* only at concentrations of 60–120 µM. The activities observed were far weaker than the reference fluconazole.[141] Several polyhydroxylated aurones were found to target specific RNA structures, the group II intron, absent in vertebrates but crucial for plants and fungi. A link was established between a high affinity for this RNA tertiary structure and an antifungal potency against *Candida parapsilosis*. Bracteatin (Figure 2) constituted the starting point of this study (K_i = 2.1 µM against the ai5γ intron and MIC of 53 µM), and compound **98** was identified as a potent analogue by removing phenol groups from the A-ring (K_i = 5.8 µM against the ai5γ intron and MIC of 30 µM). However, furan derivatives outside the hemiindigoid chemical space were found as more efficient both in terms of ai5γ intron targeting and antifungal activity.[142]

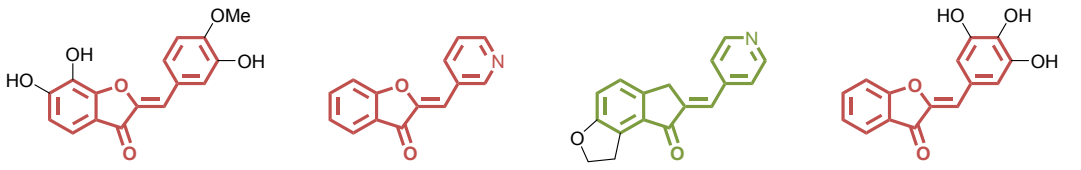

95
IC_{50} = 10–16 µM (*C. albicans, C. glabrata, C. tropicalis*)

96
IC_{50} = 10–18 µM (*C. albicans, C. glabrata, C. tropicalis*)

97
MIC = 60–120 µM (various stains)

98
K_i = 5.8 µM (ai5γ intron)
MIC = 30 µM (*C. parapsilosis*)

Figure 17. Structures and activities of antifungal compounds.

Anti-parasite activities. As parasitic diseases are responsible for almost one million of deaths annually (with almost one half being caused by *Plasmodium* species in low-income countries), the

quest for efficient and accessible anti-parasite compounds still appears as a sanitary emergency. In addition, many parasitic diseases are contained in tropical areas, and have been largely neglected by the pharmaceutical efforts of developed nations. Addressing these pathologies is an urgent need. Regarding hemiindigoids, most of the anti-parasite activities were reported against protozoan parasites, such as *Plasmodium*, *Leishmania* or *Trypanosoma* species. Hence, antimalarial aurones were first found, leading to a series of compounds with simple structure and activities in the micromolar range. If B-substituted derivatives were sometimes encouraging, compound **99** (Figure 18) was identified as the best inhibitor of the chloroquine-resistant *Plasmodium falciparum* W2 strain (IC_{50} = 1.18 μM), without any cytotoxicity measured in human cells (EC_{50} >100 μM against HEK293T cells). However, this IC_{50} value remained one order of magnitude higher than that of chloroquine.[143] Another series of various methoxy- or methyl-substituted aurones only produced inactive compounds, with the exception of two derivatives exhibiting IC_{50} values in the 10–20 μM range.[144] The transition to a hemiindigo scaffold was far more successful. The substitution of positions 3' and 4' yielded dozens of molecules with submicromolar activity against chloroquine-resistant *P. falciparum*. Compound **100** even reached the hundred nanomolar range (EC_{50} = 0.11 μM) with no toxicity reported against HEK293T cells (EC_{50} >100 μM). Interestingly, the positions 3' and 4' appeared as very tolerant for a wide variety of substituents, especially phenyl groups. The series was also active against *P. berghei* (EC_{50} = 0.81 μM for **100**). However, the intracyclic NH acetylation led to a dramatic drop of activity in all cases, highlighting the crucial role of the unsubstituted group.[145] QSAR studies were conducted in order to extract the crucial structural elements from the reported hemiindigoid series. Hence, the presence of bulky groups at positions 4 and/or 6 was pinpointed as beneficial, and overall the roles of electron-withdrawing substituents at the B-ring and of electron-donating groups at the A-ring were underlined, a statement partially consistent with the aforementioned series, including **99** and **100**.[146] A further study focusing on

hemiindigos endorsed the introduction of a bulky substituent at the *meta* position of the B-ring, and proposed four new structures derived from **100**, with heterocyclic 3'-aryl groups.[147] Antileshmanial aurones were also identified. If several methyl- and methoxy-substituted compounds only afforded weak inhibitors against *Leishmania donovani* (IC_{50} = 10–50 μM for the most active derivatives),[144] a set of molecules with closely-related structures gave more promising results against *L. infantum*. Indeed, some analogues reached micromolar values against intracellular amastigotes, especially compound **101** (IC_{50} = 1.3 μM) which in addition revealed a low cytotoxicity against THP1-differentiated macrophages, leading to a good selectivity index (57.5).[148] Aurones were also pinpointed for their ability to inhibit the ABC transporter ABCI4, responsible for the efflux of antimony, a first-line drug against leishmaniasis. Compound **102** was able to restore the susceptibility of a ABCI4-expressing *L. major* line to Sb^{III}, allowing to divide its EC_{50} value by 6, and to reach a similar level of activity than against a control *L. major* line without ABCI4. The parasites were sensitized even for control, although no significant cytotoxicity was recorded either on *L. major* (EC_{50} = 190 μM) or THP-1 cells (EC_{50} = 350 μM), indicating a probable intrinsic antiparasitic effect of **102**.[149] Finally, aurone **103** showed some activity against *Toxoplasma gondii* proliferation (IC_{50} = 10 μM) without causing cytotoxicity at this concentration.[150] The protozoan *Entamoeba histolytica* was also the target of an indanone derivative, that was identified through a virtual screening as a potential inhibitor of *E. histolytica* hexokinase 1, a crucial enzyme for glycolysis regulation. However, the compound was actually a weak inhibitor, with an IC_{50} value of 96 μM.[151] Hemiindigoid compounds were developed for other parasite species. Among them, *Schistosoma* worms are responsible for schistosomiasis, a neglected disease causing a high morbidity in Africa, South America and Asia. A natural aurone, isolated from a plant traditionally used in Chinese medicine, was evaluated against adult *S. japonicum* worms, but did not cause any worm mortality even at higher concentrations.[152] The introduction of a furane- and an indole-based

(compound **104**) B-ring on the aurone scaffold afforded two compounds with an EC_{50} of 34 µM against *S. mansoni* worms. **104** especially appeared as promising, due to its lack of general cytotoxicity against macrophages (CC_{50} >150 µM).[153] In addition, the thiophene counterpart **105** killed about 50% of *S. mansani* adult worms at a concentration of 25 µM, although no EC_{50} value was measured. The compound was still non-cytotoxic (CC_{50} >150 µM).[154] Another parasite causing a neglected disease, *Trypanosoma brucei*, was targeted by an indanone series, yielding compound **106** as the most potent derivative (IC_{50} = 0.55 µM) devoid of cytotoxicity (IC_{50} >100 µM against HeLa cells).[155]

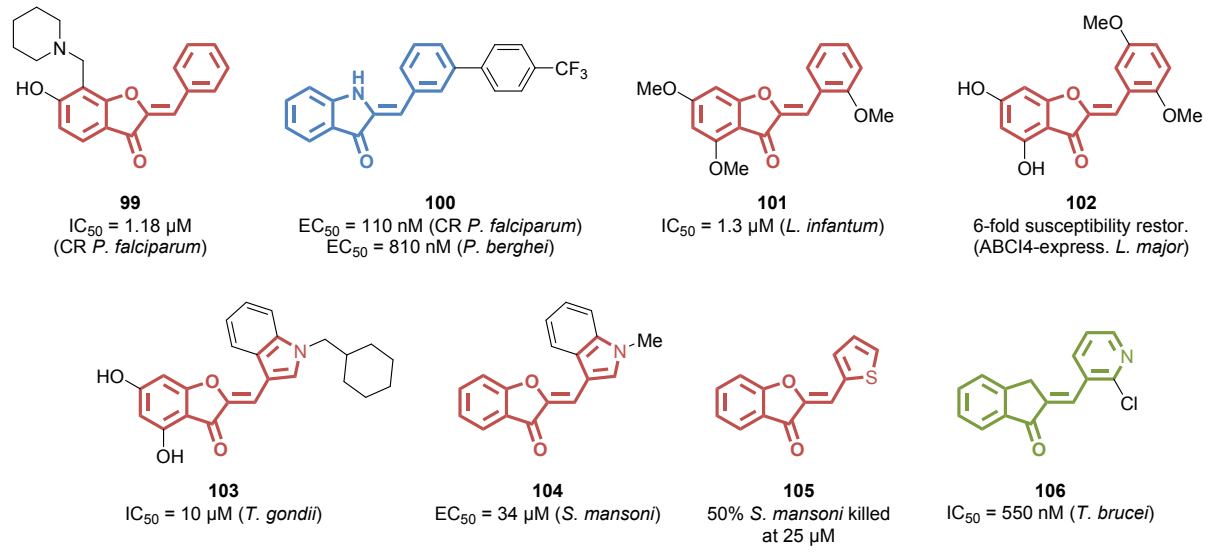

Figure 18. Structures and activities of anti-parasite compounds.

Antiviral activities. The recent (and still ongoing) COVID-19 pandemic has underlined the crucial importance of specific antiviral development, as the efficacy of vaccines globally appeared as suboptimal, an observation that also applies to some other viral infections. Indeed, new antiviral agents are still needed for a wide range of pathologies in order to reach a decent treatment response. In the hemiindigoid chemical space, aurone analogues were discovered as anti-influenza A virus (IAV) agents. First, derivatives of usnic acid were evaluated for their ability to inhibit the viral

reproduction. Among more than forty tested molecules, aurone-usnic acid hybrids were found as potent compounds, especially **107** (Figure 19) which was one of the best antiviral agents of the series (ED_{50} = 4.7 μM). The contribution of the aurone scaffold was clearly visible upon comparison with usnic acid itself (ED_{50} = 52 μM). However, it revealed a quite high level of cytotoxicity, leading to an insufficient selectivity index (8.3). The four aurones tested afforded similar results.[156] More classical aurones delivered far more efficient activities in a further study. Surprisingly, while initially developed for targeting IAV neuraminidase, the compounds exhibited only moderate action against the enzyme (IC_{50} = 37–45 μM) but managed to induce significant viral reduction at concentrations one thousand times lower (EC_{50} = 30–50 nM). Although less active than flavone counterparts, compound **108** provided a very potent profile by combining an exquisite anti-IAV activity (EC_{50} = 35 nM) with a good therapeutic index value of ~5000.[157] An additional study tried to retrieve IAV neuraminidase inhibitors from a docking-based virtual screening. The approach was overall successful, as several aurone analogues presented IC_{50} values below 50 nM in the series. Compound **109** was the most active aurone found, showing a higher affinity for IAV neuraminidase (IC_{50} = 20 nM) than the reference oseltamivir carboxylate (IC_{50} = 40 nM).[158] Some aurones were also tested in anti-HIV assays. First, Gao *et al.* performed an antiviral evaluation in their phytochemical report involving five natural aurone analogues. Among them, compound **50** (Figure 12) showed an interesting effect (EC_{50} = 2.4 μM) while being devoid of cytotoxicity at 200 μM, leading to a selectivity index >82. Maritimetin (Figure 2) was also moderately active (EC_{50} = 12 μM), but in the study the recorded values were globally far higher than the reference azidothymidine.[77] Variously substituted synthetic aurones showed very weak efficacy at inhibiting HIV-1 infection at 10 μM in another report, especially when compared with more active analogous chalcones and flavonols.[159] Regarding hepatitis viruses, a unique aurone compound was tested as an erythrocentaurin derivative against hepatitis B virus, with only

llimolar activity.[160] Other series of analogues tested against hepatitis C were more successful. lolaurones showed especially good activities against hepatitis C virus (HCV) RNA-dependent IA polymerase NS5B, reminiscently of a previous work.[15] Interestingly, the substitution of the lole part appeared as tolerant in terms of size and position, as most of the designed compounds l into the similar activity range (IC_{50} = 2.2–8 μM). Compound **110** was one of the best inhibitors NS5B, with an IC_{50} value of 2.3 μM.[161] In addition, dimeric aurones were developed, leading to :ent compounds with micromolar activity against HCV NS5B. Compound **111** showed a)mising profile (IC_{50} = 1.3 μM), and was associated with a probable binding at the palm pocket f the enzyme, as testified by mutagenesis experiments (an activity drop was recorded against the 5Q mutant). However, only low effects were seen in a J6/JFH1 cell infection model (EC_{50} = 200 l for **111**, 42 μM for the best compound).[162] A last study about the antiviral potential of aurones :used on several flavonoids from a phytochemical work. Among them, sulfuretin (Figure 2) was ınd as a very weak inhibitor of two fish viruses, infectious hematopoietic necrosis virus and viral norrhagic septicemia virus, with activity values in the hundred micromolar range.[163]

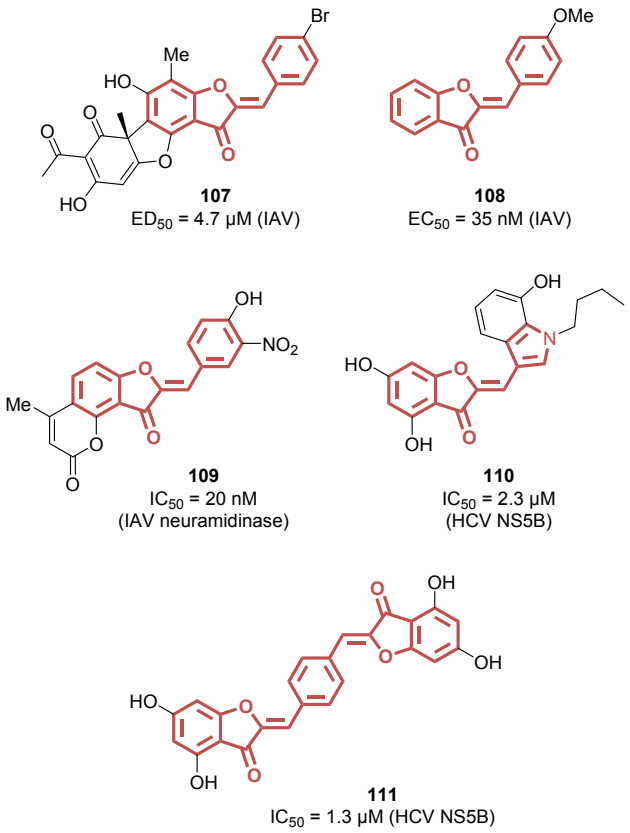

Figure 19. Structures and activities of antiviral compounds.

Anti-inflammatory and antioxidant activities.

Inflammation and oxidative stress from various sources are responsible for many chronic pathologies. In this context, the control of inflammation could be achieved through the suppression of pro-inflammatory cytokines production, such as tumor necrosis factor-alpha (TNF-α). The targeting of intracellular signaling pathways regulating cytokine expression appeared as a promising strategy. The nuclear factor kappa B (NF-κB) is directly involved in immune response and inflammation-related proteins regulation. A series of aurones managed to inhibit canonical NF-κB signaling by attenuating IκB kinase (IKK) activity, resulting in a lower TNF-α expression in

macrophages. In the case of aurone **112** (Figure 20), this expression was halved in presence of 40 μM of compound, and a concomitant reduction of the nitric oxide synthase (iNOS) level was observed (~30% at 50 μM).[164] A similar anti-inflammatory effect was recorded from aureusidin (Figure 2) at similar concentrations in a lipopolysaccharide (LPS)-induced mouse macrophage model, through inhibition of NF-κB nuclear translocation and activation of MAPKs- and ROS-dependent Nrf2/HO-1 signaling pathways.[165] Damaurone D (Figure 2) was also found as an inhibitor of the expression of LPS-stimulated pro-inflammatory enzymes iNOS and cyclooxygenase-2 (COX-2). A significant reduction was reached at concentrations of 10–20 μM. Although a series of analogues bearing various B-rings was synthesized and evaluated, **85** (Figure 15) remained the most potent derivative in the reduction of nitrite production in LPS-stimulated RAW 264.7 cells (IC_{50} = 4 μM vs. >5 μM).[166,167] An indanone series was investigated for their interleukin-5 (IL-5) inhibition properties. IL-5 is a cytokine produced by Th2 lymphocytes, involved in the immune and inflammatory response. Among the tested compounds, hydrogenated analogues without the exocyclic double bond were more promising, and analogues with a proper indanone scaffold were globally very weak inhibitors. Compound **113**, the best molecule among them, only showed 47% of IL-5 activity inhibition at 30 μM, in contrast to 100% inhibition for its reduced counterpart.[168] Direct enzymatic inhibition is another anti-inflammatory strategy. Indeed, numerous enzymes are involved in the inflammation process, especially in the arachidonic acid metabolism. A report especially focused on the inhibition of phospholipase A_2 (PLA2), cyclooxygenases (COXs) and lipoxygenases (LOXs) by various α,β-unsaturated carbonyls. Among them, three indanone derivatives exhibited moderate activities. Compound **114** especially displayed IC_{50} values of 37 μM, 2 μM and 19 μM against PLA2, COX-1 and COX-2, respectively, laying the foundations for promising multitarget anti-inflammatory molecule.[169] In addition, **114** was found as a potential immunosuppressive agent, able to inhibit polymorphonuclear neutrophils

cell movement (IC_{50} = 7 μM) and ROS production.[170] An enhanced ROS level is indeed a factor of inflammation. As the enzyme NADPH oxidase, which catalyzes the production of superoxide ions, plays a crucial role in the modulation of the macrophage ROS level, indanones were developed as potential inhibitors of NADPH oxidase. Good inhibition properties were recorded, resulting in lowered ROS levels in a LPS-induced inflammatory macrophage model, especially for compound **115** (IC_{50} = 1.33 μM).[171] Activities of hemiindigoid derivatives were also reported in specific pathological inflammatory contexts. Hispidol (Figure 2) was found as a promising agent against inflammatory bowel disease (IBD), a chronic gastrointestinal inflammatory disorder, by inhibiting TNF-α-induced adhesion of monocytes to colon epithelial cells (IC_{50} = 0.50 μM), TNF-α-induced ROS production and LPS-induced TNF-α expression (reduction of TNF-α to the level of the LPS-untreated control at 10 μM). Interestingly, hispidol caused a significant suppression of TNBS-induced rat colitis, an *in vivo* animal model of IBD, through oral administration of 30 mg/kg of hispidol. A dose of 300 mg/kg of the positive control sulfasalazine was required for reaching a similar effect.[172] Further developments provided compound **116**, which globally shared the potential of hispidol (IC_{50} = 2 μM for TNF-α-induced adhesion, and significant suppression of TNBS-induced rat colitis at 25 mg/kg).[173] Indanone **117** managed to inhibit the inflammatory response in the frame of acute lung injury both *in vitro* and *in vivo*, by interfering with myeloid differentiation 2 (MD2), an attractive target involved in the production of pro-inflammatory cytokines.[174] Aurone glucoside **118** exhibited anti-inflammatory and antioxidant properties in a Rd10 mouse model of retinitis pigmentosa, protecting the retinal morphology potentially through an activation of p38 pathway.[175] Finally, sulfuretin (Figure 2) showed a beneficial anti-inflammatory effect in both atopic dermatitis and rheumatoid arthritis contexts. It induced the suppression of Th2 cell activation at 10–20 μM and provided an improvement of atopic dermatitis symptoms in an *in vivo* mouse model, with a suppression of the immune response, at these

concentrations.[176] Sulfuretin triggered the suppression of TNF-α-induced chemokine production through inhibition of the NF-κB signaling pathway, thereby allowing an *in vivo* reduction of the paw thickness of mice with collagen-induced arthritis.[177] In addition, sulfuretin caused a decrease of ROS level in human hepatic L02 cells, providing hepatoprotection.[178] Besides, the compound was described as an antioxidant, able to scavenge DPPH (89–91%) and $ABTS^{+\bullet}$ (71%) radicals and to inhibit AAPH-induced lipid peroxidation (53%) at high concentrations (100 µM).[179] Other sporadic weak antioxidant behaviors were reported for hemiindigoids, such as compound **97** (Figure 17)[141] or ferrocenyl derivative **119**[180] using DPPH-, $ABTS^{+\bullet}$- or galvinoxyl-based assays.

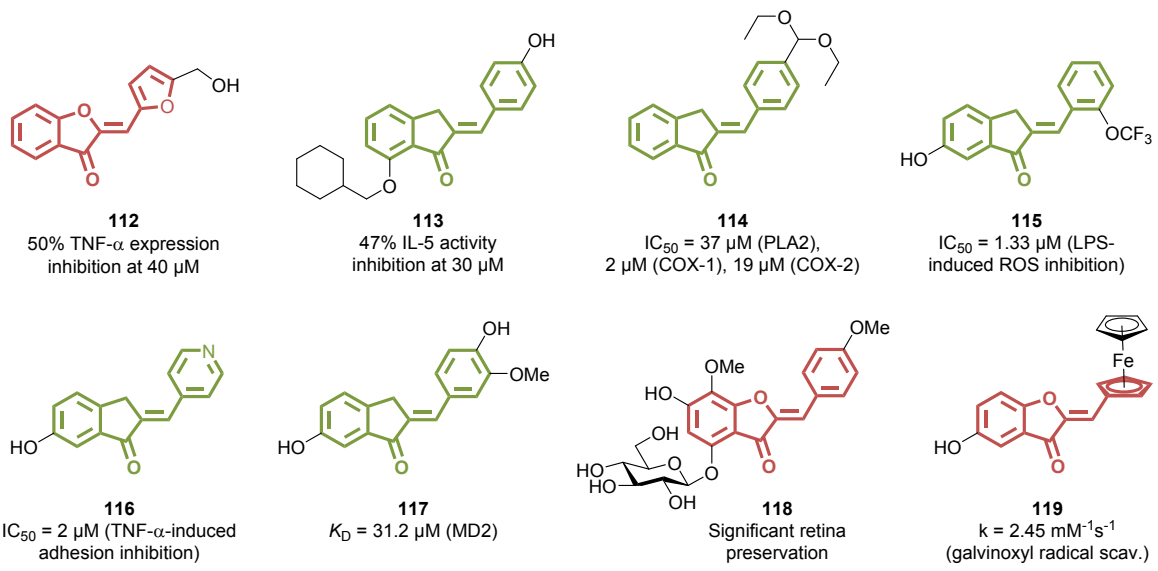

Figure 20. Structures and activities of anti-inflammatory and antioxidant compounds.

Anti-diabetic and anti-adipogenic activities.

The incidence of diabetes and obesity is increasing worldwide, and they now constitute one of the major causes of death in developed countries, while potentially leading to numerous health complications. Several biomolecules are potentially involved in type-II diabetes, making them

more or less validated therapeutic targets. Some of them were targeted by hemiindigoid derivatives in the recent years. Dual-specificity protein tyrosine phosphatase localized to mitochondrion 1 (PTPMT1), whose knockdown is known to cause an increase of insulin secretion in β-cells, was thus the target of a structure-based virtual screening. Among a wide diversity of molecules, compound **120** (Figure 21) emerged as one of the fifteen active structures retained, showing an activity in the micromolar range (IC_{50} = 12 μM).[181] The inhibition of kinase DRAK2 provided promising results regarding islet survival improvement for type-I and type-II diabetes. In this context, aurones, indanones and related scaffold were developed starting from compound **40** (Figure 10), a moderately active compound (IC_{50} = 3.15 μM). The introduction of oxygen-based chemical groups at position 5 appeared as overall beneficial, as testified by compound **121**, the best inhibitor of the series (IC_{50} = 0.25 μM). Beyond DRAK2 *in vitro* inhibition, **121** was able to induce a partial and dose-dependent recovering of glucose-stimulated insulin secretion after a palmitate-induced impairment in isolated pancreatic islets.[182] α-Glucosidase is another target of interest for antidiabetic strategies. Indeed, the enzyme catalyzes the cleavage of polysaccharides into glucose, and its modulation could thus allow a control of hyperglycemia in the frame of type-II diabetes. Aurones and benzofuranones showed some activity against this enzyme, with IC_{50} values in the micromolar range. Compound **122** was the most active aurone identified in the study (IC_{50} = 31 μM). In addition, it promoted glucose consumption in HepG2 cells at 1 μM to a similar level than positive control metformin at 1 mM.[183] The peroxisome proliferator-activated receptor gamma (PPARγ) is involved in the expression of genes regulating lipid management and blood glucose, and was thus targeted by inhibitors for antidiabetic action. While thiazolidinedione derivatives were previously developed, a series of analogous indanones provided valuable results, especially compound **123** which revealed a very good affinity for PPARγ (IC_{50} = 0.62 μM).[184] Recently, the

protein mitoNEET, a mitochondrial 2Fe-2S iron-sulfur cluster, was discovered along with its important role in both diabetes and obesity processes. Through a screening of mitoNEET potential ligands, three aurones were identified. Compound **124** exhibited a very high affinity for mitoNEET, reaching a K_i value of 6 nM.[185] Further studies are required for evaluating the antidiabetic potential of this compound, however. Lastly, sulfuretin (Figure 2) showed anti-adipogenic activities. As obesity is a global health issue and a risk factor for a series of other pathologies, including diabetes and cardiovascular diseases, a pharmacological approach allowing to regulate adipogenesis is necessary for patients with higher body mass index. A high-concentration (70 μM) sulfuretin treatment resulted in a notable reduction of lipid production in 3T3-L1 cells through the inhibition of several adipogenic factors, including PPARγ.[186] In addition, sulfuretin regulated adipogenesis in the specific context of acquired lymphedema, leading to a significant edema volume reduction in lymphedema-induced mice.[187]

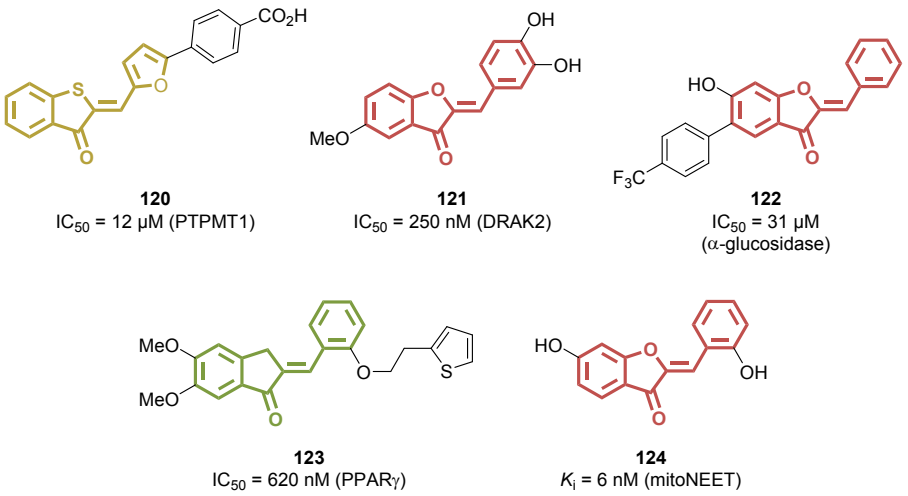

120
IC_{50} = 12 μM (PTPMT1)

121
IC_{50} = 250 nM (DRAK2)

122
IC_{50} = 31 μM
(α-glucosidase)

123
IC_{50} = 620 nM (PPARγ)

124
K_i = 6 nM (mitoNEET)

Figure 21. Structures and activities of anti-diabetic and anti-adipogenic compounds.

Potential interfering chemical reactivity and properties.

The development of molecular scaffolds dedicated to medicinal applications should avoid to trigger chemical cross-reactivity with various biological elements. In the case of hemiindigoids, the core structure of all aforementioned scaffolds contains an enone-based electrophilic Michael acceptor system, somewhat similar to the closely related chalcones. However, many reports described that the reactivity of this chemical group is particularly low, especially in aurones and hemiindigos, due to the presence of an electrodonor substituent at the α-carbon of the enone that confers to the system a conflicting enamine/enol character.[188,189] Thus, synthetic chemical methods developed for Michael addition on aurones or hemiindigos always involved highly reactive nucleophiles such as *N*-heterocyclic carbenes.[190] Indeed, among biologically relevant nucleophiles, even electron-rich thiols like glutathione or *N*-acetylcysteine failed to react with aurones derivatives.[191] Studies are lacking for the two other hemiindigoid scaffolds, but hemithioindigos, and to a lesser extent indanones, should logically undergo similar effects. As a consequence, the impact of hemiindigoids electrophilicity is expected to be minimal in their biological activity, and cross-reactivity with cell nucleophiles does not appear as a major issue. Furthermore, the overall low toxicity of hemiindigoids argue for their stability in physiological conditions. While sporadic cytotoxicity occurs, it usually affects individual compounds among other innocuous, closely-related analogues based on the same scaffold, suggesting an independent mechanism. Nevertheless, if overall hemiindigoids and their substructures have not been flagged in common pan-assay interference compounds (PAINS) libraries, it cannot be excluded that their weak electrophile character could occasionally interfere with reactive nucleophilic species used as bioassay reagents or products. Such a phenomenon was observed, for example, when evaluating aurones as tyrosinase inhibitors,

using the highly nucleophilic 3-methyl-2-benzothiazolinone hydrazone (MBTH, Besthorn's hydrazone) as a reagent for quinone capture,[192] leading to the use of alternative methods.[41,42,47] Similarly, a special attention should generally be paid when using a strong nucleophile in an assay mixture. In addition to chemical reactivity, possible PAINS-related interferences in bioassays could originate from compounds intrinsic fluorescence covering the operating wavelengths.[193] Indeed, as described below, hemiindigoids frequently show emission bands between 500 and 600 nm, thus matching output wavelengths in several biochemical assays. One must keep in mind these limitations when biochemically evaluating hemiindigoids, and should implement appropriate control experiments in order to dismiss a potential fluorescence interference.

HEMIINDIGOIDS AS SMART AGENTS FOR BIOLOGICAL AND PHOTOPHARMACOLOGICAL APPLICATIONS

Photophysical properties of hemiindigoids.

Hemiindigoids exhibit special optical properties that are conferred by their intrinsically planar structure and a fully conjugated π–π aromatic system. Thus, beyond their aforementioned activities over several biological targets, the ability of these scaffolds to absorb light can give rise to fluorescence emission[194,195] and, in the case of oxo, aza and thio analogues, to photochromism,[8,196] a marked feature especially for hemiindigos (HI) and hemithioindigos (HTI). These light-induced behaviors make hemiindigoids phototools of interest, and their potential use as fluorescent probes and photochromic units has recently started to be addressed in the photobiology and photopharmacology fields. Their fluorogenic applications in cellular medium are facilitated by

their light absorption and intense fluorescence emission in the visible region of the electromagnetic spectrum. They exhibit large Stokes shifts and, generally, possess high fluorescence quantum yields in apolar solvents. In addition, changes in their substitution patterns and *push-pull* effect modulation are known strategies to further increase the energy gap between absorption and emission and to induce bathochromic shifts.[195,197,198] Most hemiindigoids can promptly cross cell membranes due to their lipophilic character, which enables their delivery to transmembrane and intracellular targets. Another interesting characteristic is their pronounced solvatofluorochromism.[195] Indeed, the ability to generate different fluorescence outputs according to the polarity of the environment is an important property for tracing and imaging biological events. Several aurones were especially reported as promising environment-sensitive probes. One example is aurone **125** (Figure 22), which exhibited only residual fluorescence emission in water and methanol, while showing high fluorescence quantum yield in chloroform ($\Phi_F = 0.34$), with 50-fold emission increase.

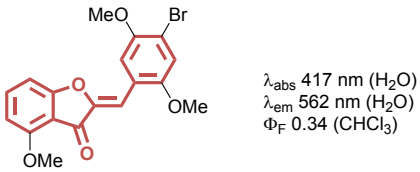

125

Figure 22. Structure and photophysical properties of compound **125**.

In a similar way, the photochromic properties of HI and HTI, especially attractive for biological applications, can be tuned by solvent polarity.[197,199] Their photoisomerization occurs through the excitation of the π–π^* electronic transition band with visible light, where one of the de-excitation pathways leads to the conversion of the thermodynamically stable *Z* isomer into the metastable *E* isomer.[194,200] For both scaffolds, this conversion occurs upon irradiation with blue or green light, whereas the backward reaction proceeds either photochemically, within the range of green to red

light, or thermally, with thermal half-lives reaching the month to year range for the most stable *E* analogues (*e.g.*, compounds **126** and **127** in Figure 23).[197,201] HI and HTI are thus positive photochroms, with the *E* form being bathochromically shifted relative to the *Z* form. Unlike other classes of photochroms well explored in biology, such as azobenzenes, HI and HTI do not require the use of harmful UV light and show considerable band separation between the two isomers, a characteristic that contributes to the quasi-complete *Z*-to-*E* and *E*-to-*Z* conversions and the subsequent high photostationary state (PSS) ratios commonly observed for these photochroms.[197,202] This feature opens the possibility to selectively address one of the forms in biological medium, a property that perfectly match the photopharmacology basis that consists in exerting a spatiotemporal control over biological activity using light as a non-invasive stimulus, in an attempt to reduce side-effects of drugs.[203] Thus, *on-off* switching of activity becomes possible when the biological target discriminates between the two isomeric forms, making these compounds very attractive for the development of drugs with localized and selective action. In addition, the replacement of the phenyl-based B-ring of HTI by a hydrogen-bond-donor pyrrole moiety confers a unique combination of high bistability and exquisite interconversion ratios at operable wavelengths, due to the stabilization of *E* isomers through hydrogen bonding with the intracyclic ketone (*e.g.*, compound **128** in Figure 23).[202] Similarly, substituting the intracyclic nitrogen atom of the HI scaffold provided analogues with very stable *Z* and *E* forms, a consequence of the additional steric hindrance between the *N*-substituent and the aromatic B-ring in the *Z* configuration (*e.g.*, compound **129** in Figure 23).[197] These studies yielded photoswitchable systems that would in theory perfectly meet the requirements for *in vivo* photopharmacological applications. Last but not least, HTI are highly resistant to photofatigue and can undergo many photoisomerization cycles without being degraded.[202,204] The photoisomerization mechanism is well described for the naked HTI scaffold. It occurs through the excitation of the π–π^* electronic transition band in the visible

range with $S_0 \rightarrow S_1$ promotion. From S_1, conformational changes lead to competitive pathways where the molecule can either follow a radiative decay and emit fluorescence, or undergo an internal conversion and cross to the S_2 potential energy surface. Then, S_2 can decay with equal probabilities to the S_0 of the metastable *E*-isomer or return to the S_0 of the thermodynamically stable *Z*-isomer, after reaching the conical intersection.[198]

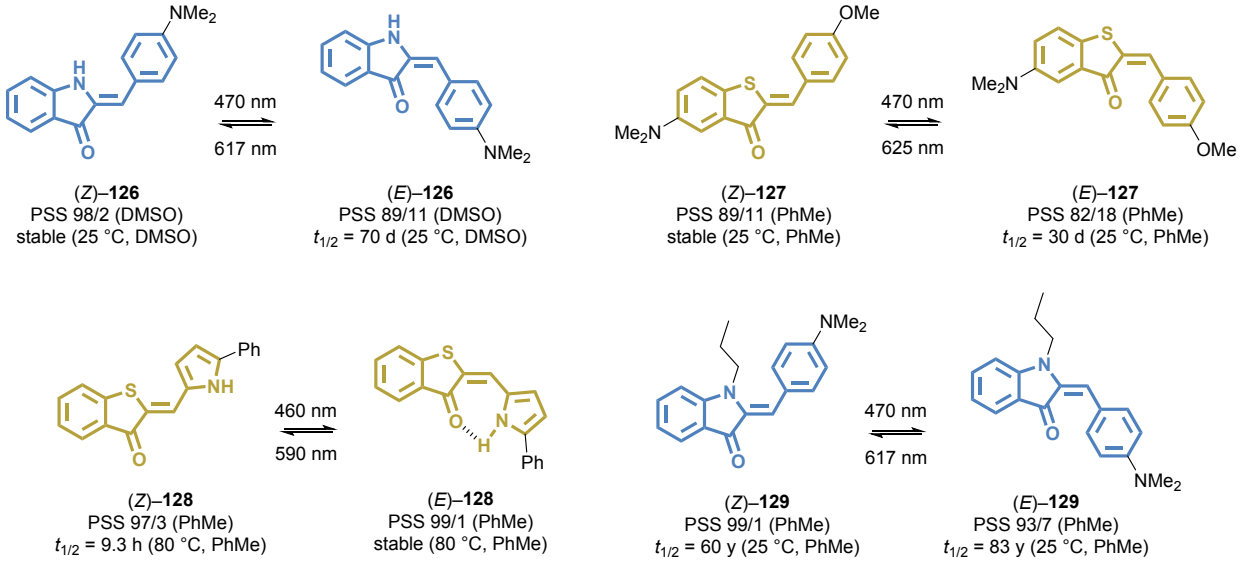

Figure 23. Examples of HI/HTI-based photoswitchable compounds in fundamental studies.

Fluorescent biosensors based on hemiindigoid scaffolds.

Hemiindigoids are solvatochromic dyes. In living systems, environmental changes around these chromophores produced by their interaction with proteins, lipids, metal ions and small molecules often trigger significant shifts in fluorescence emission wavelength and/or intensity. As a general tendency, their fluorescence emission increases with decreasing environmental polarity, a phenomenon that theoretical calculations linked to the existence of a charge transfer character of the excited states, *e.g.*, in the context of aurones and HTI. In polar environments, this HOMO–

LUMO π–π* transition is stabilized, reducing fluorescence quantum yields. To take profit of these effects, some applications of hemiindigoids as sensing probes have been developed in the last ten years.

First, the fluorescent tracking of proteins, peptides and small molecules constitutes a powerful tool to monitor biochemical pathways and pathological processes. Studies providing proof-of-concept principle for *off-on* fluorescence of hemiindigoids are available and highlight the increments in fluorescence emission of hemiindigoids in contact with hydrophobic sites of biomolecules, in a concentration-dependent manner. The aforementioned aurone **125** (Figure 22) was able to detect the presence of compound-binding biomolecules such as human serum albumin or poly-L-glutamic acid, triggering a ~25-fold increase of fluorescence upon binding,[195] a result that confirmed an earlier work focusing on other aurone derivatives such as **130** (Figure 24).[194] Lipid sensing was also explored, and aurones were incorporated into L-α-dipalmitoylphosphatidylcholine bilayers. The authors noticed that the fluorescence emission of aurone **125** increased when the molecule was located inside the liposomes.[195] Applying this principle, Wang *et al.* developed three different solvatochromic aurones (**57**, **131**, **132**, Figures 13 and 24) conjugated with dimethylamino, *N*-ethylcarbazoyl and pyrene moieties to monitor the dynamics between lipid droplets (LD) and mitochondria under oxidative stress conditions.[205] LD are fatty acid storage organelles that participate in energy homeostasis and play a role in oxidative stress regulation. An accumulation of these organelles is observed in pathologies such as cancer and obesity. For the first time, their interaction with mitochondria in the presence of an excess of H_2O_2 were directly monitored through two-photon fluorescence. In this context, the authors verified that the aurones were able to selectively stain LD inside cells with superior photobleaching resistance than BODIPY 493/503, a common probe widely used for fluorescent staining of lipids. In another study, Nan *et al* evaluated

a series of indanones for their binding affinity and fluorescence staining capacity towards β-amyloid plaques in AD. *In vitro* evaluations using brains from AD patients revealed a high staining profile for compound **84** (Figure 15). In addition, *in vivo* studies performed with the same molecule over normal mice confirmed its ability to cross the blood brain barrier and to undergo brain uptake followed by fast washout.[118] These results attest for the potential application of indanones as β-amyloid plaque probes, and more generally for the appropriate physicochemical profile of hemiindigoids to operate in living environments. In addition, chemical reaction sensing allows to specifically detect small molecules in a complex environment, a desirable tool for early diagnosis and disease monitoring. To enable such applications, the intrinsic solvatochromic properties of hemiindigoids could be mitigated by an appropriate design, in order to provide bright fluorescence in aqueous environments. Indeed, by reducing aromatic aggregation, restraining the donor-acceptor character and allowing the formation of a hydrogen-bond network with the solvent, water-fluorescent indanones were obtained.[206] This concept was explored for cysteine detection. This semi-essential amino acid is involved in several biological processes and is associated with metabolic disorders and increased risk for health problems when present at high levels. Fang *et al* introduced an acrylate group able to react with cysteine at position 5 of indanone **133** (Figure 24).[207] In the presence of the target, the acrylate group was hydrolyzed to the corresponding phenol **134**, which, in turn, possesses higher fluorescence quantum yield (0.73) compared to the acrylate (0.13). Therefore, increments in fluorescence intensity, generated by the formation of 5-hydroxyindanone, were quantitatively correlated to cysteine concentration in the medium. In some cases, even anti-solvatochromic behaviors were observed. For example, **135** was able to selectively detect H_2S, a small molecule generating during the cirrhosis process, through the reduction of the azido group to amino (**136**), which triggers an increase of the quantum yield, allowing two-photon fluorescence imaging of liver cells (Figure 24).[206] The aminoindanone showed remarkable anti-solvatochromic

properties, as the quantum yield increased with the solvent polarity (0.80 in PBS buffer, 0.53 in EtOH, 0.12 in MeCN and 0.02 in CH_2Cl_2). Overall, these promising results offer a glimpse of the versatility of hemiindigoids and could endorse future research about applications of the scaffolds as biosensors.

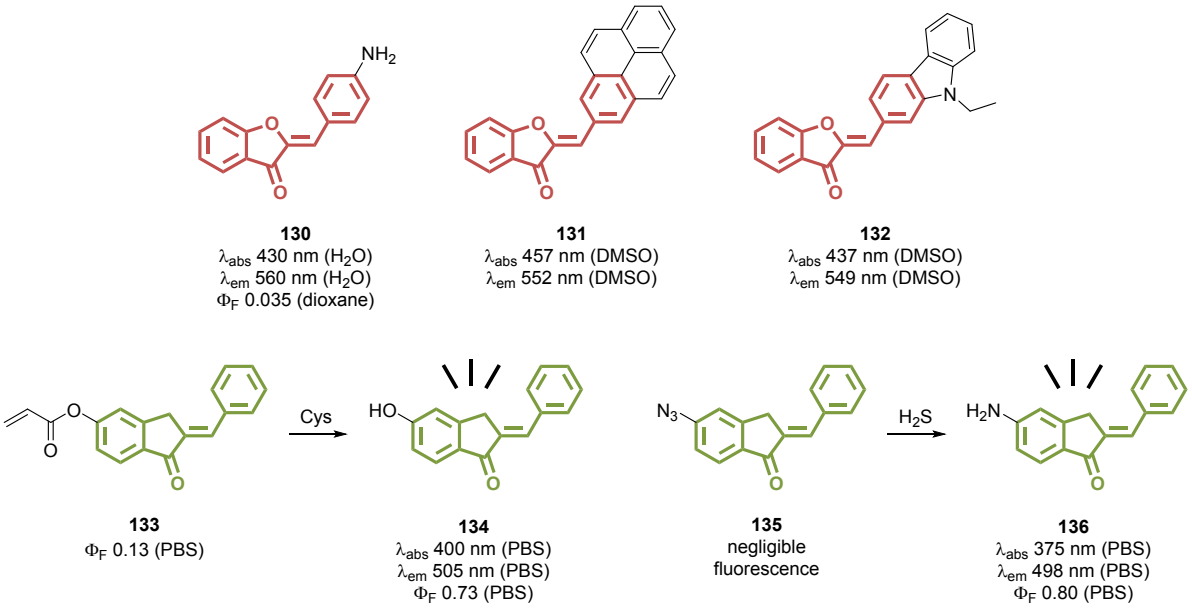

Figure 24. Examples of aurone/indanone-based fluorogenic probes.

Biological applications of photoswitchable hemiindigoids.

A *Z/E* photoisomerization triggers geometric changes immediately accompanied by changes in electronic and physicochemical properties of hemiindigoid photochroms (photoswitches), such as dipolar moment and solubility. As the interactions between small molecules and biological targets can be quite sensitive to minimal structural modifications, photoswitches find a direct application in the development of photocontrolable drugs and probes. Indeed, selectivity constitutes a crucial feature in the development of new drugs and is also a main axe of photopharmacology, where it is

directly related to modifications in pharmacokinetic and pharmacodynamic parameters undergone by photochroms upon switching. To date, photopharmacology has been dominated by azobenzenes, but HI and HTI recently started to find their way in this field, with promising results. It is worth noting that these molecules are closely related to aurones and indanones. These last two classes convey numerous biological activities, as previously described in this review, and could guide the elucidation of the biological potential of HI and HTI, still far from being completely known. In the context of photopharmacology, a special interest should be directed to skin and eye-related activities, where light in the blue-to-red range can easily penetrate; but with adaptations, a wider range of biological tissues could be targeted such as the gastrointestinal tract, the throat, the respiratory system and even inner organs.[208] Few examples of HI/HTI photoswitches dedicated to biological applications are available in the literature. Indeed, the scaffolds initially experienced some drawbacks in aqueous media, such as intrinsic low solubility, loss of photoswitching efficiency and reduced thermal stability in water. However recent reports tended to mitigate these issues by providing insightful results. In a study from Berdnikova, new HI with photoswitching properties in water or water-containing medium were identified and their ability to bind HIV-1 RNA was investigated.[209,210] Except for **126**, all derivatives presented overall good solubility and ability to isomerize in water or water/co-solvent mixtures upon irradiation at 470 nm for the forward reaction, and 590 nm for the backward reaction. Compound **137** was able to switch in pure water and to associate with HIV-1 RNA with high affinity and photoswitchable fluorescence (Figure 25). The derivative showed decent photostationary states (PSS^{470} = 20/80 (%*Z*/*E*) and PSS^{590} = 97/3 (%*Z*/*E*)), with a thermal half-life of 10.8 h at 25 °C for the *E* form in a phosphate buffer. Upon RNA binding, the photoswitch properties were maintained, with huge increments in fluorescence emission for the *Z*-isomer (up to 75-fold), while the *E*-isomer remained only weakly fluorescent. This study provided a remarkable proof-of-concept for the development of new HI-

based biomolecule binders operable in physiological contexts. Interestingly, a common feature of **126**, **137** and the other compounds of the series is the presence of sp^3 carbon atoms, which increases the flexibility of these scaffolds, avoiding molecular stacking or assembling and promoting water solubility.[211] As already stated in the literature for HTI, strong amine donor groups at position 4 of the stilbene fragment induce pronounced mesomeric effects, with bathochromic absorption and fluorescence shifts. This effect is due to the stabilization of the S_1, increasing the S_1–S_2 barrier preceding the conical intersection and reducing the efficiency of photoisomerization.[198] A similar behavior could be expected for HI **126**, considering its structural analogy with HTI. The presence of weaker electron-donor substituents such as a methoxy did not compromise the capacity of the molecules to switch in aqueous environments (HI **137**). Hemiindigoids were also covalently attached to biomolecules, and some examples can be found for HTI compounds incorporated into proteins and peptides with the aim of studying folding processes. However, the photophysical properties of these derivates were studied in MeOH or DMSO, with no analysis being performed in water.[212–214] Reports exploring true photopharmacological activities of HI and HTI in living systems are still rare in the literature, probably due to the yet underexplored biological potential of these compounds. In addition, predictability of substituent and solvent effects in their photophysical properties remains challenging, and most of the existing examples involve the HTI scaffold. A first study employing HTI **138** as a 12/15-lipoxygenase (12/15-LOX) pathway inhibitor was published in 2006.[215] It described the differential activity of the compound in its native *Z* configuration (IC_{50} = 700 μM) and as a 38/62 *Z*/*E* mixture corresponding to the PSS reached after irradiation at 405 nm (IC_{50} = 41 μM). The higher potency of the *E* isomer was confirmed by a separate evaluation in its pure form (IC_{50} = 21 μM) upon isolation using chromatography. While *Z*-**138** was not directly converted in the *E* isomer in the biological medium, and despite the PSS ratio obtained, insufficient for further applications, the study demonstrated the possibility to reach

an operable activity gap between the *Z* and *E* forms (a ~30-fold difference). Indeed, even if both isomers of HTI, and more generally of hemiindigoids, could appear as superimposable, with a lower geometrical change as compared to azobenzenes, an appropriate incorporation of substituents at some key positions (*e.g.*, positions 4 and 7) should be sufficient to break the apparent symmetry. More recently, HTI **139** was reported as a potent antimitotic *in cellulo*.[216] Its structure was inspired from colchicine and several indanones previously reported as inhibitors of tubulin polymerization. Initially intended as a switch-on inhibitor, **139** was finally found more active in its 'dark' form (mainly *Z* configuration, EC_{50} = 1 μM) than in its 'lit' form (mainly *E* configuration, EC_{50} = 4 μM). However, the study highlighted for the first time the potential of HTI to switch upon irradiation in a cell-based context. Additional insights were provided by compound **140**, a close analogue of **139** with a similar activity profile ('lit'/'dark' EC_{50} ratio of 4.1).[217] Whereas no photoswitching was observed in aqueous medium, an unequivocal activity drop was measured in an antimitotic cellular assay following sample irradiation at 450 nm (Figure 26). The authors hypothesized that photoswitching can occur in intracellular medium, where water-excluded lipidic membranes and vesicles are present and could favor the photochromic behavior of the HTI inhibitor, even if interconversion fails in pure water. The exact mechanism that explains this difference in activity is uncertain, but it opens new avenues for biological applications of hemiindigoids that did not show optimal photoswitching in aqueous environments. However, compound **140** suffered from its polar protic chemical group at position 4' which led to a far less stable *E* isomer, reminiscently of azobenzenes. Finally, replacing the B-ring by a pyrrole counterpart afforded a series of alternative tubulin ligands. Among them, compound **141** (Figure 25) showed a reverse selective antimitotic activity: the 'lit' form, mainly *E*-**141**, was found more active than the 'dark' form, mainly *Z*-**141** (IC_{50} = 4.5 μM vs. >50 μM, respectively).[218] Cell-precise photoisomerization of this compound

allowed to block microtubule dynamics only in selected cells with temporal precision, a result that puts HTI and hemiindigoids on the exciting path of *in vivo* photopharmacological applications.

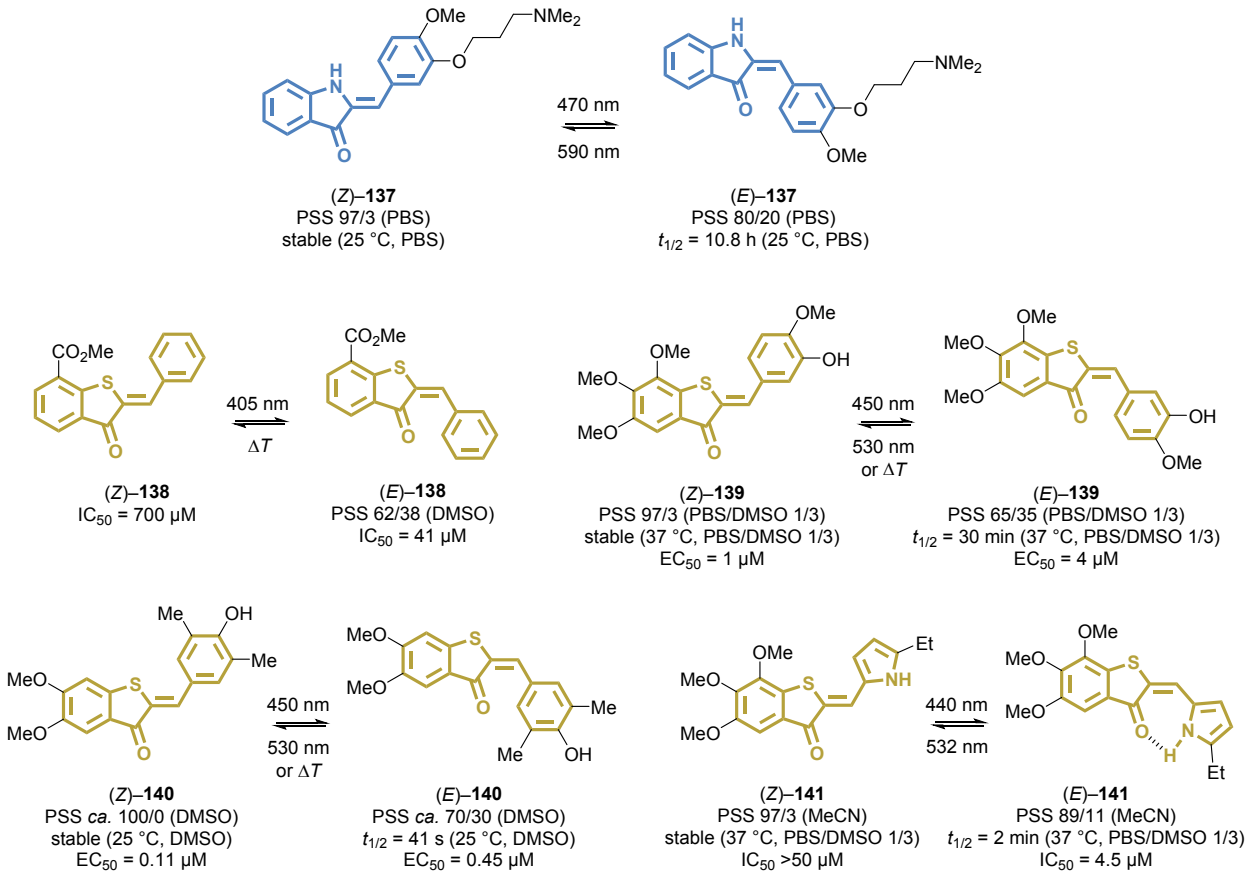

Figure 25. Structures of HI/HTI-based photoswitchable compounds developed for biological and photopharmacological applications.

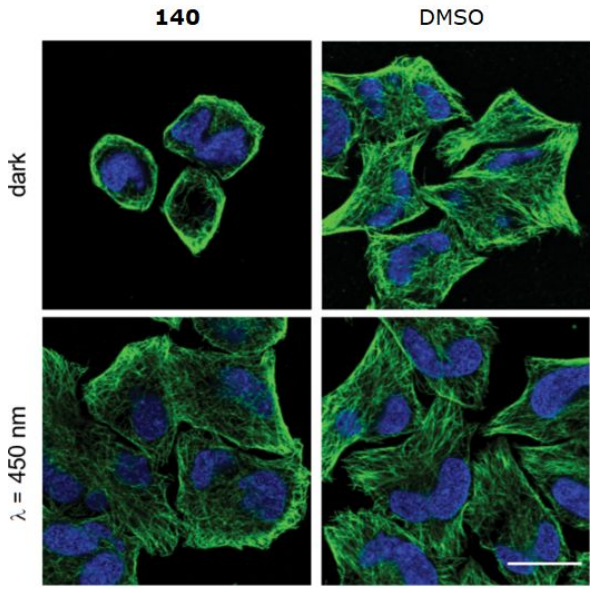

Figure 26. Confocal microscopy images of immunofluorescently labelled microtubule networks with or without treatment with **140** in 'lit' (irradiation at 450 nm) and 'dark' conditions. Microtubules are visualized in green. Reproduced and modified from ref 217 (Creative Commons, CC BY 4.0 license).

CONCLUSION AND PROSPECTS

Hemiindigoids have attracted attention in medicinal chemistry within the past ten years, with multiple and increasingly reported biological activities reports in various therapeutic fields, including anticancer, anti-infective, neurochemical or anti-inflammatory. In the frame of cancer, aurone derivatives were especially found as low nanomolar inhibitors of two emerging targets, PARP-1 and PIM1 kinase, and their interaction patterns were rationalized through the resolution of crystal structure of ligand–protein complexes. Indanocine and its indanone-based analogues were developed as colchicine alternatives, for their potent antimitotic action. Acetylcholinesterase inhibition was the most explored neurochemical action, with the aim to transpose donepezil activity in aurone and indanone scaffolds, sometimes with very promising results. In addition, structurally-

diverse hemiindigoid compounds were identified for their anti-infective effect against a large set of pathogenic bacteria, fungi, parasites and virus, and sometimes against resistant strains. Thus, a large ensemble of various biological activities appears reachable by an appropriate substitution and/or B-ring heterocycle introduction, even if the recorded effects often remain to be confirmed by *in vivo* studies involving appropriate selectivity, toxicity and pharmacokinetics assessments. Overall, hemiindigoids are especially engaging for the rapid access they offer to a full range of substituents at both aromatic rings, and for the facile assembly of the aurone, indanone, HI and HTI scaffolds themselves. Their flatness also enables a precise control of their geometry and interaction patterns inside protein pockets. With the recent rise of photochemical studies dedicated to HI and HTI photochromic properties and early "proof-of-concept" uses in photopharmacological applications, a new avenue is opening up that endorses further investigations about hemiindigoid potential as biological photoswitches. Indeed, hemiindigoids bring a set of advantageous properties for medicinal applications, first and foremost their possibility of thermal bistability and near-quantitative interconversion using visible light. Yet, to date, most examples of bioactive hemiindigoids still rely on the more explored aurone and indanone backbones. HI and HTI still received less attention, but they now appear as light-controllable counterparts whose close structural analogy with aurones and indanones could orientate the elucidation of their biological potential for more ambitious applications in photopharmacology. The replacement of existing bioactive aurones and indanones by HI or HTI versions could even represent a promising strategy for turning simple medicinal agents into photoswitchable entities, able to deliver their activity with a high spatiotemporal precision. As many of the biological effects described within this review could easily trigger undesirable events (*e.g.*, off-target cytotoxic activities, rise of resistances to antibacterial action, collateral neurochemical modifications), the possibility to "turn-off" the activity on demand is often highly attractive. Early results drawn from existing studies tended to

demonstrate that the HI/HTI scaffolds are fully compatible with such an objective. While they share some drawbacks with other known scaffolds, the first reported examples have shown that these issues could be circumvented through a careful molecular design. First, despite the apparent symmetry between the *Z* and *E* isomers, an appropriate substitution pattern (*i.e.*, substitution at position 7) successfully led to an important (~30-fold) discrimination between their respective activities in the case of compound **138**.[215] Second, while several examples of HI/HTI photoswitches in water were reported, their conversion in aqueous environments is often challenging. However, even compounds containing strong protic electron donor substituents at position 4', known to severely jeopardize photoswitching in water and photostability of the *E* isomer, showed good conversions in cellular contexts, possibly relying on cell water-excluded microenvironments.[217] Third, optimal interconversion wavelengths could be easily tuned by molecular design adjustments, leading to a wide set of possibilities covering the entire visible spectrum, ranging from ~400 to ~600 nm for *Z*-to-*E* conversion, and from ~500 to ~750 nm for *E*-to-*Z* conversion. These properties were exploited for the conception of practicable HTI photoswitching agents, optimized to be fully compatible with the limited set of fixed-wavelength lasers available in biology, thereby addressing a common issue met with more classical scaffolds like azobenzenes.[218] To date, antimitotic agents **139**–**141** are the only known set of true photopharmacological agents based on HI/HTI scaffolds. Indeed, solid cancers are ideal targets in the field as they are usually localized, and as their classical treatments most often trigger severe side effects, possibly mitigated by a subsequent *off*-switching of the active photodrug. But upon examination of targets easily accessible for irradiation, from the systematic classification proposed by Feringa *et al.*,[219] many other research perspectives spring to mind. For example, hemiindigoid-based HDAC inhibitors described above could become potent photoswitchable agents able to address cutaneous T-cell lymphoma, a 'class 1' target, directly accessible for irradiation. An HDAC2-inhibiting azobenzene derivative was already developed for

the treatment of lymphoma, but the need of skin-damaging UV light dismissed the compound for clinical applications, an obstacle that could be overcome by using visible-light-operating hemiindigoid scaffolds.[220] Localized infectious diseases are also good candidates: in the case of tuberculosis, the respiratory system is accessible by endoscopy. *M. tuberculosis* was thus targeted by several photoswitching scaffolds through various mechanisms of action, but with limiting issues related to irradiation wavelengths and times. Antitubercular hemiindigoids could provide improved photophysical properties for enabling clinical use. Even 'class 3' targets, gathering organs lying under the skin and requiring a deeper light penetration in living tissues, could benefit from the globally redshifted interconversion wavelengths of HI/HTI, compared to other photoswitches. An example of application could be the light-controlled inhibition of PARP-1 by HI/HTI versions of aurones **18**–**23** in the frame of mammary tumor treatment. When photopharmaceuticals based on more classical scaffolds such as azobenzene derivatives often require heavy modifications of a pre-existing active compound, an uncertain time- and resource-consuming process, the development of bioactive HI- and HTI-based photoswitchable agents could rely on the already well-established medicinal chemistry of aurones and indanones. With the blossoming of photopharmacology as a full-blown therapeutic field, hemiindigoids represent exciting opportunities to associate effective biological actions with unique photophysical properties.

AUTHOR INFORMATION

Corresponding author

*E-mail: Romain.Haudecoeur@univ-grenoble-alpes.fr

ORCID

Romain Haudecoeur: 0000-0002-6271-4717

Notes

The authors declare no competing financial interest.

Biographies

Letícia M. Lazinski received her Bachelor of Pharmacy from the Federal University of Paraná (Brazil) in 2016. She did her Master in Chemistry for Life Sciences at University Grenoble Alpes (France), where she started her Ph.D. in 2021 under the supervision of Dr. Romain Haudecoeur and Dr. Guy Royal. Her studies focus on the development of hemiindigoid photoswitches to control tyrosinase activity.

Guy Royal is full professor at University of Grenoble Alpes (France). He obtained his Ph.D. in Dijon (University of Burgundy) under the supervision of Prof. Roger Guilard, in the fields of organic and coordination chemistry. He then spent one year in the group of Prof. Karl Kadish at University of Houston (U.S.) where he studied molecular electrochemistry. In 1999 he joined the University of Grenoble where he is currently developing molecular switches and in particular photochromic systems that can be used for information storage, smart devices or biological applications.

Maxime Robin obtained his Ph.D. in Organic Chemistry from Aix-Marseille University (France) in 2000, under the supervision of Prof. Jean-Pierre Galy. He joined the group of Dr. Duy Hua at Kansas State University (U.S.) as a postdoctoral researcher before being hired in 2002 at Aix-Marseille University (France) as an Assistant Professor. His research focuses on the design and synthesis of new scaffolds (small-molecule entities) as future therapeutics to address diverse pharmacological problems.

Marc Maresca is a researcher at Aix-Marseille University since 2006, working at identifying, developing and characterizing new molecules (natural, synthetic or bio-inspired) with therapeutic properties, such as antimicrobial, antitumoral, antioxidant and/or anti-inflammatory actions.

Romain Haudecoeur obtained his Ph.D. in Chemical Biology from University Grenoble Alpes (France) in 2011, under the supervision of Prof. Ahcène Boumendjel. He joined the group of Dr. David Monchaud at the University of Burgundy (Dijon, France) as a postdoctoral associate in the same year. He was then appointed as Researcher in 2012 in the Department of Medicinal Chemistry of University Grenoble Alpes and received in 2020 the Accreditation to Supervise Research (HDR). His research work essentially focuses on the rational targeting of biological macromolecules, with the aim of developing new bioinspired, bioactive and smart compounds for modulating the function of proteins such as tyrosinases, viral polymerases and membrane ABC transporters.

ACKNOWLEDGEMENTS

The authors are grateful to ANR ("Agence Nationale de la Recherche") for financial support through Labex ARCANE and CBH-EUR-GS (ANR-17-EURE-0003) and through ANR project EPIDERMIS (ANR-19-CE44-0002). The authors thank Labex ARCANE for the fellowship grant of L.M.L in the frame of project SHAPESHIFT.

ABBREVIATIONS USED

AAPH, 2,2'-azobis(2-amidinopropane) dihydrochloride; ABC, ATP-binding cassette; ABTS, 2,2'-azino-bis(3-ethylbenzothiazoline-6-sulfonic acid); AURKB, aurora B kinase; BODIPY 493/503, 4,4-difluoro-1,3,5,7,8-pentamethyl-4-bora-3a,4a-diaza-*s*-indacene; CDK5, cyclin-dependent kinase 5; CK2, casein kinase 2; COVID-19, coronavirus disease 2019; DPPH, 2,2-diphenyl-1-picrylhydrazyl; DRAK2, death-associated protein-kinase-related 2 ; Dvl, disheveled protein; GSK3, glycogen synthase kinase 3; HI, hemiindigo; HOPNO, hydroxypyridine-*N*-oxide; HTI, hemithioindigo; HtrA, high-temperature requirement A; IAV, influenza A virus; IKK, IκB kinase; IL-5, interleukin-5; iNOS, nitric oxide synthase; LD, lipid droplets; LOW, lipoxygenase; MAO, monoamine oxidase; MD2, myeloid differentiation 2; MPP^+, 1-methyl-4-phenylpyridinium; MRP1, multidrug resistance protein 1; MTT, 3-(4,5-dimethylthiazol-2-yl)-2,5-diphenyltetrazolium bromide; NFT, neurofibrillary tangle; Nrf2, nuclear factor erythroid 2-related factor 2; NS5B, nonstructural protein 5B; PARP, poly(ADP-ribose)polymerase; PLA2, phospholipase A_2; PSS, photostationary state; PTPMT1, Protein tyrosine phosphatase mitochondrial 1 ; RAR, retinoid receptor; SIRT-1, sirtuin 1; TDP1, tyrosyl-DNA phosphodiesterase; TNKS, poly(ADP-ribose)polymerase tankyrase

REFERENCES

(1) Baeyer, A. Ueber die Verbindungen der Indigogruppe. *Ber. Dtsch. Chem. Ges.* **1883**, *16*, 2188–2204.

(2) Boucherle, B.; Peuchmaur, M.; Boumendjel, A.; Haudecoeur, R. Occurrences, biosynthesis and properties of aurones as high-end evolutionary products. *Phytochemistry* **2017**, *142*, 92–111.

(3) Haudecoeur, R.; Boumendjel, A. Recent advances in the medicinal chemistry of aurones. *Curr. Med. Chem.* **2012**, *19*, 2861–2875.

(4) Friedländer, P. Ueber schwefelhaltige Analoga der Indigogruppe. *Chem. Ber.* **1906**, *39*, 1060–1066.

(5) Geissman, T. A.; Heaton, C. D. Anthochlor pigments. IV. The pigments of *Coreopsis grandiflora*, Nutt. I. *J. Am. Chem. Soc.* **1943**, *65*, 677–683.

(6) Daisley, R. W.; Elagbar, Z. A.; Walker, J. Reaction of indol-3-(2*H*)-one derivatives with some active methylene compounds. *J. Heterocyclic Chem*. **1982**, *19*, 1013–1016.

(7) Chalkha, M.; Bakhouch, M.; Akhazzane, M.; Bourass, M.; Nicolas, Y.; Al Houari, G.; El Yazidi, M. Design, synthesis and characterization of functionalized pyrazole derivatives bearing amide and sulfonamide moieties from aza-aurones. *J. Chem. Sci.* **2020**, *132*, 86.

(8) Wiedbrauk, S.; Dube, H. Hemithioindigo—an emerging photoswitch. *Tetrahedron Lett.* **2015**, *56*, 4266–4274.

(9) Mukherjee, C.; De, A. Application of directed metalation in synthesis, part 2: an expedient synthesis of methoxybenzo[*b*]thiophenes. *Synlett* **2002**, 2, 325–327.

(10) Huang, Y-S.; Liu, J-Q.; Zhang, L-J.; Lu, H-L. Synthesis of 1-indanones from benzoic acids. *Ind. Eng. Chem. Res*. **2012**, *51*, 1105–1109.

(11) Cui, D-M.; Zhang, C.; Kawamura, M.; Shimada, S. Synthesis of 1-indanones by intramolecular Friedel-Crafts reaction of 3-arylpropionic acids catalyzed by $Tb(OTf)_3$. *Tetrahedron Lett.* **2004**, *45*, 1741–1745.

(12) Premasagar, V.; Palaniswamy, V. A.; Eisenbraun, E. J. Methanesulfonic acid catalyzed cyclization of 3-arylpropanoic and 4-arylbutanoic acids to 1-indanones and 1-tetralones. *J. Org. Chem.* **1981**, *46*, 2974–2976.

(13) Sheng, R.; Xu, Y.; Hu, C.; Zhang, J.; Lin, X.; Li, J.; Yang, B. ; He, Q.; Hu, Y. Design, synthesis and AChE inhibitory activity of indanone and aurone derivatives. *Eur. J. Med. Chem*. **2009**, *44*, 7–17.

(14) Jung, H. J.; Noh, S. G.; Park, Y.; Kang, D.; Chun, P.; Chung, H. Y.; Moon, H. R. *In vitro* and *in silico* insights into tyrosinase inhibitors with (*E*)-benzylidene-1-indanone derivatives. *Comp. Struct. Biotechnol. J.* **2019**, *17*, 1255–1264.

(15) Haudecoeur, R.; Ahmed-Belkacem, A.; Yi, W.; Fortuné, A.; Brillet, R.; Belle, B.; Nicolle, E.; Pallier, C.; Pawlotsky, J.-M.; Boumendjel, A. Discovery of naturally occurring aurones that are potent allosteric inhibitors of hepatitis C virus RNA-dependent RNA polymerase. *J. Med. Chem.* **2011**, *54*, 5395–5402.

(16) Varma, R. S.; Varma, M. Alumina-mediated condensation. A simple synthesis of aurones. *Tetrahedron Lett.* **1992**, *33*, 5937–5940.

(17) Venkateswarlu, S.; Murty, G. N.; Satyanarayana, M. "On water" synthesis of aurones: first synthesis of 4,5,3',4',5'-pentamethoxy-6-hydroxyaurone from *Smilax riparia*. *Arkivoc* **2017**, 303–314.

(18) Narsinghani, T.; Sharma, M. C.; Bhargav, S. Synthesis, docking studies and antioxidant activity of some chalcone and aurone derivatives. *Med. Chem. Res.* **2013**, *22*, 4059–4068.

(19) Regenass, P.; Abboud, D.; Daubeuf, F.; Lehalle, C.; Gizzi, P.; Riché, S.; Hachet-Haas, M.; Rohmer, F.; Gasparik, V.; Boeglin, D.; Haiech, J.; Knehans, T.; Rognan, D.; Heissler, D.; Marsol, C.; Villa, P.; Galzi, J.-L.; Hibert, M.; Frossard, N.; Bonnet, D. Discovery of a locally and orally active CXCL12 neutraligand (LIT-927) with anti-inflammatory effect in a murine model of allergic airway hypereosinophilia. *J. Med. Chem.* **2018**, *61*, 7671–7686.

(20) Nguyen, T. B.; Retailleau, P. DIPEA-promoted reaction of 2-nitrochalcones with elemental sulfur: an unusual approach to 2-benzoylbenzothiophenones. *Org. Lett*. **2017**, *19*, 4858–4860.

(21) Harkat, H.; Blanc, A.; Weibel, J.-M.; Pale, P. Versatile and expeditious synthesis of aurones via Au^{I}-catalyzed cyclization. *J. Org. Chem.* **2008**, *73*, 1620–1623.

(22) Kraus, G. A.; Gupta, V. Divergent approach to flavones and aurones via dihaloacrylic acids. Unexpected dependence on the halogen atom. *Org. Lett.* **2010**, *12*, 5278–5280.

(23) Kaur, R.; Kaur, G.; Gill, R. K.; Soni, R.; Bariwal, J. Recent developments in tubulin polymerization inhibitors: an overview. *Eur. J. Med. Chem.* **2014**, *87*, 89–124.

(24) Leoni, L. M.; Hamel, E.; Genini, D.; Shih, H.; Carrera, C. J.; Cottam, H. B.; Carson, D. A. Indanocine, a microtubule-binding indanone and a selective inducer of apoptosis in multidrug-resistant cancer cells. *J. Natl. Cancer Inst.* **2000**, *92*, 217–224.

(25) Hu, J.; Yan, J.; Chen, J.; Pang, Y.; Huang, L.; Li, X. Synthesis, biological evaluation and mechanism study of a class of benzylideneindanone derivatives as novel anticancer agents. *Med. Chem. Commun.* **2015**, *6*, 1318–1327.

(26) Chen, J.; Yan, J.; Hu, J.; Pang, Y.; Huang, L.; Li, X. Synthesis, biological evaluation and mechanism study of chalcone analogues as novel anti-cancer agents. *RSC Adv.* **2015**, *5*, 68128–68135.

(27) Lewin, G.; Aubert, G.; Thoret, S.; Dubois, J.; Cresteil, T. Influence of the skeleton on the cytotoxicity of flavonoids. *Bioorg. Med. Chem.* **2012**, *20*, 1231–1239.

(28) Singh, A.; Fatima, K.; Srivastava, A.; Khwaja, S.; Priya, D.; Singh, A.; Mahajan, G.; Alam, S.; Saxena, A. K.; Mondhe, D. M.; Luqman, S.; Chanda, D.; Khan, F.; Negi, A. S. Anticancer activity of gallic acid template-based benzylidene indanone derivative as microtubule destabilizer. *Chem. Biol. Drug Des.* **2016**, *88*, 625–634.

(29) Tripathi, S.; Srivastava, G.; Singh, A.; Prakasham, A. P.; Negi, A. S.; Sharma, A. Insight into microtubule destabilization mechanism of 3,4,5-trimethoxyphenyl indanone derivatives using molecular dynamics simulation and conformational modes analysis. *J. Comput. Aided Mol. Des.* **2018**, *32*, 559–572.

(30) Prakasham, A. P.; Saxena, A. K.; Luqman, S.; Chandra, D.; Kaur, T.; Gupta, A.; Yadav, D. K.; Chanotiya, C. S.; Shanker, K.; Khan, F.; Negi, A. S. Synthesis and anticancer activity of 2-benzylidene indanones through inhibiting tubulin polymerization. *Bioorg. Med. Chem.* **2012**, *20*, 3049–3057.

(31) Singh, A.; Fatima, K.; Singh, A.; Behl, A.; Mintoo, M. J.; Hasanain, M.; Ashraf, R.; Luqman, S.; Shaker, K.; Mondhe, D. M.; Sarkar, J.; Chanda, D.; Negi, A. S. Anticancer activity and toxicity profiles of 2-benzylidene indanone lead molecule. *Eur. J. Pharm. Sci.* **2015**, *76*, 57–67.

(32) Srivastava, A.; Fatima, K.; Fatima, E.; Singh, A.; Singh, A.; Shukla, A.; Luqman, S.; Shanker, K.; Chanda, D.; Khan, F.; Negi, A. S. Fluorinated benzylidene indanone exhibits antiproliferative activity through modulation of microtubule dynamics and antiangiogenic activity. *Eur. J. Pharm. Sci.* **2020**, *154*, 105513.

(33) Pérès, B.; Nasr, R.; Zarioh, M.; Lecerf-Schmidt, F.; Di Pietro, A.; Baubichon-Cortay, H.; Boumendjel, A. Ferrocene-embedded flavonoids targeting the Achilles heel of multidrug-resistant cancer cells through collateral sensitivity. *Eur. J. Med. Chem.* **2017**, *130*, 346–353.

(34) Toth, S.; Szepesi, A.; Tran-Nguyen, V.-K.; Sarkadi, B.; Nemet, K.; Falson, P.; Di Pietro, A.; Szakacs, G.; Boumendjel, A. Synthesis and anticancer cytotoxicity of azaaurones overcoming multidrug resistance. *Molecules* **2020**, *25*, 764.

(35) Lord, C. J.; Ashworth, A. PARP inhibitors: synthetic lethality in the clinic. *Science* **2017**, *355*, 1152–1158.

(36) Patel, M. R.; Bhatt, A.; Steffen, J. D.; Chergui, A.; Murai, J.; Pommier, Y.; Pascal, J. M.; Trombetta, L. D.; Fronczek, F. R.; Talele, T. T. Discovery and structure−activity relationship of novel 2,3-dihydrobenzofuran-7-carboxamide and 2,3-dihydrobenzofuran-3(2*H*)-one-7-carboxamide derivatives as poly(ADP-ribose)polymerase-1 inhibitors. *J. Med. Chem.* **2014**, *57*, 5579–5601.

(37) Velagapudi, U. K.; Langelier, M.-F.; Delgado-Martin, C.; Diolaiti, M. E.; Bakker, S.; Ashworth, A.; Patel, B. A.; Shao, X.; Pascal, J. M.; Talele, T. T. Design and synthesis of poly(ADP-ribose) polymerase inhibitors: impact of adenosine pocket-binding motif appendage to the 3-oxo-2,3-dihydrobenzofuran-7-carboxamide on potency and selectivity. *J. Med. Chem.* **2019**, *62*, 5330–5357.

(38) Buitrago, E.; Hardré, R.; Haudecoeur, R.; Jamet, H.; Belle, C.; Boumendjel, A.; Bubacco, L.; Réglier, M. Are human tyrosinase and related proteins suitable targets for melanoma therapy? *Curr. Top. Med. Chem.* **2016**, *16*, 3033–3047.

(39) Roulier, B.; Pérès, B.; Haudecoeur, R. Advances in the design of genuine human tyrosinase inhibitors for targeting melanogenesis and related pigmentations. *J. Med. Chem.* **2020**, *63*, 13428–13443.

(40) Okombi, S.; Rival, D.; Bonnet, S.; Mariotte, A.-M.; Perrier, E.; Boumendjel, A. Discovery of benzylidenebenzofuran-3(2*H*)-one (aurones) as inhibitors of tyrosinase derived from human melanocytes. *J. Med. Chem.* **2006**, *49*, 329–333.

(41) Dubois, C.; Haudecoeur, R.; Orio, M.; Belle, C.; Bochot, C.; Boumendjel, A.; Hardré, R.; Jamet, H.; Réglier, M. Versatile effects of aurone structure on mushroom tyrosinase activity. *ChemBioChem* **2012**, *13*, 559–565.

(42) Haudecoeur, R.; Gouron, A.; Dubois, C.; Jamet, H.; Lightbody, M.; Hardré, R.; Milet, A.; Bergantino, E.; Bubacco, L.; Belle, C.; Réglier, M.; Boumendjel, A. Investigation of the binding-site homology of mushroom and bacterial tyrosinases by aurones as effectors. *ChemBioChem* **2014**, *15*, 1325–1333.

(43) Markova, E.; Kotik, M.; Krenkova, A.; Man, P.; Haudecoeur, R.; Boumendjel, A.; Hardré, R.; Mekmouche, Y.; Courvoisier-Dezord, E.; Réglier, M.; Martinkova, L. Recombinant tyrosinase from *Polyporus arcularius*: overproduction in *Escherichia coli*, characterization, and use in a study of aurones as tyrosinase effectors. *J. Agric. Food Chem.* **2016**, *64*, 2925–2931.

(44) Radhakrishnan, S.; Shimmon, R.; Conn, C.; Baker, A. Inhibitory kinetics of novel 2,3-dihydro-1*H*-inden-1-one chalcone-like derivatives on mushroom tyrosinase. *Bioorg. Med. Chem. Lett.* **2015**, *25*, 5495–5499.

(45) Choi, H.; Ryu, I. Y.; Choi, I.; Ullah, S.; Jung, H. J.; Park, Y.; Hwang, Y.; Jeong, Y.; Hong, S.; Chun, P.; Chung, H. Y.; Moon, H. R. Identification of (Z)-2-benzylidene-dihydroimidazothiazolone derivatives as tyrosinase inhibitors: anti-melanogenic effects and *in silico* studies. *Comp. Struct. Biotechnol. J.* **2022**, *20*, 899–912.

(46) Bukhari, S. N. A.; Jantan, I.; Tan, O. U.; Sher, M.; Naeem-ul-Hassan, M.; Qin, H.-L. Biological activity and molecular docking studies of curcumin-related α,β-unsaturated carbonyl-based synthetic compounds as anticancer agents and mushroom tyrosinase inhibitors. *J. Agric. Food Chem.* **2014**, *62*, 5538–5547.

(47) Haudecoeur, R.; Carotti, M.; Gouron, A.; Maresca, M.; Buitrago, E.; Hardré, R.; Bergantino, E.; Jamet, H.; Belle, C.; Réglier, M.; Bubacco, L.; Boumendjel, A. 2-Hydroxypyridine-*N*-oxide-embedded aurones as potent human tyrosinase inhibitors. *ACS Med. Chem. Lett.* **2017**, *8*, 55–60.

(48) Asati, V.; Mahapatra, D. K.; Bharti, S. K. PIM kinase inhibitors: structural and pharmacological perspectives. *Eur. J. Med. Chem.* **2019**, *172*, 95–108.

(49) Tsuganezawa, K.; Watanabe, H.; Parker, L.; Yuki, H.; Taruya, S.; Nakagawa, Y.; Kamei, D.; Mori, M.; Ogawa, N.; Tomabechi, Y.; Handa, N.; Honma, T.; Yokoyama, S.; Kojima, H.; Okabe, T.; Nagano, T.; Tanaka, A. A novel Pim-1 kinase inhibitor targeting residues that bind the substrate peptide. *J. Mol. Biol.* **2012**, *417*, 240–252.

(50) Parker, L. J.; Watanabe, H.; Tsuganezawa, K.; Tomabechi, Y.; Handa, N.; Shirouzu, M.; Yuki, H.; Honma, T.; Ogawa, N.; Nagano, T.; Yokoyama, S.; Tanaka, A. Flexibility of the P-loop of Pim-1 kinase: observation of a novel conformation induced by interaction with an inhibitor. *Acta Cryst.* **2012**, *F68*, 860–866.

(51) Nakano, H.; Saito, N.; Parker, L.; Tada, Y.; Abe, M.; Tsuganezawa, K.; Yokoyama, S.; Tanaka, A.; Kojima, H.; Okabe, T.; Nagano, T. Rational evolution of a novel type of potent and selective proviral integration site in moloney murine leukemia virus kinase 1 (PIM1) inhibitor from a screening-hit compound. *J. Med. Chem.* **2012**, *55*, 5151–5164.

(52) Nakano, H.; Hasegawa, T.; Saito, N.; Furukawa, K.; Mukaida, N.; Kojima, H.; Okabe, T.; Nagano, T. Design and synthesis of an in vivo-efficacious PIM3 kinase inhibitor as a candidate anti-pancreatic cancer agent. *Bioorg. Med. Chem. Lett.* **2015**, *25*, 5687–5693.

(53) Nakano, H.; Hasegawa, T.; Kojima, H.; Okabe, T.; Nagano, T. Design and synthesis of potent and selective PIM kinase inhibitors by targeting unique structure of ATP-binding pocket. *ACS Med. Chem. Lett.* **2017**, *8*, 504–509.

(54) Park, H.; Jeon, J.; Kim, K.; Choi, S.; Hong, S. Structure-based virtual screening and de novo design of PIM1 inhibitors with anticancer activity from natural products. *Pharmaceuticals* **2021**, *14*, 275.

(55) Fujii, N.; You, L.; Xu, Z.; Uematsu, K.; Shan, J.; He, B.; Mikami, I.; Edmondson, L. R.; Neale, G.; Zheng, J.; Guy, R. K.; Jablons, D. M. An antagonist of dishevelled protein-protein interaction suppresses β-catenin–dependent tumor cell growth. *Cancer Res.* **2007**, *67*, 573–579.

(56) Choi, J.; Ma, S.; Kim, H.-Y.; Yun, J.-H.; Heo, J.-N.; Lee, W.; Choi, K.-Y.; No, K. T. Identification of small-molecule compounds targeting the dishevelled PDZ domain by virtual screening and binding studies. *Bioorg. Med. Chem.* **2016**, *24*, 3259–3266.

(57) Altucci, L.; Leibowitz, M. D.; Oglivie, K. M.; de Lera, A. R.; Gronemeyer, RAR and RXR modulation in cancer and metabolic disease. *Nat. Rev. Drug Discov.* **2007**, *6*, 793–810.

(58) Lorenzo, P.; Ortiz, M. A.; Alvarez, R.; Piedrafita, F. J.; de Lera, A. R. Adamantyl arotinoids that inhibit IκB kinase α and IκB kinase β. *ChemMedChem* **2013**, *8*, 1184–1198.

(59) Rajagopalan, P.; Alahmari, K. A.; Elbessoumy, A. A.; Baladubramaniam, M.; Suresh, R.; Shariff, M. E. A.; Chandramoorthy, H. C. Biological evaluation of 2‐arylidene‐4, 7‐dimethyl indan‐1‐one (FXY‐1): a novel Akt inhibitor with potent activity in lung cancer. *Cancer Chemother. Pharmacol.* **2016**, *77*, 393–404.

(60) Balasubramaniam, M.; Lakkaniga, N. R.; Dera, A. A.; Al Fayi, M.; Abohashrh, M.; Ahmad, I.; Chandramoorthy, H. C.; Nalini, G.; Rajagopalan, P. FCX-146, a potent allosteric inhibitor of Akt kinase in cancer cells: Lead optimization of the second-generation arylidene indanone scaffold. *Biotechnol. Appl. Biochem.* **2021**, *68*, 82–91.

(61) Xie, F.; Zhu, H.; Zhang, H.; Lang, Q.; Tang, L.; Huang, Q.; Yu, L. *In vitro* and *in vivo* characterization of a benzofuran derivative, a potential anticancer agent, as a novel Aurora B kinase inhibitor. *Eur. J. Med. Chem.* **2015**, *89*, 310–319.

(62) Nakanishi, I.; Murata, K.; Nagata, N.; Kurono, M.; Kinoshita, T.; Yasue, M.; Miyazaki, T.; Takei, Y.; Nakamura, S.; Sakurai, A.; Iwamoto, N.; Nishiwaki, K.; Nakaniwa, T.; Sekiguchi, Y.; Hirasawa, A.; Tsujimoto, G.; Kitaura, K. Identification of protein kinase CK2 inhibitors using solvent dipole ordering virtual screening. *Eur. J. Med. Chem.* **2015**, *96*, 396–404.

(63) Park, H.; Lee, S.; Hong, S. Discovery of dual inhibitors for wild type and D816V mutant of c‐KIT kinase through virtual and biochemical screening of natural products. *J. Nat. Prod.* **2016**, *79*, 293–299.

(64) Protopopov, M. V.; Vdovin, V. S.; Starosyla, S. A.; Borysenko, I. P.; Prykhod'ko, A. O.; Lukashov, S. S.; Bilokin, Y. V.; Bdzhola, V. G.; Yarmoluk, S. M. Flavone inspired discovery of benzylidenebenzofuran-3(2*H*)-ones (aurones) as potent inhibitors of human protein kinase CK2. *Bioorg. Chem.* **2020**, *102*, 104062.

(65) Zwick, V.; Chatzivasileiou, A.-O.; Deschamps, N.; Roussaki, M.; Simões-Pires, C. A.; Nurisso, A.; Denis, I.; Blanquart, C.; Martinet, N.; Carrupt, P.-A.; Detsi, A.; Cuendet, M. Aurones as histone deacetylase inhibitors: identification of key features. *Bioorg. Med. Chem. Lett.* **2014**, *24*, 5497–5501.

(66) Itoh, Y.; Suzuki, M.; Matsui, T.; Ota, Y.; Hui, Z.; Tsubaki, K.; Suzuki, T. False HDAC inhibition by aurone compound. *Chem. Pharm. Bull.* **2016**, *64*, 1124–1128.

(67) Kumboonma, P.; Senawong, T.; Saenglee, S.; Yenjai, C.; Phaosiri, C. New histone deacetylase inhibitors from the twigs of *Melanorrhoea usitata*. *Med. Chem. Res.* **2018**, *27*, 2004–2015.

(68) Manjulatha, K.; Srinivas, S.; Mulakayala, N.; Rambabu, D.; Prabhakar, M.; Arunasree, K. M.; Alvala, M.; Basaveswara, Rao, M. V.; Pal, M. Ethylenediamine diacetate (EDDA) mediated synthesis of aurones under ultrasound: their evaluation as inhibitors of SIRT1. *Bioorg. Med. Chem. Lett.* **2012**, *22*, 6160–6165.

(69) Zakharova, O.; Luzina, O.; Zakharenko, A.; Sokolov, D.; Filimonov, A.; Dyrkheeva, N.; Chepanova, A.; Ilina, E.; Ilyina, A.; Klabenkova, K.; Chelobanov, B.; Stetsenko, D.; Zafar, A.; Eurtivong, C.; Reynisson, J.; Volcho, K.; Salakhutdinov, N.; Lavrik, O. Synthesis and evaluation of aryliden- and hetarylidenfuranone derivatives of usnic acid as highly potent Tdp1 inhibitors. *Bioorg. Med. Chem.* **2018**, *26*, 4470–4480.

(70) Diveshkumar, K. V.; Sakrikar, S.; Rosu, F.; Harikrishna, S.; Gabelica, V.; Pradeepkumar, P. I. Specific stabilization of c-MYC and c-KIT G-quadruplex DNA structures by indolylmethyleneindanone scaffolds. *Biochemistry* **2016**, *55*, 3571–3585.

(71) Tugrak, M.; Yamali, C.; Sakagami, H.; Gul, H. I. Synthesis of mono Mannich bases of 2-(4-hydroxybenzylidene)-2,3-dihydroinden-1-one and evaluation of their cytotoxicities. *J. Enzyme Inhib. Med. Chem.* **2016**, *31*, 818–823.

(72) Tugrak, M.; Gul, H. I.; Sakagami, H.; Mete, E. Synthesis and anticancer properties of mono Mannich bases containing vanillin moiety. *Med. Chem. Res.* **2017**, *26*, 1528–1534.

(73) Gul, H. I.; Tugrak, M.; Gul, M.; Mazlumoglu, S.; Sakagami, H.; Gulcin, I.; Supuran, C. T. New phenolic Mannich bases with piperazines and their bioactivities. *Bioorg. Chem.* **2019**, *90*, 103057.

(74) Tugrak, M.; Gul, H. I.; Bandow, K.; Sakagami, H.; Gulcin, I.; Ozkay, Y.; Supuran, C. T. Synthesis and biological evaluation of some new mono Mannich bases with piperazines as possible anticancer agents and carbonic anhydrase inhibitors. *Bioorg. Chem.* **2019**, *90*, 103095.

(75) Tiwari, K. N.; Monserrat, J.-P.; Hequet, A.; Ganem-Elbaz, C.; Cresteil, T.; Jaouen, G.; Vessières, A.; Hillard, E. A.; Jolivalt, C. *In vitro* inhibitory properties of ferrocene-substituted chalcones and aurones on bacterial and human cell cultures. *Dalton Trans.* **2012**, *41*, 6451–6457.

(76) Shaik, A. B.; Rao, G. K.; Kumar, G. B.; Patel, N.; Reddy, V. S.; Khan, I.; Routhu, S. R.; Kumar, C. G.; Veena, I.; Shekar, K. C.; Barkume, M.; Jadhav, S.; Juvekar, A.; Kode, J.; Pal-Bhadra, M.; Kamal, A. Design, synthesis and biological evaluation of novel pyrazolochalcones as potential modulators of PI3K/Akt/mTOR pathway and inducers of apoptosis in breast cancer cells. *Eur. J. Med. Chem.* **2017**, *139*, 305–324.

(77) Gao, X.-M.; Yang, L.-Y.; Huang, X.-Z.; Shu, L.-D.; Shen, Y.-Q.; Hu, Q.-F.; Chen, Z.-Y. Aurones and isoaurones from the flowers of Rosa damascene and their biological activities. *Heterocycles* **2013**, *87*, 583–589.

(78) Hu, Q.; Meng, Y.; Yao, J.; Qin, Y.; Yang, Z.; Zhao, G.; Yang, Z.; Gao, X.; Li, T. Flavonoids from *Garcinia paucinervis* and their biological activities. *Chem. Nat. Comp.* **2014**, *50*, 994–997.

(79) Wang, H.; Yang, J.-X.; Lou, J.; Li, L.; Liu, G.-Y.; Hu, Q.-F.; Ye, Y.-Q.; Gao, X.-M. A new isoprenylated aurone from the flowers of *Rosa damascene* and Its cytotoxicities. *Asian J. Chem.* **2014**, *26*, 7122–7124.

(80) Paidakula, S.; Nerella, S.; Vadde, R.; Kamal, A.; Kankala, S. Design and synthesis of 4β-acetamidobenzofuranone-podophyllotoxin hybrids and their anti-cancer evaluation. *Bioorg. Med. Chem. Lett.* **2019**, *29*, 2153–2156.

(81) Ragab, F. A.; Yahya, T. A. A.; El-Naa, M. M.; Arafa, R. K. Design, synthesis and structure-activity relationship of novel semisynthetic flavonoids as antiproliferative agents. *Eur. J. Med. Chem.* **2014**, *82*, 506–520.

(82) Lozano-Gonzalez, M.; Ramirez-Apan, M. T.; Nieto-Camacho, A.; Toscano, R. A.; Sanchez-Sandoval, A. L.; Alvarez-Toledano, C. Anticarcinogenic and metal chelation properties of novel hydroxybenzylidene-1-indanone derivatives in the U-251 glioblastoma cell line. *New. J. Chem.* **2018**, *42*, 3878–3884.

(83) Popova, A. V.; Frasinyuk, M. S.; Bondarenko, S. P.; Zhang, W.; Xie, Y.; Martin, Z. M.; Cai, X.; Fiandalo, M. V.; Mohler, J. L.; Liu, C.; Watt, D. S.; Sviripa, V. M. Efficient synthesis of aurone Mannich bases and evaluation of their antineoplastic activity in PC-3 prostate cancer cells. *Chem. Papers* **2018**, *72*, 2443–2456.

(84) Huang, L.; Lu, C.; Sun, Y.; Mao, F.; Luo, Z.; Su, T.; Jiang, H.; Shan, W.; Li, X. Multitarget-directed benzylideneindanone derivatives: anti-β-amyloid (Aβ) aggregation, antioxidant, metal chelation, and monoamine oxidase B (MAO-B) inhibition properties against Alzheimer's disease. *J. Med. Chem.* **2012**, *55*, 8483–8492.

(85) Geldenhuys, W. J.; Funk, M. O.; Van der Schyf, C. J.; Carroll, R. T. A scaffold hopping approach to identify novel monoamine oxidase B inhibitors. *Bioorg. Med. Chem. Lett.* **2012**, *22*, 1380–1383.

(86) Li, Y.; Qiang, X.; Luo, L.; Li, Y.; Xiao, G.; Tan, Z.; Deng, Y. Synthesis and evaluation of 4-hydroxyl aurone derivatives as multifunctional agents for the treatment of Alzheimer's disease. *Bioorg. Med. Chem.* **2016**, *24*, 2342–2351.

(87) Baek, S. C.; Lee, H. W.; Ryu, H. W.; Kang, M.-G.; Park, D.; Kim, S. H.; Cho, M.-L.; Oh, S.-R.; Kim, H. Selective inhibition of monoamine oxidase A by hispidol. *Bioorg. Med. Chem. Lett.* **2018**, *28*, 584–588.

(88) Badavath, V. N.; Nath, C.; Ganta, N. M.; Ucar, G.; Sinha, B. N.; Jayaprakash, V. Design, synthesis and MAO inhibitory activity of 2-(arylmethylidene)-2,3-dihydro-1-benzofuran-3-one derivatives. *Chin. Chem. Lett.* **2017**, *28*, 1528–1532.

(89) Nel, M. S.; Petzer, A.; Petzer, J. P.; Legoabe, L. J. 2-Heteroarylidene-1-indanone derivatives as inhibitors of monoamine oxidase. *Bioorg. Chem.* **2016**, *69*, 20–28.

(90) Nel, M. S.; Petzer, A.; Petzer, J. P.; Legoabe, L. J. 2-Benzylidene-1-indanone derivatives as inhibitors of monoamine oxidase. *Bioorg. Med. Chem. Lett.* **2016**, *26*, 4599–4605.

(91) Affini, A.; Hagenow, S.; Zivkovic, A.; Marco-Contelles, J.; Stark, H. Novel indanone derivatives as MAO B/H_3R dual-targeting ligands for treatment of Parkinson's disease. *Eur. J. Med. Chem.* **2018**, *148*, 487–497.

(92) Guglielmi, P.; Secci, D.; Petzer, A.; Bagetta, D.; Chimenti, P.; Rotondi, G.; Ferrante, C.; Recinella, L.; Leone, S.; Alcaro, S.; Zengin, G.; Petzer, J. P.; Ortuso, F.; Carradori, S. Benzo[*b*]thiophen-3-ol derivatives as effective inhibitors of human monoamine oxidase: design, synthesis, and biological activity. *J. Enz. Inhib. Med. Chem.* **2019**, *34*, 1511–1525.

(93) Wang, K.; Yu, L.; Shi, J.; Liu, W.; Sang, Z. Multifunctional indanone–chalcone hybrid compounds with anti-β-amyloid (Aβ) aggregation, monoamine oxidase B (MAO-B) inhibition and neuroprotective properties against Alzheimer's disease. *Med. Chem. Res.* **2019**, *28*, 1912–1922.

(94) Takao, K.; U, S.; Kamauchi, H.; Sugita, Y. Design, synthesis and evaluation of 2-(indolylmethylidene)-2,3-dihydro-1-benzofuran-3-one and 2-(indolyl)-4*H*-chromen-4-one derivatives as novel monoamine oxidases inhibitors. *Bioorg. Chem.* **2019**, *87*, 594–600.

(95) Lan, J.-S.; Zhang, T.; Liu, Y.; Yang, J.; Xie, S.-S.; Liu, J.; Miao, Z.-Y.; Ding, Y. Design, synthesis and biological activity of novel donepezil derivatives bearing *N*-benzyl pyridinium moiety as potent and dual binding site acetylcholinesterase inhibitors. *Eur. J. Med. Chem.* **2017**, *133*, 184–196.

(96) Nadri, H.; Pirali-Hamedani, M.; Moradi, A.; Sakhteman, A.; Vahidi, A.; Sheibani, V.; Asadipour, A.; Hosseinzadeh, N.; Abdollahi, M.; Shafiee, A.; Foroumadi, A. 5,6-Dimethoxybenzofuran-3-one derivatives: a novel series of dual acetylcholinesterase/butyrylcholinesterase inhibitors bearing benzyl pyridinium moiety. *DARU J. Pharm. Sci.* **2013**, *21*, 15.

(97) Alipour, M.; Khoobi, M.; Nadri, H.; Sakhteman, A.; Moradi, A.; Ghandi, M.; Foroumadi, A.; Shafiee, A. Synthesis of some new 3-coumaranone and coumarin derivatives as dual inhibitors of acetyl- and butyrylcholinesterase. *Arch. Pharm. Chem. Life Sci.* **2013**, *346*, 577–587.

(98) Meng, F.-C.; Mao, F.; Shan, W.-J.; Qin, F.; Huang, L.; Li, X.-S. Design, synthesis, and evaluation of indanone derivatives as acetylcholinesterase inhibitors and metal-chelating agents. *Bioorg. Med. Chem. Lett.* **2012**, *22*, 4462–4466.

(99) Huang, L.; Miao, H.; Sun, Y.; Meng, F.; Li, X. Discovery of indanone derivatives as multi-target-directed ligands against Alzheimer's disease. *Eur. J. Med. Chem.* **2014**, *87*, 429–439.

(100) Lee, Y. H.; Shin, M. C.; Yun, Y. D.; Shin, S. Y.; Kim, J. M.; Seo, J. M.; Kim, N.-J.; Ryu, J. H.; Lee, Y. S. Synthesis of aminoalkyl-substituted aurone derivatives as acetylcholinesterase inhibitors. *Bioorg. Med. Chem.* **2015**, *23*, 231–240.

(101) Liew, K.-F.; Chan, K.-L.; Lee, C.-Y. Blood-brain barrier permeable anticholinesterase aurones: synthesis, structure-activity relationship, and drug-like properties. *Eur. J. Med. Chem.* **2015**, *94*, 195–210.

(102) Mozaffarnia, S.; Parsaee, F.; Payami, E.; Karami, H.; Soltani, S.; Rashidi, M.-R.; Teimuri-Mofrad, R. Design, synthesis and biological assessment of novel 2-(4-alkoxybenzylidine)-2,3-dihydro-5,6-dimethoxy-1*H*-inden-1-one derivatives as hAChE and hBuChE enzyme inhibitors. *ChemistrySelect* **2019**, *4*, 9376–9380.

(103) Li, Y.; Qiang, X.; Luo, L.; Yang, X.; Xiao, G.; Liu, Q.; Ai, J.; Tan, Z.; Deng, Y. Aurone Mannich base derivatives as promising multifunctional agents with acetylcholinesterase inhibition, anti-*β*-amyloid aggregation and neuroprotective properties for the treatment of Alzheimer's disease. *Eur. J. Med. Chem.* **2017**, *126*, 762–775.

(104) Saglik, B. N.; Ilgin, S.; Özkay, Y. Synthesis of new donepezil analogues and investigation of their effects on cholinesterase enzymes. *Eur. J. Med. Chem.* **2016**, *124*, 1026–1040.

(105) Mishra, C. B.; Kumari, S.; Manral, A.; Prakash, A.; Saini, V.; Lynn, A. M.; Tiwari, M. Design, synthesis, in-silico and biological evaluation of novel donepezil derivatives as multi-target-directed ligands for the treatment of Alzheimer's disease. *Eur. J. Med. Chem.* **2017**, *125*, 736–750.

(106) Mozaffarnia, S.; Teimuri-Mofrad, R.; Rashidi, M.-R. Design, synthesis and biological evaluation of 2,3-dihydro-5,6-dimethoxy-1*H*-inden-1-one and piperazinium salt hybrid derivatives as hAChE and hBuChE enzyme inhibitors. *Eur. J. Med. Chem.* **2020**, *191*, 112140.

(107) Mughal, E. U.; Sadiq, A.; Murtaza, S.; Rafique, H.; Zafar, M. N.; Riaz, T.; Khan, B. A.; Hameed, A.; Khan, K. M. Synthesis, structure–activity relationship and molecular docking of 3-oxoaurones and 3-thioaurones as acetylcholinesterase and butyrylcholinesterase inhibitors. *Bioorg. Med. Chem.* **2017**, *25*, 100–106.

(108) Gabr, M. T.; Abdel-Raziq, M. S. Structure-based design, synthesis, and evaluation of structurally rigid donepezil analogues as dual AChE and BACE-1 inhibitors. *Bioorg. Med. Chem. Lett.* **2018**, *28*, 2910–2913.

(109) Shahrivar-Gargari, M.; Hamzeh-Mivehroud, M.; Hemmati, S.; Mojarrad, J. S.; Notash, B.; Kücükkilinc, T. T.; Ayazgök, B.; Dastmalchi, S. Design, synthesis, and biological evaluation of novel indanone-based hybrids as multifunctional cholinesterase inhibitors for Alzheimer's disease. *J. Mol. Struct.* **2021**, *1229*, 129787.

(110) Churches, Q. I.; Caine, J.; Cavanagh, K.; Chandana Epa, V.; Waddington, L.; Tranberg, C. E.; Meyer, A. G.; Varghese, J. N.; Streltsov, V.; Duggan, P. J. Naturally occurring polyphenolic inhibitors of amyloid beta aggregation. *Bioorg. Med. Chem. Lett.* **2014**, *24*, 3108–3112.

(111) Rampa, A.; Mancini, F.; De Simone, A.; Falchi, F.; Belluti, F.; Di Martino, R. M. C.; Gobbi, S.; Andrisano, V.; Tarozzi, A.; Bartolini, M.; Cavalli, A.; Bisi, A. From AChE to BACE1 inhibitors: the role of the amine on the indanone scaffold. *Bioorg. Med. Chem. Lett.* **2015**, *25*, 2804–2808.

(112) Lunven, L.; Bonnet, H.; Yahiaoui, S.; Yi, W.; Da Costa, L.; Peuchmaur, M.; Boumendjel, A.; Chierici, S. Disruption of fibers from the tau model AcPHF6 by naturally occurring aurones and synthetic analogues. *ACS Chem. Neurosci.* **2016**, *7*, 995–1003.

(113) Boukherrouba, E.; Larosa, C.; Nguyen, K.-A.; Caburet, J.; Lunven, L.; Bonnet, H.; Fortuné, A.; Boumendjel, A.; Boucherle, B.; Chierici, S.; Peuchmaur, M. Exploring the structure-activity relationship of benzylidene-2,3-dihydro-1*H*-inden-1-one compared to benzofuran-3(2*H*)-one derivatives as inhibitors of tau amyloid fibers. *Eur. J. Med. Chem.* **2022**, *231*, 114139.

(114) Kobayashi, H.; Nishimura, H.; Kudo, N.; Osada, H.; Yoshida, M. A novel GSK3 inhibitor that promotes self-renewal in mouse embryonic stem cells. *Biosci. Biotechnol. Biochem.* **2020**, *84*, 2113–2120.

(115) Qhobosheane, M. A.; Beteck, R. M.; Baratte, B.; Robert, T.; Ruchaud, S.; Bach, S.; Legoabe, L. J. Exploration of 7-azaindole-coumaranone hybrids and their analogues as protein kinase inhibitors. *Chem. Biol. Interact.* **2021**, *343*, 109478.

(116) Watanabe, H.; Ono, M.; Kimura, H.; Matsumura, K.; Yoshimura, M.; Okamoto, Y.; Ihara, M.; Takahashi, R.; Saji, H. Synthesis and biological evaluation of novel oxindole derivatives for imaging neurofibrillary tangles in Alzheimer's disease. *Bioorg. Med. Chem. Lett.* **2012**, *22*, 5700–5703.

(117) Qiao, J.-P.; Gan, C.-S.; Wang, C.-W.; Ge, J.-F.; Nan, D.-D.; Pan, J.; Zhou, J.-N. Novel indanone derivatives as potential imaging probes for β-amyloid plaques in the brain. *ChemBioChem* **2012**, *1*3, 1652–1662.

(118) Nan, D.-D.; Gan, C.-S.; Wang, C.-W.; Qiao, J.-P.; Wang, X.-M.; Zhou, J.-N. 6-Methoxy-indanone derivatives as potential probes for β-amyloid plaques in Alzheimer's disease. *Eur. J. Med. Chem.* **2016**, *124*, 117–128.

(119) Sun, X.; Admane, P.; Starosolski, Z. A.; Eriksen, J. L.; Annapragada, A. V.; Tanifum, E. A. 1-Indanone and 1,3-indandione derivatives as ligands for misfolded α-synuclein aggregates. *ChemMedChem* **2022**, *17*, e202100611.

(120) Shrestha, S.; Natarajan, S.; Park, J.-H.; Lee, D.-Y.; Cho, J.-G.; Kim, G.-S.; Jeon, Y.-J.; Yeon, S.-W.; Yang, D.-C.; Baek, N.-I. Potential neuroprotective flavonoid-based inhibitors of CDK5/p25 from *Rhus parviflora*. *Bioorg. Med. Chem. Lett.* **2013**, *23*, 5150–5154.

(121) Shrestha, S.; Lee, D.-Y.; Park, J.-H.; Cho, J.-G.; Lee, D.-S.; Li, B.; Kim, Y.-C.; Jeon, Y.-J.; Yeon, S.-W.; Baek, N.-I. Flavonoids from the fruits of Nepalese sumac (*Rhus parviflora*) attenuate glutamate-induced neurotoxicity in HT22 cells. *Food Sci. Biotechnol.* **2013**, *22*, 895–902.

(122) Yang, E.-J.; Kim, M.; Woo, J. E.; Lee, T.; Jung, J.-W.; Song, K.-S. The comparison of neuroprotective effects of isoliquiritigenin and its Phase I metabolites against glutamate-induced HT22 cell death. *Bioorg. Med. Chem. Lett.* **2016**, *26*, 5639–5643.

(123) Seo, Y. H.; Trinh, T. A.; Ryu, S. M.; Kim, H. S.; Choi, G.; Moon, B. C.; Shim, S. H.; Jang, D. S.; Lee, D.; Kang, K. S.; Lee, J. Chemical constituents from the aerial parts of *Elsholtzia ciliata* and their protective activities on glutamate-induced HT22 cell death. *J. Nat. Prod.* **2020**, *83*, 3149–3155.

(124) Kwon, S.-H.; Ma, S.-X.; Lee, S.-Y.; Jang, C.-G. Sulfuretin inhibits 6-hydroxydopamine-induced neuronal cell death via reactive oxygen species-dependent mechanisms in human neuroblastoma SH-SY5Y cells. *Neurochem. Int.* **201**4, *74*, 53–64.

(125) Kwon, S.-H.; Ma, S.-X.; Hwang, J.-Y.; Lee, S.-Y.; Jang, C.-G. Involvement of the Nrf2/HO-1 signaling pathway in sulfuretin-induced protection against amyloid beta$_{25–35}$ neurotoxicity. *Neuroscience* **2015**, *304*, 14–28.

(126) Pariyar, R.; Lamichhane, R.; Jung, H. J.; Kim, S. Y.; Seo, J. Sulfuretin attenuates MPP+-induced neurotoxicity through Akt/GSK3β and ERK signaling pathways. *Int. J. Mol. Sci.* **2017**, *18*, 2753.

(127) Lee, S. H.; Han, Y. T.; Cha, D. S. Neuroprotective effect of damaurone D in a *C. elegans* model of Parkinson's disease. *Neurosci. Lett.* **2021**, *747*, 135623.

(128) Ma, Q.; Wei, R.; Sang, Z. Neuroprotective aurones from *Sophora japonica*. *Chem. Nat. Comp.* **2019**, *55*, 265–268.

(129) Li, H.; Li, X.; Luo, W.; Zhu, X. (*Z*)-7,4'-Dimethoxy-6-hydroxy-aurone-4-O-*β*-glucopyranoside exerts neuroprotective effects *in vitro* and anxiolytic activity *in vivo*. *NeuroReport* **2019**, *30*, 280–287.

(130) Oh, J. M.; Lee, H.-S.; Baek, S. C.; Lee, J. P.; Jeong, G. S.; Paik, M.-J.; Kim, H. Antidepressant-like activities of hispidol and decursin in mice and analysis of neurotransmitter monoamines. *Neurochem. Res.* **2020**, *45*, 1930–1940.

(131) Jardosh, H. H.; Patel, M. P. Antimicrobial and antioxidant evaluation of new quinolone based aurone analogs. *Arab. J. Chem.* **2017**, *10*, S3781–S3791.

(132) Kumar, G.; Lathwal, E.; Saroha, B.; Kumar, S.; Kumar, S.; Chauhan, N. S.; Kumar, T. Synthesis and biological evaluation of quinoline-based novel aurones. *ChemistrySelect* **2020**, *5*, 3539–3543.

(133) Pervaram, S.; Ashok, D.; Reddy, C. V. R.; Sarasija, M.; Rao, B. A. Synthesis and antimicrobial activity of (*Z*)-3-{[3-oxobenzofuran-2(3*H*)-ylidene]methyl}-4*H*-chromen-4-one derivatives. *Russ. J. Gen. Chem.* **2018**, *88*, 566–572.

(134) Ashok, D.; Rangu, K.; Gundu, S.; Lakkadi, A.; Tigulla, P. Microwave-assisted synthesis, molecular docking, and biological evaluation of 2-arylidene-2*H*-furo[2,3-*f*]chromen-3(7*H*)-ones as antioxidant and antimicrobial agents. *Med. Chem. Res.* **2017**, *26*, 1735–1746.

(135) Ashok, D.; Ziauddin, M.; Lakshmi, B. V.; Sarasija, M. Microwave assisted synthesis of substituted (*Z*)-2-{[1-phenyl-3-(thiophen-2-yl)-1*H*-pyrazol-4-yl]methylene}benzofuran-3(2*H*)-ones and their antimicrobial activity. *Russ. J. Gen. Chem.* **2016**, *86*, 1753–1757.

(136) Olleik, H.; Yahiaoui, S.; Roulier, B.; Courvoisier-Dezord, E.; Perrier, J.; Pérès, B.; Hijazi, A.; Baydoun, E.; Raymond, J.; Boumendjel, A.; Maresca, M.; Haudecoeur, R. Aurone derivatives as promising antibacterial agents against resistant Gram-positive pathogens. *Eur. J. Med. Chem.* **2019**, *165*, 133–141.

(137) Reynolds, R. C.; Ananthan, S.; Faaleolea, E.; Hobrath, J. V.; Kwong, C. D.; Maddox, C.; Rasmussen, L.; Sosa, M. I.; Thammasuvimol, E.; White, E. L.; Zhang, W.; Secrist III, J. A. High throughput screening of a library based on kinase inhibitor scaffolds against *Mycobacterium tuberculosis* H37Rv. *Tuberculosis* **2012**, *92*, 72–83.

(138) Campaniço, A.; Carrasco, M. P.; Njoroge, M.; Seldon, R.; Chibale, K.; Perdigão, J.; Portugal, I.; Warner, D. F.; Moreira, R.; Lopes, F. Azaaurones as potent antimycobacterial agents active against MDR- and XDR-TB. *ChemMedChem* **2019**, *14*, 1537–1546.

(139) Perna, A. M.; Rodrigues, T.; Schmidt, T. P.; Böhm, M.; Stutz, K.; Reker, D.; Pfeiffer, B.; Altmann, K.-H.; Backert, S.; Wessler, S.; Schneider, G. Fragment-based de novo design reveals a small-molecule inhibitor of *Helicobacter pylori* HtrA. *Angew. Chem. Int. Ed.* **2015**, *54*, 10244–10248.

(140) Sutton, C. L.; Taylor, Z. E.; Farone, M. B.; Handy, S. T. Antifungal activity of substituted aurones. *Bioorg. Med. Chem. Lett.* **2017**, *27*, 901–903.

(141) Adole, V. A.; More, R. A.; Jagdale, B. S.; Pawar, T. B.; Chobe, S. S.; Shinde, R. A.; Dhonnar, S. L.; Koli, P. B.; Patil, A. V.; Bukane, A. R.; Gacche, R. N. Microwave prompted solvent-free synthesis of new series of heterocyclic tagged 7-arylidene indanone hybrids and their computational, antifungal, antioxidant, and cytotoxicity study. *Bioorg. Chem.* **2021**, *115*, 105259.

(142) Fedorova, O.; Jagdmann, G. E. Jr.; Adams, R. L.; Yuan, L.; Van Zandt, M. C.; Pyle, A. M. Small molecules that target group II introns are potent antifungal agents. *Nat. Chem. Biol.* **2018**, *14*, 1073–1078.

(143) Carrasco, M. P.; Newton, A. S.; Gonçalves, L.; Gois, A.; Machado, M.; Gut, J.; Nogueira, F.; Hänscheid, T.; Guedes, R. C.; dos Santos, D. J. V. A.; Rosenthal, P. J.; Moreira, R. Probing the aurone scaffold against *Plasmodium falciparum*: design, synthesis and antimalarial activity. *Eur. J. Med. Chem.* **2014**, *80*, 523–534.

(144) Morimoto, M.; Cantrell, C. L.; Khan, S.; Tekwani, B. L.; Duke, S. O. Antimalarial and antileishmanial activities of phytophenolics and their synthetic analogues. *Chem. Biodiversity* **2017**, *14*, e1700324.

(145) Carrasco, M. P.; Machado, M.; Gonçalves, L.; Sharma, M.; Gut, J.; Lukens, A. K.; Wirth, D. F.; André, V.; Duarte, M. T.; Guedes, R. C.; dos Santos, D. J. V. A.; Rosenthal, P. J.; Mazitschek, R.; Prudêncio, M.; Moreira, R. Probing the azaaurone scaffold against the hepatic and erythrocytic stages of malaria parasites. *ChemMedChem* **2016**, *11*, 2194–2204.

(146) Sharma, M. C.; Sharma, S.; Sharma, P.; Kumar, A. Pharmacophore and QSAR modeling of some structurally diverse azaaurones derivatives as anti-malarial activity. *Med. Chem. Res.* **2014**, *23*, 181–198.

(147) Hadni, H.; Elhallaoui, M. 2D and 3D-QSAR, molecular docking and ADMET properties *in silico* studies of azaaurones as antimalarial agents. *New. J. Chem.* **2020**, *44*, 6553–6565.

(148) Roussaki, M.; Costa Lima, S.; Kypreou, A.-M.; Kefalas, P.; Cordeiro da Silva, A.; Detsi, A. Aurones: a promising heterocyclic scaffold for the development of potent antileishmanial agents. *Int. J. Med. Chem.* **2012**, 196921.

(149) Manzano, J. I.; Lecerf-Schmidt, F.; Lespinasse, M.-A.; Di Pietro, A.; Castanys, S.; Boumendjel, A.; Gamarro, F. Identification of specific reversal agents for *Leishmania* ABCI4-mediated antimony resistance by flavonoid and trolox derivative screening. *J. Antimicrob. Chemother.* **2014**, *69*, 664–672.

(150) Touquet, B.; Pelissier, L.; Cavailles, P.; Yi, W.; Bellini, V.; Mercier, C.; Cesbron-Delauw, M.-F.; Boumendjel, A.; Aldebert, D. High-content imaging assay to evaluate *Toxoplasma gondii* infection and proliferation: a multiparametric assay to screen new compounds. *PLoS One* **2018**, *13*, e0201678.

(151) Saucedo-Mendiola, M. L.; Salas-Pacheco, J. M.; Najera, H.; Rojo-Dominguez, A.; Yepez-Mulia, L.; Avitia-Dominguez, C.; Tellez-Valencia, A. Discovery of *Entamoeba histolytica* hexokinase 1 inhibitors through homology modeling and virtual screening. *J. Enz. Inhib. Med. Chem.* **2014**, *29*, 325–332.

(152) Xiao, C.-J.; Zhang, Y.; Qiu, L.; Dong, X.; Jiang, B. Schistosomicidal and antioxidant flavonoids from *Astragalus englerianus*. *Planta Med.* **2014**, *80*, 1727–1731.

(153) Silva Torres, D.; de Oliveira, B. A.; da Silveira, L. S.; Silva, M. P.; Pereira, V. R. D.; Moraes, J.; Couri, M. R. C.; Queiroz, R. F. G.; Parreiras, P. M.; Silva, M. R.; Alves, L. A.; de Souza, V. C.; Goliatt, P. V. Z. C.; Vasconcelos, E. G.; da Silva Filho, A. A.; Pinto, P. F. Synthetic aurones: new features for *Schistosoma mansoni* therapy. *Chem. Biodiversity* **2021**, *18*, e2100439.

(154) Pereira, V. R. D.; da Silveira, L. S.; Mengarda, A. C.; Alves Junior, I. J.; da Silva, O. O. Z.; Miguel, F. B.; Silva, M. P.; Almeida, A. C.; da Silva Torres, D.; Pinto, P. F.; Coimbra, E. S.; Moraes, J.; Couri, M.

R. C.; da Silva Filho, A. A. Antischistosomal properties of aurone derivatives against juvenile and adult worms of *Schistosoma mansoni*. *Acta Tropica* **2021**, *213*, 105741.

(155) Beteck, R. M.; Legoabe, L. J.; Isaacs, M.; Hoppe, H. C. In vitro anti-trypanosomal activities of indanone-based chalcones. *Drug Res.* **2019**, *69*, 337–341.

(156) Shtro, A. A.; Zarubaev, V. V.; Luzina, O. A.; Sokolov, D. N.; Kiselev, O. I.; Salakhutdinov, N. F. Novel derivatives of usnic acid effectively inhibiting reproduction of influenza A virus. *Bioorg. Med. Chem.* **2014**, *22*, 6826–2836.

(157) Chintakrindi, A. S.; Gohil, D. J.; Chowdhary, A. S.; Kanyalkar, M. A. Design, synthesis and biological evaluation of substituted flavones and aurones as potential anti-influenza agents. *Bioorg. Med. Chem.* **2020**, *28*, 115191.

(158) Zhong, Z. J.; Cheng, L. P.; Pang, W.; Zheng, X. S.; Fu, S. K. Design, synthesis and biological evaluation of dihydrofurocoumarin derivatives as potent neuraminidase inhibitors. *Bioorg. Med. Chem. Lett.* **2021**, *37*, 127839.

(159) Cole, A. L.; Hossain, S.; Cole, A. M.; Phanstiel, O. Synthesis and bioevaluation of substituted chalcones, coumaranones and other flavonoids as anti-HIV agents. *Bioorg. Med. Chem.* **2016**, *24*, 2768–2776.

(160) Geng, C.-A.; Huang, X.-Y.; Ma, Y.-B.; Zhang, X.-M.; Chen, J.-J. Synthesis of erythrocentaurin derivatives as a new class of hepatitis B virus inhibitors. *Bioorg. Med. Chem. Lett.* **2015**, *25*, 1568–1571.

(161) Meguellati, A.; Ahmed-Belkacem, A.; Yi, W.; Haudecoeur, R.; Crouillère, M.; Brillet, R.; Pawlotsky, J.-M.; Boumendjel, A.; Peuchmaur, M. B-ring modified aurones as promising allosteric inhibitors of hepatitis C virus RNA-dependent RNA polymerase. *Eur. J. Med. Chem.* **2014**, *80*, 579-592.

(162) Meguellati, A.; Ahmed-Belkacem, A.; Nurisso, A.; Yi, W.; Brillet, R.; Berqouch, N.; Chavoutier, L.; Fortuné, A.; Pawlotsky, J.-M.; Boumendjel, A.; Peuchmaur, M. New pseudodimeric aurones as palm pocket inhibitors of Hepatitis C virus RNA-dependent RNA polymerase. *Eur. J. Med. Chem.* **2016**, *115*, 217–229.

(163) Kang, S. Y.; Kang, J.-Y.; Oh, M.-J. Antiviral activities of flavonoids isolated from the bark of *Rhus verniciflua* Stokes against fish pathogenic viruses *in vitro*. *J. Microbiol.* **2012**, *50*, 293–300.

(164) Park, H. S.; Nelson, D. E.; Taylor, Z. E.; Hayes, J. B.; Cunningham, K. D.; Arivett, B. A.; Ghosh, R.; Wolf, L. C.; Taylor, K. M.; Farone, M. B.; Handy, S. T.; Farone, A. L. Suppression of LPS-induced NF-κB activity in macrophages by the synthetic aurone, (Z)-2-((5-(hydroxymethyl) furan-2-yl)methylene) benzofuran-3(2H)-one. *Int. Immunopharmacol.* **2017**, *43*, 116–128.

(165) Ren, J.; Su, D.; Li, L.; Cai, H.; Zhang, M.; Zhai, J.; Li, M.; Wu, X.; Hu, K. Anti-inflammatory effects of aureusidin in LPS-stimulated RAW264.7 macrophages via suppressing NF-κB and activating ROS- and MAPKs-dependent Nrf2/HO-1 signaling pathways. *Toxicol. Appl. Pharmacol.* **2020**, *387*, 114846.

(166) Han, Y. T.; Wang, Z.; Bae, E. J. Synthesis of the proposed structure of damaurone D and evaluation of its anti-inflammatory activity. *Chem. Pharm. Bull.* **2015**, *63*, 907–912.

(167) Wang, Z.; Bae, E. J.; Han, Y. T. Synthesis and anti-inflammatory activities of novel dihydropyranoaurone derivatives. *Arch. Pharm. Res.* **2017**, *40*, 695–703.

(168) Boggu, P. R.; Cho, J.; Kim, Y.; Jung, S.-H. Identification of novel 2-benzyl-1-indanone analogs as interleukin-5 inhibitors. *Eur. J. Med. Chem.* **2018**, *152*, 65–75.

(169) Bukhari, S. N. A.; Lauro, G.; Jantan, I.; Bifulco, G.; Amjad, M. W. Pharmacological evaluation and docking studies of α,β-unsaturated carbonyl based synthetic compounds as inhibitors of secretory phospholipase A_2, cyclooxygenases, lipoxygenase and proinflammatory cytokines. *Bioorg. Med. Chem.* **2014**, *22*, 4151–4161.

(170) Arshad, L.; Jantan, I.; Bukhari, S. N. A.; Jamil, S. Inhibitory effects of α,β-unsaturated carbonyl-based compounds and their pyrazoline derivatives on the phagocytosis of human neutrophils. *Med. Chem. Res.* **2018**, *27*, 1460–1471.

(171) Shrestha, A.; Oh, H. J.; Kim, M. J.; Pun, N. T.; Magar, T. B. T.; Bist, G.; Choi, H.; Park, P.-H.; Lee, E.-S. Design, synthesis, and structure-activity relationship study of halogen containing 2-benzylidene-1-

indanone derivatives for inhibition of LPS-stimulated ROS production in RAW 264.7 macrophages. *Eur. J. Med. Chem.* **2017**, *133*, 121–138.

(172) Kadayat, T. M.; Banskota, S.; Gurung, P.; Bist, G.; Magar, T. B. T.; Shrestha, A.; Kim, J.-A.; Lee, E.-S. Discovery and structure-activity relationship studies of 2-benzylidene-2,3-dihydro-1*H*-inden-1-one and benzofuran-3(2*H*)-one derivatives as a novel class of potential therapeutics for inflammatory bowel disease. *Eur. J. Med. Chem.* **2017**, *137*, 575–597.

(173) Kadayat, T. M.; Banskota, S.; Bist, G.; Gurung, P.; Magar, T. B. T.; Shrestha, A.; Kim, J.-A.; Lee, E.-S. Synthesis and biological evaluation of pyridine-linked indanone derivatives: potential agents for inflammatory bowel disease. *Bioorg. Med. Chem. Lett.* **2018**, *28*, 2436–2441.

(174) Zhang, Y.-L.; Zhang, W.-X.; Yan, J.-Q.; Tang, Y.-L.; Jia, W.-J.; Xu, M.-J.; Chattipakorn, N.; Wang, Y.; Feng, J.-P.; Liu, Z.-G.; Liang, G. Chalcone derivatives ameliorate lipopolysaccharide-induced acute lung injury and inflammation by targeting MD2. *Acta Pharmacol. Sinica* **2022**, *43*, 76–85.

(175) Chen, Y.; Yang, M.; Wang, Z.-J. (Z)-7,4'-Dimethoxy-6-hydroxy-aurone-4-O-β-glucopyranoside mitigates retinal degeneration in Rd10 mouse model through inhibiting oxidative stress and inflammatory responses. *Cutaneous Ocular Toxicol.* **2020**, *39*, 36–42.

(176) Jiang, P.; Sun, H. Sulfuretin alleviates atopic dermatitis-like symptoms in mice via suppressing Th2 cell activity. *Immunol. Res.* **2018**, *66*, 611–619.

(177) Lee, Y.-R.; Hwang, J.-K.; Koh, H.-W.; Jang, K. Y.; Lee, J. H.; Park, J.-W.; Park, B.-H. Sulfuretin, a major flavonoid isolated from *Rhus verniciflua*, ameliorates experimental arthritis in mice. *Life Sci.* **2012**, *90*, 799–807.

(178) Lu, Y.-T.; Xiao, Y.-F.; Li, Y.-F.; Li, J.; Nan, F.-J.; Li, J.-Y. Sulfuretin protects hepatic cells through regulation of ROS levels and autophagic flux. *Acta Pharmacol. Sinica* **2019**, *40*, 908–918.

(179) Kostopoulou, I.; Tzani, A.; Polyzos, N.-I.; Karadendrou, M.-A.; Kritsi, E.; Pontiki, E.; Liargkova, T.; Hadjipavlou-Litina, D.; Zoumpoulakis, P.; Detsi, A. Exploring the 2'-hydroxy-chalcone framework for the development of dual antioxidant and soybean lipoxygenase inhibitory agents. *Molecules* **2021**, *26*, 2777.

(180) Chen, J.-F.; Liu, Z.-Q. Ferrocenyl-appended aurone and flavone: which possesses higher inhibitory effects on DNA oxidation and radicals? *Chem. Res. Toxicol.* **2015**, *28*, 451–459.

(181) Park, H.; Kim, S. Y.; Kyung, A.; Yoon, T.-S.; Ryu, S. E.; Jeong, D. G. Structure-based virtual screening approach to the discovery of novel PTPMT1 phosphatase inhibitors. *Bioorg. Med. Chem. Lett.* **2012**, *22*, 1271–1275.

(182) Wang, S.; Xu, L.; Lu, Y.-T.; Liu, Y.-F.; Han, B.; Liu, T.; Tang, J.; Li, J.; Wu, J.; Li, J.-Y.; Yu, L.-F.; Yang, F. Discovery of benzofuran-3(2*H*)-one derivatives as novel DRAK2 inhibitors that protect islet b-cells from apoptosis. *Eur. J. Med. Chem.* **2017**, *130*, 195–208.

(183) Sun, H.; Ding, W.; Song, X.; Wang, D.; Chen, M.; Wang, K.; Zhang, Y.; Yuan, P.; Ma, Y.; Wang, R.; Dodd, R. H.; Zhang, Y.; Lu, K.; Yu, P. Synthesis of 6-hydroxyaurone analogues and evaluation of their αglucosidase inhibitory and glucose consumption-promoting activity: development of highly active 5,6-disubstituted derivatives. *Bioorg. Med. Chem. Lett.* **2017**, *27*, 3226–3230.

(184) Chaturvedi, R. N.; Pendem, K.; Patel, V. P.; Sharma, M.; Malhotra, S. Design, synthesis, molecular docking, and in vitro antidiabetic activity of novel PPARγ agonist. *Monatsch. Chem.* **2018**, *149*, 2069–2084.

(185) Geldenhuys, W. J.; Yonutas, H. M.; Morris, D. L.; Sullivan, P. G.; Darvesh, A. S.; Leeper, T. C. Identification of small molecules that bind to the mitochondrial protein mitoNEET. *Bioorg. Med. Chem. Lett.* **2016**, *26*, 5350–5353.

(186) Lamichhane, R.; Kim, S.-G.; Kang, S.; Lee, K.-H.; Pandeya, P. R.; Jung, H.-J. Exploration of underlying mechanism of anti-adipogenic activity of sulfuretin. *Biol. Pharm. Bull.* **2017**, *40*, 1366–1373.

(187) Roh, K.; Kim, S.; Kang, H.; Ku, J.-M.; Park, K. W.; Lee, S. Sulfuretin has therapeutic activity against acquired lymphedema by reducing adipogenesis. *Pharmacol. Res.* **2017**, *121*, 230–239.

(188) Zhang, L.-J.; Wang, Y.; Hu, X.-Q.; Xu, P.-F. Hydrogen-bonding network promoted [3+2] cycloaddition: asymmetric catalytic construction of spiro-pseudoindoxyl derivatives. *Chem. Asian J.* **2016**, *11*, 834–838.

(189) Wang, M.; Rong, Z.-Q.; Zhao, Y. Stereoselective synthesis of ε-lactones or spiro-heterocycles through NHC-catalyzed annulation: divergent reactivity by catalyst control. *Chem. Commun.* **2014**, *50*, 15309–15312.

(190) Guo, C.; Schedler, M.; Daniliuc, G.; Glorius, F. N-heterocyclic carbene catalyzed formal [3+2] annulation reaction of enals: an efficient enantioselective access to spiro-heterocycles. *Angew. Chem. Int. Ed.* **2014**, *53*, 10232–10236.

(191) Lee, C.-Y.; Chew, E.-H.; Go, M.-L. Functionalized aurones as inducers of NAD(P)H:quinone oxidoreductase 1 that activate AhR/XRE and Nrf2/ARE signaling pathways: synthesis, evaluation and SAR. *Eur. J. Med. Chem.* **2010**, *45*, 2957–2971.

(192) Haudecoeur, R. Pharmacochimie des aurones pour la modulation d'enzymes. Ph.D. Thesis, University of Grenoble, 2011.

(193) Yang, Z.-Y; Yang, Z.-J.; He, J.-H.; Lu, A.-P.; Liu, S.; Hou, T.-J.; Cao, D.-S. Benchmarking the mechanisms of frequent hitters: limitation of PAINS alerts. *Drug Discov. Today* **2021**, *26*, 1353–1358.

(194) Shanker, N.; Dilek, O.; Mukherjee, K.; McGee, D. W.; Bane, S. L. Aurones: small molecule visible range fluorescent probes suitable for biomacromolecules. *J. Fluoresc*. **2011**, *21*, 2173–2184.

(195) Espinosa-Bustos, C.; Cortés-Arriagada, D.; Soto-Arriaza, M. A.; Duggon, J. R.; Pizarro, N.; Cabrera, A. R.; Fuentealba, D.; Salas, C. O. Fluorescence properties of aurone derivatives: an experimental and theoretical study with some preliminary biological applications. *Photochem. Photobiol. Sci.* **2017**, *16*, 1268–1272.

(196) Petermayer, C.; Dube, H. Indigoid photoswitches: visible light responsive molecular tools. *Acc. Chem. Res.* **2018**, *51*, 1153–1163.

(197) Petermeyer, C.; Thumser, S.; Kink, F.; Mayer, P.; Dube, H. Hemiindigo: highly bistable photoswitching at the biooptical window. *J. Am. Chem. Soc*. **2017**, *139*, 15060–15067.

(198) Maerz, B.; Wiedbrauk, S.; Oesterling, S.; Samoylova, E.; Nenov, A.; Mayer, P.; de Vivie-Riedle, R.; Zinth, W.; Dube, H. Making fast photoswitches faster—using Hammett analysis to understand the limit of donor-acceptor approaches for faster hemithioindigo photoswitches. *Chem. Eur. J.* **2014**, *20*, 13984–13992.

(199) Zhao, X.; Yang, S. Photoinduced excited-state hydrogen bonding strengthening of hemiindigo for the drastically fluorescence quenching in protic solvent and water sensing in aprotic solvent. *J. Lumin.* **2020**, *220*, 116993.

(200) Plotner, J.; Dreuw, A. Molecular mechanism of the Z/E isomerization of hemithioindigo stilbene. *J. Phys. Chem*. **2009**, *43*, 11882–11887.

(201) Kink, F.; Collado, M. P.; Wiedbrauk, S.; Mayer, P.; Dube, H. Bistable photoswitching of hemithioindigo with green and red light: entry point to advanced molecular digital information processing. *Chem. Eur. J.* **2017**, *23*, 6237–6243.

(202) Zweig, J. E.; Newhouse, T. R. Isomer-specific hydrogen bonding as a design principle for bidirectionally quantitative and redshifted hemithioindigo photoswitches. *J. Am. Chem. Soc.* **2017**, *139*, 10956–10959.

(203) Welema, W. A.; Szymanski, W.; Feringa, B. L. Photopharmacology: beyond the proof-of-principle. *J. Am. Chem. Soc*. **2014**, *136*, 2178–2191.

(204) Sailer, A.; Ermer, F.; Kraus, Y.; Bingham, R.; Lutter, F. H.; Ahlfeld, J.; Thorn-Seshold, O.; Potent hemithioindigo-based antimitotics photocontrol the microtubules cytoskeleton in cellulo. *Beilstein J. Org. Chem.* **2020**, *16*, 125–134.

(205) Wang, K.; Ma, S.; Ma, Y.; Zhao, Y.; Xing, M.; Zhou, L.; Cao, D.; Lin, W. Aurone derivative revealing the metabolism of lipid droplets and monitoring oxidative stress in living cells. *Anal. Chem.* **2020**, *92*, 6631–6636.

(206) Ren, T.-B.; Xu, W.; Zhang, Q.-L.; Zhang, X.-X.; Wen, S.-Y.; Yi, H.-B.; Yuan, L.; Zhang, X.-B. Enhancing the anti-solvatochromic two-photon fluorescence for cirrhosis imaging by forming a hydrogen-bond network. *Angew. Chem. Int. Ed.* **2018**, *130*, 7595–7599.

(207) Fang, L.; Zhang, X.-Y.; Yuan, Q.; Li, D.-D.; Jiao, Q.-C.; Yang, Y.-S.; Zhu, H.-L. A novel indanone-derivated fluorescence sensor for Cysteine detection and biological imaging. *Dyes Pigments* **2020**, *175*, 108122.

(208) Lerch, M. M.; Hansen, M. J.; van Dam, G. M.; Szymanski, W.; Feringa, B. L. Emerging targets in photopharmacology. *Angew. Chem. Int. Ed.* **2016**, *55*, 10978–10999.

(209) Berdnikova, D. V. Design, synthesis and investigation of water-soluble hemi-indigo photoswitches for bioapplications. *Beilstein J. Org. Chem*. **2019**, *15*, 2822–2829.

(210) Berdnikova, D. V. Visible-range hemi-indigo photoswitch: ON–OFF fluorescent binder for HIV-1 RNA. *Chem. Commun.* **2019**, *55*, 8402–8405.

(211) Volaric, J.; Szymanski, W.; Simeth, N. A.; Feringa, B. L. Molecular photoswitches in aqueous environments. *Chem. Soc. Rev.* **2021**, *50*, 12337–12449.

(212) Erdélyi, M.; Varedian, M.; Skold, C.; Niklasson, I. B.; Nurbo, J.; Persson, A.; Bergquist, J.; Gogoll, A. Chemistry and folding of photomodulable peptides-stilbene and thioaurone-type candidates for conformational switches. *Org. Biomol. Chem*. **2008**, *6*, 4356–4373.

(213) Cordes, T.; Weinrich, D.; Kempa, S.; Riesselmann, K.; Herre, S.; Hoppmann, C.; Ruck – Braun, K.; Zinth, W. Hemithioindigo-based photoswitches as ultrafast light trigger in chromopeptides. *Chem. Phys. Lett.* **2006**, *428*, 167–173.

(214) Regner, N.; Herzog, T. T.; Haiser, K.; Hoppmann, C.; Beyermann, M.; Sauermann, J.; Engelhard, M.; Cordes, T.; Ruck-Braun, K.; Zinth, W. Light-switchable hemithioindigo-hemistilbene-containing peptides: ultrafast spectroscopy of the Z→E isomerization of the chromophore and the structural dynamics of the peptide moiety. *J. Phys. Chem. B* **2012**, *116*, 4181–4191.

(215) Herre, S.; Schadendorf, T.; Ivanov, I.; Herrberger, C.; Steinle, W.; Rück-Braun, K.; Preissner, R.; Kuhn, H. Photoactivation of an inhibitor of the 12/15-lipoxygenase pathway. *ChemBioChem* **2006**, *7*, 1089–1095.

(216) Sailer, A.; Ermer, F.; Kraus, Y.; Lutter, F. H.; Donau, C.; Bremerich, M.; Ahlfled, J.; Thorn-Seshold, O. Hemithioindigos for cellular photopharmacology: desymmetrised molecular switch scaffolds enabling design control over the isomer-dependency of potent antimitotic bioactivity. *ChemBioChem* **2019**, *20*, 1305–1314.

(217) Sailer, A.; Ermer, F.; Kraus, Y.; Bingham, R.; Lutter, F. H.; Ahlfeld, J.; Thorn-Seshold, O. Potent hemithioindigo-based antimitotics photocontrol the microtubule cytoskeleton in cellulo. *Beilstein J. Org. Chem.* **2020**, *16*, 125–134.

(218) Sailer, A.; Meiring, J. C. M.; Heise, C.; Pettersson, L. N.; Akhmanova, A.; Thorn-Seshold, J.; Thorn-Seshold, O. Pyrrole hemithioindigo antimitotics with near-quantitative bidirectional photoswitching that photocontrol cellular microtubule dynamics with single-cell precision. *Angew. Chem. Int. Ed.* **2021**, *60*, 23695–23704.

(219) Lerch, M. M.; Hansen, M. J.; van Dam, G. M.; Szymanski, W.; Feringa, B. L. Emerging targets in photopharmacology. *Angew. Chem. Int. Ed.* **2016**, *55*, 10978–10999.

(220) Szymanski, W.; Ourailidou, M. E.; Velema, W. A.; Dekker, F. J.; Feringa, B. L. Light-controlled histone deacetylase (HDAC) inhibitors: towards photopharmacological chemotherapy. *Chem. Eur. J.* **2015**, *21*, 16517–16524.

Table of Contents Graphic